

NAVAL POSTGRADUATE SCHOOL MONTEREY, CALIFORNIA



19970305 043

THESIS

EXPERIMENTAL INVESTIGATION OF FLOW CONTROL BY MEANS OF AIRFOIL FLAPPING

by

Jiannwoei Yue

September, 1996

Thesis Advisor:

M. F. Platzer

Co-Advisors:

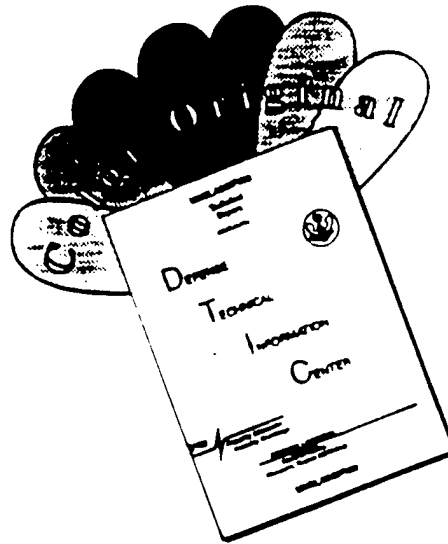
J. C. S. Lai

M. D. Kelleher

Approved for public release; distribution is unlimited.

DTIC QUALITY INSPECTED 3

DISCLAIMER NOTICE



THIS DOCUMENT IS BEST QUALITY AVAILABLE. THE COPY FURNISHED TO DTIC CONTAINED A SIGNIFICANT NUMBER OF COLOR PAGES WHICH DO NOT REPRODUCE LEGIBLY ON BLACK AND WHITE MICROFICHE.

REPORT DOCUMENTATION PAGE			Form Approved OMB No. 0704-0188	
Public reporting burden for this collection of information is estimated to average 1 hour per response, including the time for reviewing instruction, searching existing data sources, gathering and maintaining the data needed, and completing and reviewing the collection of information. Send comments regarding this burden estimate or any other aspect of this collection of information, including suggestions for reducing this burden, to Washington Headquarters Services, Directorate for Information Operations and Reports, 1215 Jefferson Davis Highway, Suite 1204, Arlington, VA 22202-4302, and to the Office of Management and Budget, Paperwork Reduction Project (0704-0188) Washington DC 20503.				
1. AGENCY USE ONLY (Leave blank)	2. REPORT DATE September, 1996	3. REPORT TYPE AND DATES COVERED Master's Thesis		
4. TITLE AND SUBTITLE EXPERIMENTAL INVESTIGATION OF FLOW CONTROL BY MEANS OF AIRFOIL FLAPPING		5. FUNDING NUMBERS		
6. AUTHOR(S) Jiannwoei Yue				
7. PERFORMING ORGANIZATION NAME(S) AND ADDRESS(ES) Naval Postgraduate School Monterey CA 93943-5000		8. PERFORMING ORGANIZATION REPORT NUMBER		
9. SPONSORING/MONITORING AGENCY NAME(S) AND ADDRESS(ES) Office of Naval Research, Arlington, VA 22217-5660		10. SPONSORING/MONITORING AGENCY REPORT NUMBER		
11. SUPPLEMENTARY NOTES The views expressed in this thesis are those of the author and do not reflect the official policy or position of the Department of Defense or the U.S. Government.				
12a. DISTRIBUTION/AVAILABILITY STATEMENT Approved for public release; distribution is unlimited.			12b. DISTRIBUTION CODE	
13. ABSTRACT (maximum 200 words) Flapping airfoils generate thrust-producing jet-like wakes. It therefore is the objective of this investigation to explore whether this feature can be used for effective flow control. To this end, the flow characteristics of flapping airfoils are first explored in a water tunnel experiment, using dye flow visualization and laser-doppler velocimeter. The effect of airfoil flapping frequency and amplitude of oscillation and of flow velocity on the wake flow characteristics are determined. This is followed by a second water tunnel experiment, where a small flapping airfoil is mounted in and near the separated flow region caused by the flow over a backward-facing step. The effect of airfoil size, location, frequency, and amplitude of oscillation on the separated flow region is again determined by means of laser-doppler velocimeter. It is found that the reattachment length of the separated flow region can be reduced by as much as 70%.				
14. SUBJECT TERMS : Vortical Wake Visualization, Jet Thrust, Backward-Facing Step, Oscillation Amplitude, Frequency, Location of Airfoils			15. NUMBER OF PAGES : 93	
			16. PRICE CODE	
17. SECURITY CLASSIFICATION OF REPORT Unclassified	18. SECURITY CLASSIFICATION OF THIS PAGE Unclassified	19. SECURITY CLASSIFICATION OF ABSTRACT Unclassified	20. LIMITATION OF ABSTRACT UL	

NSN 7540-01-280-5500

Standard Form 298 (Rev. 2-89)
Prescribed by ANSI Std. Z39-18 298-102

DTIC QUALITY INSPECTED 3

Approved for public release; distribution is unlimited.

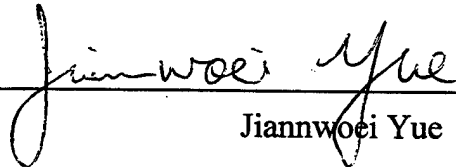
**EXPERIMENTAL INVESTIGATION OF FLOW CONTROL BY MEANS
OF AIRFOIL FLAPPING**

Giannwoei Yue
Lieutenant Colonel, Republic of China Army
M.S., Chung-Cheng Institute of Technology, 1984

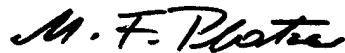
Submitted in partial fulfillment
of the requirements for the degree of

MASTER OF SCIENCE IN MECHANICAL ENGINEERING
from the
NAVAL POSTGRADUATE SCHOOL
September 1996

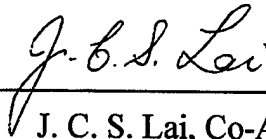
Author:


Giannwoei Yue

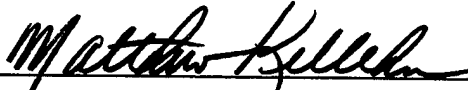
Approved by:



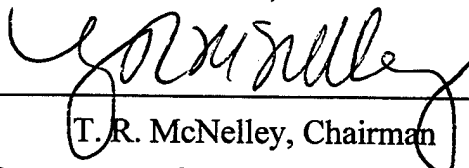
M. F. Platzter, Thesis Advisor



J. C. S. Lai, Co-Advisor



M. D. Kelleher, Co-Advisor



T. R. McNelley, Chairman

Department of Mechanical Engineering

ABSTRACT

Flapping airfoils generate thrust-producing jet-like wakes. It therefore is the objective of this investigation to explore whether this feature can be used for effective flow control. To this end, the flow characteristics of flapping airfoils are first explored in a water tunnel experiment, using dye flow visualization and laser-doppler velocimeter. The effect of airfoil flapping frequency and amplitude of oscillation and of flow velocity on the wake flow characteristics are determined. This is followed by a second water tunnel experiment, where a small flapping airfoil is mounted in and near the separated flow region caused by the flow over a backward-facing step. The effect of airfoil size, location, frequency, and amplitude of oscillation on the separated flow region is again determined by means of laser-doppler velocimeter. It is found that the reattachment length of the separated flow region can be reduced by as much as 70%.

TABLE OF CONTENT

I.	INTRODUCTION	1
II.	REVIEW OF PREVIOUS WORK	3
	A. FLOW OVER FLAPPING AIRFOIL	3
	B. FLOW OVER BACKWARD-FACING STEP	4
III.	EXPERIMENTAL APPARATUS	7
	A. WATER TUNNEL	7
	B. SHAKER	7
	C. AIRFOILS	9
	D. MODEL OF BACKWARD-FACING STEP	9
	E. LASER DOPPLER VELOCIMETER	10
IV.	EXPERIMENTAL PROCEDURE	11
	A. FLOW VELOCITY	11
	B. FREQUENCY OF AIRFOIL OSCILLATION	11
	C. AMPLITUDE OF AIRFOIL OSCILLATION	12
	D. VISUALIZATION BY DYE INJECTION	12
	E. PHOTOGRAPHY	13
	F. LASER DOPPLER VELOCIMETRY	13
	G. MATRIX OF EXPERIMENTS	14
V.	RESULTS	17
	A. VISUALIZATION OF FLOW OVER FLAPPING AIRFOIL	17
	B. LDV MEASUREMENT OF FLOW OVER FLAPPING AIRFOIL	21
	C. BACKWARD-FACING STEP FLOW	31
	D. CONTROL OF BACKWARD-FACING STEP FLOW WITH A FLAPPING AIRFOIL	36
	1. Flow Visualization	36
	2. LDV Measurements	36
	3. Effect of Stationary Airfoil	43
	4. Effect of Frequency of Oscillation	43
	5. Effect of Amplitude of Oscillation	48
	6. Effect of Airfoil Size	56
	7. Effect of Airfoil Location	56
	8. Effect of Three-Dimensionality of Upstream Flow	60
VI.	CONCLUSIONS	71
	LIST OF REFERENCES	73
	INITIAL DISTRIBUTION LIST	75

LIST OF FIGURES

Figure 3.1	Layout of the water tunnel	8
Figure 3.2	Layout of the backward-facing step	9
Figure 4.1	Calibration of the LVDT	13
Figure 5.1.1	$U_o=0.14$ m/s, no flapping case	18
Figure 5.1.2	$U_o=0.14$ m/s, $f=5$ Hz, $H'=0.02$, $V_p=0.43$	18
Figure 5.1.3	$U_o=0.14$ m/s, $f=5$ Hz, $H'=0.04$, $V_p=0.76$	19
Figure 5.1.4	$U_o=0.14$ m/s, $f=5$ Hz, $H'=0.06$, $V_p=0.98$	19
Figure 5.1.5	$U_o=0.05$ m/s, $f=5$ Hz, $H'=0.04$, $V_p=1.23$	20
Figure 5.1.6	$U_o=0.0$ m/s, $f=5$ Hz, $H'=0.06$, $V_p=1.41$	20
Figure 5.2.1	$(U-U_o)/U_p$, $f=5$ Hz, $H'=0.02$	22
Figure 5.2.2	$(U-U_o)/U_p$, $f=5$ Hz, $H'=0.04$	23
Figure 5.2.3	$(U-U_o)/U_p$, $f=5$ Hz, $H'=0.06$	24
Figure 5.2.4	$(U-U_o)/U_p$, $f=5$ Hz, $H'=0.08$	25
Figure 5.2.5	$(U-U_o)/U_p$, $f=2.5$ Hz, $H'=0.04$	26
Figure 5.2.6	$(U-U_o)/U_p$, $f=10$ Hz, $H'=0.04$	27
Figure 5.2.7	y/H , $H=4$ mm, $U_o=0$ m/s	28
Figure 5.2.8	y/H , $H=4$ mm, $U_o=0.05$ m/s	29
Figure 5.2.9	y/H , $H=4$ mm, $U_o=0.14$ m/s	30
Figure 5.3.1	Three dimensionality of the short blunt plate	33
Figure 5.3.2	10mm airfoil at $(1.83h, 0.2h)$, stationary. Short blunt leading upstream plate	34
Figure 5.3.3	Two-dimensionality of the modified sharp leading edge plate	35
Figure 5.4.1(a)	$Re_h=10,000$, airfoil at $(1.83h, 0.2h)$, stationary	40
Figure 5.4.1(b)	$Re_h=10,000$, airfoil at $(1.83h, 0.2h)$, $f=5$ Hz, $H'=0.25$	40
Figure 5.4.2(a)	$Re_h=10,000$, airfoil at $(1.83h, 0.2h)$, $f=10$ Hz, $H'=0.25$	41
Figure 5.4.2(b)	$Re_h=10,000$, airfoil at $(1.83h, 0.2h)$, $f=20$ Hz, $H'=0.125$	41
Figure 5.4.3	(a) velocity, (b) turbulence intensity, (c) streamlines of the backward- facing step, no airfoil	42

Figure 5.4.4	(a) velocity, (b) turbulence intensity, (c) streamlines of the backward-facing step, 10mm airfoil at (1.83h, 0.2h), stationary.	44
Figure 5.4.5	(a) velocity, (b) turbulence intensity, (c) streamlines of the backward-facing step, 10mm airfoil at (1.83h, 0.6h), stationary.	45
Figure 5.4.6	(a) velocity, (b) turbulence intensity, (c) streamlines of the backward-facing step, 10mm airfoil at (1.83h, 1.0h), stationary.	46
Figure 5.4.7	(a) velocity, (b) turbulence intensity, (c) streamlines of the backward-facing step, 10mm airfoil at (1.83h, 1.3h), stationary.	47
Figure 5.4.8	(a) velocity, (b) turbulence intensity, (c) streamlines of the backward-facing step, 10mm airfoil at (1.83h, 0.2h), oscillation frequency $f=5$ Hz, amplitude $H'=0.25$	49
Figure 5.4.9	(a) velocity, (b) turbulence intensity, (c) streamlines of the backward-facing step, 10mm airfoil at (1.83h, 0.2h), oscillation frequency $f=10$ Hz, amplitude $H'=0.25$	50
Figure 5.4.10	(a) velocity, (b) turbulence intensity, (c) streamlines of the backward-facing step, 10mm airfoil at (1.83h, 0.2h), oscillation frequency $f=20$ Hz, amplitude $H'=0.125$	51
Figure 5.4.11	(a) velocity, (b) turbulence intensity, (c) streamlines of the backward-facing step, 10mm airfoil at (1.83h, 1.0h), oscillation frequency $f=10$ Hz, amplitude $H'=0.25$	52
Figure 5.4.12	(a) velocity, (b) turbulence intensity, (c) streamlines of the backward-facing step, 10mm airfoil at (1.83h, 1.0h), oscillation frequency $f=10$ Hz, amplitude $H'=0.5$	53
Figure 5.4.13	(a) velocity, (b) turbulence intensity, (c) streamlines of the backward-facing step, 10mm airfoil at (2.5h, 0.9h), oscillation frequency $f=10$ Hz, amplitude $H'=0.25$	54
Figure 5.4.14	(a) velocity, (b) turbulence intensity, (c) streamlines of the backward-facing step, 10mm airfoil at (2.5h, 0.9h), oscillation frequency $f=10$ Hz, amplitude $H'=0.5$	55

Figure 5.4.15	(a) velocity, (b) turbulence intensity, (c) streamlines of the backward-facing step, 20mm airfoil at (1.83h, 0.2h), stationary	57
Figure 5.4.16	(a) velocity, (b) turbulence intensity, (c) streamlines of the backward-facing step, 20mm airfoil at (1.83h, 0.2h), oscillation frequency $f=5$ Hz, amplitude $H'=0.25$	58
Figure 5.4.17	(a) velocity, (b) turbulence intensity, (c) streamlines of the backward-facing step, 20mm airfoil at (1.83h, 0.2h), oscillation frequency $f=10$ Hz, amplitude $H'=0.25$	59
Figure 5.4.18	(a) velocity, (b) turbulence intensity, (c) streamlines of the backward-facing step, 20mm airfoil at (1.83h, 0.6h), oscillation frequency $f=10$ Hz, amplitude $H'=0.25$	62
Figure 5.4.19	(a) velocity, (b) turbulence intensity, (c) streamlines of the backward-facing step, 20mm airfoil at (1.83h, 1.3h), oscillation frequency $f=10$ Hz, amplitude $H'=0.25$	63
Figure 5.4.20	The streamwise velocity profile 2 mm above the plate, airfoil at the location $x/h=1.83$. (a) stationary, (b) flapping at $f=10$ Hz, $H'=0.25$	64
Figure 5.4.21	The streamwise velocity profile 2 mm above the plate, airfoil at the location $x/h=2.5$. (a) stationary, (b) flapping at $f=10$ Hz, $H'=0.25$	65
Figure 5.4.22	The streamwise velocity profile 2 mm above the plate, airfoil at the location $x/h=4.0$. (a) stationary, (b) flapping at $f=10$ Hz, $H'=0.25$	66
Figure 5.4.23	The streamwise velocity profile 2 mm above the plate, airfoil at the location $x/h=2.5$. (a) flapping at same frequency $f=10$ Hz, (b) flapping at same amplitude, $H'=0.25$	67
Figure 5.4.24	(a) velocity, (b) turbulence intensity, (c) streamlines of the backward-facing step, 10mm airfoil at (1.83h, 0.2h), oscillation frequency $f=10$ Hz, amplitude $H'=0.25$. short, blunt leading edge upstream plate	68
Figure 5.4.25	(a) velocity, (b) turbulence intensity, (c) streamlines of the backward-facing step, 10mm airfoil at (1.83h, 0.2h), oscillation frequency $f=20$ Hz, amplitude $H'=0.125$. short, blunt leading edge upstream plate	69

Figure 5.4.26 (a) velocity, (b) turbulence intensity, (c) streamlines of the backward-facing step, 10mm airfoil at $(1.83h, 0.2h)$, oscillation frequency $f=5$ Hz. amplitude $H'=0.25$. short, blunt leading edge upstream plate70

LIST OF TABLES

Table 4.1	Calibration of flowmeter and LDV	11
Table 4.2	LDV measurements of airfoil flapping in the free-stream flow	14
Table 4.3	LDV measurements of BSF	15
Table 5.1	List of Dye Flow Visualization	17
Table 5.2	Dye Injection Visualization of BSF	39

LIST OF SYMBOLS

c :	chord length, m.
f :	plunging frequency, Hz.
h :	step height of the backward-facing step, mm.
H :	maximum amplitude of oscillation of airfoil, m.
H' :	normalized amplitude, $H' = H/c$.
H_i :	height, upstream of backward-facing step, mm.
H_o :	height, downstream of backward-facing step, mm.
k_o :	reduced frequency, $k_o = \omega c / U_o$.
k_e :	effective reduced frequency, $k_e = \omega c / U_e$.
L_1 :	length, blunt upstream plate of the backward-facing step, mm
L_2 :	length, downstream plate of the backward-facing step, mm
L_3 :	length, modified extended upstream plate of the backward-facing step, mm
Re_h :	Reynolds number, $Re_h = \frac{U_o h}{\nu}$
t :	thickness of the backward-facing step, mm
u :	streamwise turbulence intensity, m/s.
U :	mean streamwise velocity, m/s.
U_o :	free-stream velocity, m/s.
U_p :	plunging velocity (r.m.s), m/s. $U_p = H\omega / \sqrt{2}$.
U_e :	effective velocity, m/s. $U_e = \sqrt{U_o^2 + U_p^2}$.
V_p :	nondimensional flapping velocity, $= H' * k$
ω :	plunging frequency, rad/s.

ACKNOWLEDGMENT

The author would like to acknowledge the financial support of the Office of Naval Research for allowing the purchase of equipment used in this study.

I would like to express my sincere gratitude to Dist. Professor M. F. Platzner for his love, care and patient guidance. His constant encouragement and support were instrumental in accomplishing this work.

Thanks are also due to Visiting Professor J. C. S. Lai for his assistance in the model designing, trouble shooting and Co-advising.

Special thanks to my wife, Yali, for her persistence and spiritual support.

I. INTRODUCTION

It was first recognized by Knoller (1909) and by Betz (1912) that a flapping airfoil generates thrust. This Knoller-Betz effect was first confirmed experimentally by Katzmayer (1922). Recently, Dohring et al. (1996) showed, both experimentally and computationally, that when an airfoil is oscillated in plunge with appropriate combination of frequency and amplitude, a jet (instead of a wake) is produced downstream of the trailing edge. The entrainment induced by the jet structure of a flapping airfoil may provide a mechanism whereby the reattachment of a separated shear layer may be controlled. The separated flow region caused by the flow over a backward-facing step is an obvious example to demonstrate the possibility of flow control.

Backward-facing step flows have received considerable attention in the past primarily because of two reasons. Firstly, separated and reattached flows are encountered in many practical applications, such as flow in diffusers, combustors, turbomachinery, and flow around airfoils, etc. Secondly, backward-facing step flows are the simplest flow for studying the reattachment process and for providing data for turbulence modeling and CFD validation. With improved understanding of the flow, the objective of research often becomes one of studying means whereby the flow can be controlled to suit individual applications. The controlled excitation may be implemented using various means, among which mechanical, acoustic or fluidic devices are more commonly used.

The objectives of this study were, therefore, to explore

- A. the entrainment and the jet structure induced by a flapping airfoil in a zero and low velocity flow;
- B. if the recirculation flow region in backward-facing step flows can be controlled by a small flapping airfoil;
- C. the effects of frequency and amplitude of oscillation of a small flapping airfoil on the flow dynamics in a backward-facing step flow; and

D. the effects of the location of a small flapping airfoil on backward-facing step flow.

II. REVIEW OF PREVIOUS WORK

A. FLOW OVER FLAPPING AIRFOIL

Katzmayr (1922) appeared to have been the first one to perform wind tunnel tests to determine the effect of flow oscillations on the drag of airfoils. He found that under certain conditions the airfoil produced a net thrust rather than a drag and thus confirmed the theoretical explanations of thrust generation due to wing flapping advanced by Knoller (1909) and Betz (1912). Halfman (1952) presented lift and moment measurements due to airfoil oscillations in either pure translatory (flapping) or pitching motion. At the same time, Bratt (1953) visualized the flow patterns in the wake of a flapping airfoil. Additional investigations of the behavior of vortex wakes from oscillating airfoils were published by Katz and Weihs (1978), Freymuth (1988) and Koochesfahani (1989). Freymuth showed the difference between a drag-producing and a thrust-producing wake behind a flapping airfoil. In the former case the wake is similar to the Karman vortex street shed from a cylinder, i.e., the upper row of vortices turns clockwise, and the lower row turns counterclockwise. The thrust producing wake, in contrast, has counterclockwise vortices in the upper row and clockwise vortices in the lower row, thus generating a jet flow. Koochesfahani (1989) limited himself to the investigation of sinusoidally pitching airfoils. He visualized the wake as a function of amplitude and frequency of the oscillation and he showed that the switch from a drag-producing wake to a thrust-producing wake occurs only if a certain relatively high critical reduced frequency is exceeded.

At the Naval Postgraduate School, Professor Platzer and his associates have conducted a series of tests on flapping airfoils. Dohring (1996) and Jones et al. (1996) presented systematic visualizations and measurements of the flow past flapping airfoils. They confirmed the earlier findings, but they also identified an asymmetric wake mode which occurs when a certain critical plunge velocity is exceeded.

B. FLOW OVER BACKWARD-FACING STEP

Backward-Facing Step flows (BSF) are of fundamental importance for a better understanding of separating and reattaching flows. Therefore, they have already been studied in considerable detail. Comprehensive reviews of experiments on BSF prior to 1980 have been given by Bradshaw and Wong (1972) and by Eaton and Johnston (1981).

As pointed out by Eaton and Johnston, there are many variables involved in the flow, step height (h), free stream velocity (U_o), boundary layer thickness (δ) at separation, momentum thickness (θ) at separation, expansion ratio (ER), streamwise pressure gradient and aspect ratio (channel width to step ratio) etc.

Different investigators have used different definitions of Reynolds number to characterize the flow over backward-facing steps, by using either the boundary layer thickness (δ) or the step height (h) or the momentum thickness (θ). It is, therefore, not surprising that there is a scatter of 20~50 % in the reattachment lengths reported in the literature even for nominally similar flows conditions, as shown by Adams and Johnston (1988). The documentation of the upstream initial condition and other variables mentioned above for backward-facing step flows cannot be overemphasized. Adams and Johnston argued for using Re_h (Reynolds number based on step height), expansion ratio (ER) and δ/h as three relevant non-dimensional parameters. The effects of the state of separation boundary layer, expansion ratio and streamwise pressure gradient on reattachment lengths have been studied in detail and are summarized as follows.

It has been shown by Eaton and Johnston (1981) and Adams and Johnston (1988), among others, that the reattachment length is greatly influenced by the state of the separating boundary layer. Generally, at low Reynolds number ($Re_h < 1000$), the flow is laminar at separation and at reattachment and the reattachment length increases with increasing Reynolds number. As Reynolds number increases further, transition to turbulence occurs in the separated free shear layer and the reattachment length decreases

with increasing Reynolds number. At higher Reynolds number ($Re_h > 100,000$), the reattachment length becomes almost independent of Reynolds number. The increases in reattachment length from upstream laminar condition to turbulent condition can be as much as over 30%. The shorter reattachment length for laminar separation boundary layer has been attributed to the initial faster growth of laminar shear layer than turbulent shear layer (Bradshaw, 1966, Otugen, 1991) which results in faster entrainment in the separated shear layer. Reattachment length decreases with increasing boundary layer thickness at separation (Adams and Johnston, 1988) but the trend is weak. Eaton and Johnston (1981) and Isomoto and Hyonami (1989) have found that reattachment length shortens as the free-stream turbulence level increases. Moreover, by placing a rod or cavity near the wall at separation point, Isomoto and Hyonami (1989) showed that only a change in 2% of turbulence near the wall caused a change of two step heights in the reattachment length.

It can be inferred from the experimental results documented by Eaton and Johnston (1981) and Adams and Johnston (1988) that for expansion ratios less than 1.8, reattachment length increases with expansion ratio. This trend is also supported by the results of numerical simulation of laminar backward-facing step flows for expansion ratio 1.25~1.75 (Thangam and Knight, 1989) and 1.11~10 (Barton, 1994). On the other hand, Otugen (1991) has found experimentally that for expansion ratios between 1.5 and 3.13, reattachment length decreases as expansion ratio increases. This has been attributed by Otugen (1991) to the increase in higher turbulence intensities inside the separated shear layer at large expansion ratios although the cause for increased turbulence activity is not clear.

All the studies reviewed so far deal with the determination of reattachment length and the statistical description of the velocity field. Although coherent structures were identified almost two decades ago in plane mixing layers (Brown and Roshko, 1974) and in asymmetric mixing layers (Zaman and Hussain, 1980), it is only until recently that research in backward-facing step flows has been directed to identifying the existence of

coherent structures and to studying the role played by these structures in influencing the recirculation zone. By using flow visualization, Roos and Kegelman (1986) showed that the vortex roll-up and merging process is also present in a reattaching shear layer.

Manipulation of coherent structures to influence the flow dynamics of the reattachment zone has been achieved by Bhattacharjee et al (1986) using global acoustic excitation, by Roos and Kegelman (1986) using an oscillating flap at the point of shear-layer separation and by Hasan (1992) using localized acoustic excitation at the point of shear-layer separation. By introducing acoustic excitation at $St_h=0.2\sim0.4$ and a constant forcing amplitude of 92 dB at the step edge, Bhattacharjee et al (1986) found that the spreading rate in the separated shear layer was increased, resulting in 10~15% reduction in reattachment length. Their results seem to be relatively independent of Reynolds number Re_h over the range 26,000~76,000. Roos and Kegelman (1986) applied a constant oscillating flap amplitude of 1% at the flap trailing edge at $St_h=0.29$. They found that the reattachment length was reduced at least one step height for a laminar separating shear layer and by at least two step heights for a fully turbulent separating shear layer. Controlled perturbation was introduced by Hasan at $St_h=0.218, 0.49$ and 0.845 with an amplitude of $U/U_0=0.015$ at $x=0, y=y_{0.9}$ (where $U/U_0=0.9$) for $Re_h=11,000$. His results indicate a reduction in reattachment length of 18%, 12.5% and 12% respectively. Other attempts in modifying the flow dynamics of backward-facing step flows are mainly based on increasing the local turbulence intensity. Isomoto (1989) showed that only an increase of 2% of turbulence intensity near the wall at the separation point caused a reduction of two step heights in the reattachment length. By inserting a cylinder of diameter $0.4h$ at three different locations ($0.6h, 0.8h$), ($0.6h, 1h$) and ($0.6h, 1.5h$) for $Re_h=700, 100$ and 1400 , Suzuki et al (1991) showed that the velocity characteristics in the backward-facing step flow could be changed significantly, resulting in increased heat transfer.

III. EXPERIMENTAL APPARATUS

The experiments were conducted in the water tunnel laboratory of the Aeronautics Department of the Naval Postgraduate School. The facilities include:

- A. Water Tunnel
- B. Shaker
- C. Airfoils
- D. Model of Backward-Facing Step
- E. Laser Doppler Velocimeter

A. WATER TUNNEL (Figure 3.1)

The Flow Visualization Water Tunnel (Eidetics, 1988), made by Eidetics International Inc. model 1520, is a closed circuit continuous system with a contraction ratio of 6:1 driven by a three horsepower electric pump. The capacity is around 1000 gallons. The tunnel speed is monitored by a flow meter assembled at the end of the test section, the graduation is 0.01 ft/sec, the speed is regulated by a dial, the maximum velocity is approximately 0.5 m/s. The test section is 60 in x 20 in x 15 in. The side and bottom walls are made of glass that provides excellent accessibility for flow visualization and Laser experiments. To maintain the flow uniformity, the side walls are slightly diverged to compensate for boundary layer effects. For flow visualization, six pressurized canisters are available for different water soluble coloring. The pressure is provided by a compressor and a pressure regulator.

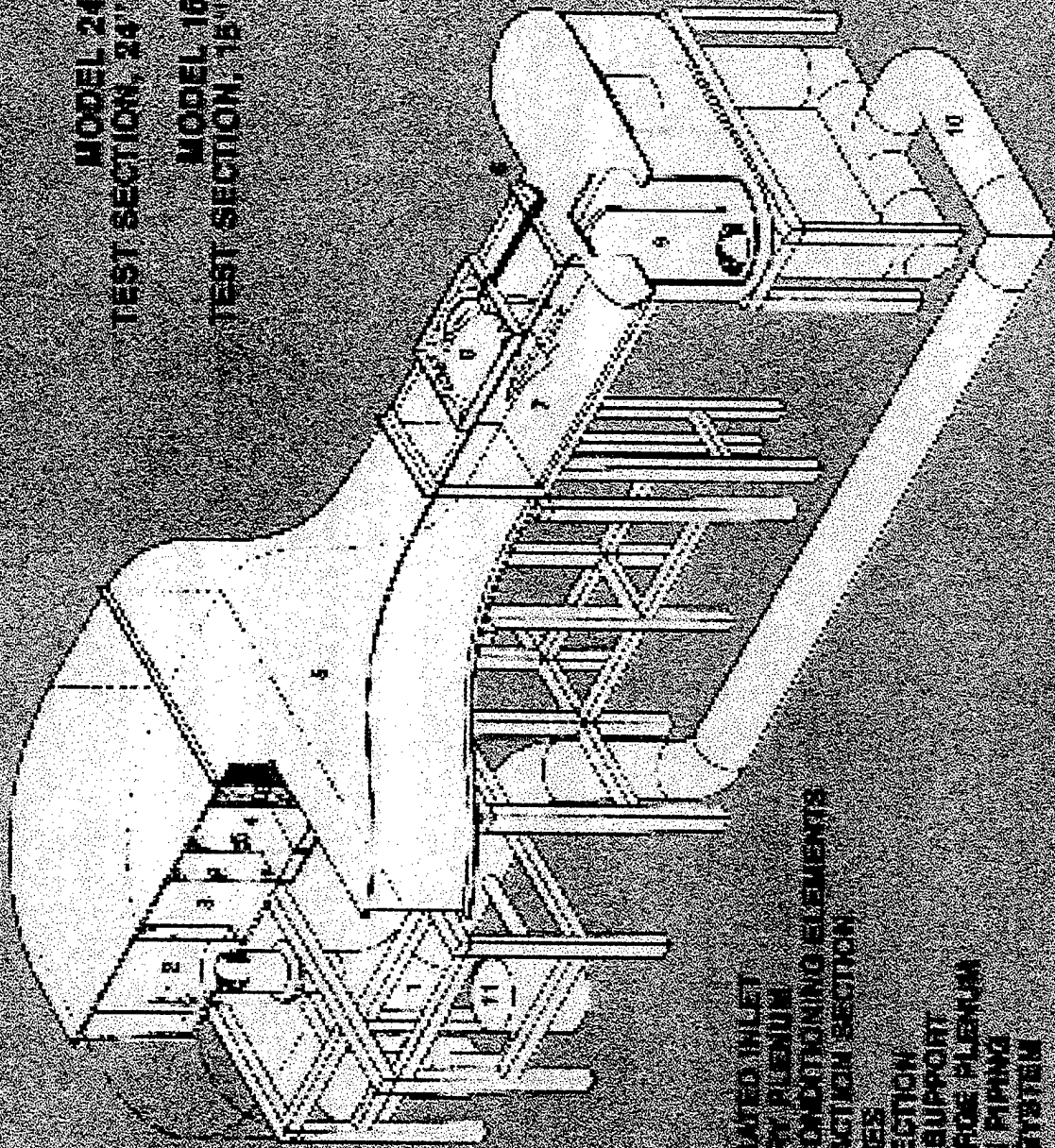
B. SHAKER

The Shaker (APS Dynamics, 1994), made by APS Dynamics Inc. model ELEKTRO-SEIS 113, is used to provide the plunging motion of the airfoil. The airfoil is attached to the bottom of the shaker. The oscillation is generated by an amplifier (APS model 114) and a frequency generator. The frequency generator is able to be operated in a frequency range up to 60 Hz, and a suitable range of amplitude.

EIDETICS INTERNATIONAL FLOW VISUALIZATION WATER TUNNEL

MODEL 2436
TEST SECTION, 24" X 36" X 72"

MODEL 1620
TEST SECTION, 16" X 20" X 60"



KEY

1. PUMP
2. PERFORATED INLET
3. DELIVERY PLENUM
4. FLOW CONDITIONING ELEMENTS
5. CONTRACTION SECTION
6. DYE LINES
7. TEST SECTION
8. MODEL SUPPORT
9. EXPANSION PLENUM
10. DISCHARGE PIPING
11. FILTER SYSTEM
12. RETURN LINE

Figure 3.1 Layout of the water tunnel

The oscillation frequency and amplitude of the shaker are monitored by an oscilloscope. The amplitude is measured by a Lucas Schaevitz sensor Model DC-E 500 LVDT (Linear Variable Differential Transformer) device.

C. AIRFOILS

The airfoils used in this study are a 10 mm chord length NACA0010 airfoil, a 20 mm NACA0018 airfoil, a 62 mm NACA0015 airfoil, and a 100 mm NACA0012 airfoil. The span of each airfoil is close to 370 mm that matches the width of the water tunnel. For the backward-facing step flow, the smallest airfoil is primarily used. For the airfoil plunging in the low (and zero) tunnel velocity flow, the largest airfoil is primarily studied for its better profile and dye injection accessibility.

D. MODEL OF BACKWARD-FACING STEP (Figure 3.2)

Figure 3.2 shows the configuration of the backward-facing step and the airfoil. The backward-facing step is made of 4.76 mm thick aluminum plate. The step height (h) is 30 mm and the width is 370 mm, thus giving an aspect ratio of 12.33 that reduces the three-dimensionality effect of the flow. The floor plate downstream of the step is 700 mm long. The plate with a blunt front leading edge upstream of the step is 310 mm long, and one extended plate with a sharp leading edge is 610 mm long, thus giving a total length of 910 mm for the flow to develop before the step.

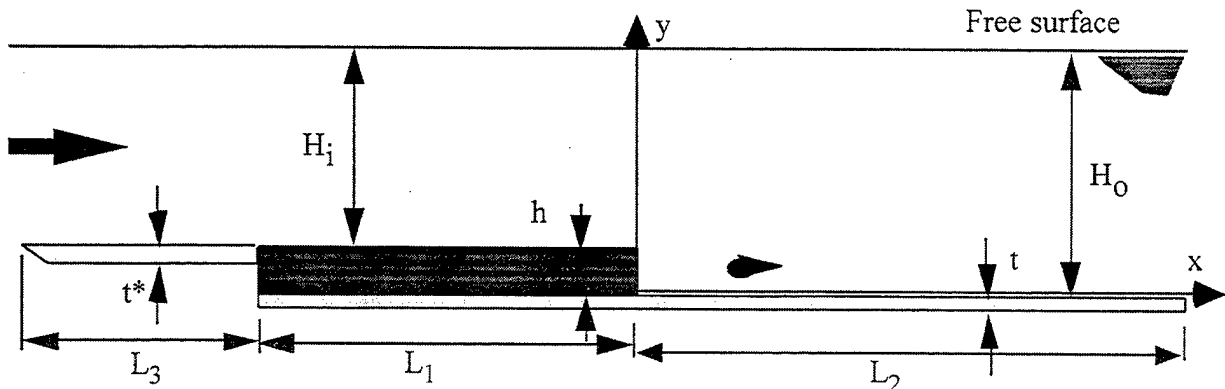


Figure 3.2 The configuration of the backward-facing step, $h=30$, $t=4.76$, $L_1=300$, $L_2=700$, $L_3=610$, $H_i=242$, $H_o=272$, unit in mm.

E. LASER-DOPPLER VELOCIMETER

The LASER-DOPPLER VELOCIMETER (LDV), provided by TSI, has the following Omnichrome components:

- a. Model 543-300A air cooled Argon Ion Laser system. The system also includes a model 160 power supply and a model RC1 remote control. The maximum power rating is 300 mW, and is operated by remote control.
- b. The TSI model 9201 Colorburst Multicolor beam separator converts the Argon ion laser beam into six laser beams to perform the Laser Doppler Velocimetry (LDV). This conversion produces three pairs of shifted and unshifted beams. The wave lengths of green, blue, and violet beams are 514.5, 488, and 476.5 nanometer respectively.
- c. TSI model 9162 photomultiplier system. The system also includes a power supply, TSI model 9165.
- d. TSI model 9275 two component fiberoptic probe. It can have two output colors. The beam separation is 50 mm, focusing length is 350 mm. The half angle is 4.08 degree.
- e. TSI LV frequency shifter, model 9186A-4 is used to shift the beam at 100k Hz.
- f. Lintech model 41583 traverse table. The traverse table is driven by Applied Motion Products system 1618 with an increment of 0.01 mm.
- g. TSI IFA 550 Intelligent Flow Analyzer.
- h. TSI FIND (Flow INformation Display) version 4.5
- i. Pentium 150 Personal computer. It processes and displays the collected raw data.

IV. EXPERIMENTAL PROCEDURE

A. FLOW VELOCITY

The speed of the water tunnel is regulated by a potential meter, and the maximum uniform velocity which can be reached is approximately 0.5 m/s. A turbine flow meter, attached at the end of the tunnel test section, is used to measure the average flow velocity, and it is displayed on a LED (Light Emitting Diode Display) with a precision of 0.01 ft/s.

For most cases, the location of the flow meter is too far away from the test location. The alternative is the LDV measurement. In addition, the reading of the flow meter differs slightly from the LDV measurement as shown on table 4.1. All the velocity data, therefore, were based on the LDV measurement.

Rev. (turn)	flowmeter (ft/s)	flowmeter (m/s)	LDV (m/s)
0.5	0.01	0.00	0.02
1.0	0.11	0.03	0.05
1.5	0.22	0.07	0.08
2.0	0.32	0.10	0.11
2.5	0.42	0.13	0.13
3.0	0.52	0.16	0.16
3.5	0.63	0.19	0.19
4.0	0.73	0.22	0.21
4.5	0.83	0.25	0.24
5.0	0.93	0.28	0.27
5.5	1.04	0.32	0.29
6.0	1.12	0.34	0.31

Table 4.1 Calibration of flowmeter with LDV

B. FREQUENCY OF AIRFOIL OSCILLATION

The frequency of the shaker is regulated by a frequency generator. Because of the airfoil jittering problem produced in the higher frequency range, most experiments were conducted below 10 Hz.

Conventionally, the reduced frequency of an airfoil flapping in a free stream is defined as $k_o = \frac{\omega c}{U_o}$, $\omega = 2\pi f$, where c is the chord length of the airfoil and U_o is the free stream velocity. Obviously, k_o tends to be infinite as U_o approaches zero. Therefore, an effective reduced frequency is defined as $k_e = \frac{\omega c}{U_e}$, where $U_e = \sqrt{U_o^2 + U_p^2}$, $U_p = \omega H / \sqrt{2}$ and H is the maximum oscillation amplitude. Table 5.1 lists the frequencies, amplitudes, and the velocities which were used in the experiments.

From table 5.1, we can see the low velocity effect on the reduced frequency k_o . When the flow velocity U_o is small or zero, the flapping velocity U_p is the dominant parameter. When the flow velocity U_o is high, the flapping velocity is less effective.

C. AMPLITUDE OF AIRFOIL OSCILLATION

The amplitude of oscillation is controlled by an amplifier and regulated by a frequency generator. The oscillation is measured by a LVDT (Linear Variable Differential Transformer) device.

Prior to the experiments, the LVDT was calibrated by a video camera and a recorder, and the calibration curve is shown in Figure 4.1. The conversion factor was determined to be 8.09volts/cm. Furthermore, the flow characteristics are very sensitive to the angle of attack. To keep the AOA as close to zero as possible, the heights of the leading edge and trailing edge were adjusted to be level by measuring the heights.

D. VISUALIZATION BY DYE INJECTION

Water soluble food coloring was injected through a plastic tube at the appropriate flow field location or through 0.8 mm holes in the BSF plate using pressurized canisters. The pressure in the canisters was maintained by a small compressor and controlled by a pressure regulator. There are twentyfour ports along the centerline of the BSF plate for dye injection, the distance between the ports is 0.5 step heights.

Calibration of LVDT

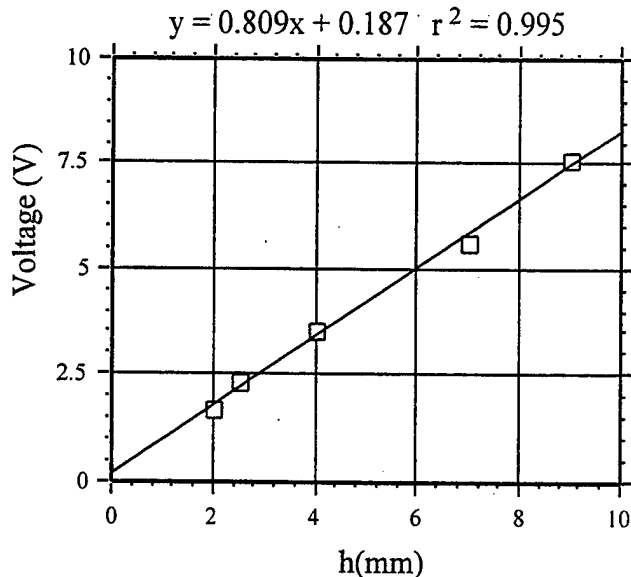


Figure 4.1 Calibration of LVDT, the calibration curve is 8.09 volt vs. 10 mm

E. PHOTOGRAPHY

The still pictures were taken by a 35 mm NIKON 2000 camera. The motion pictures were taken by a SONY DXC-3000A video camera, and were recorded by a SONY Vmatic VO5850 videocassette recorder. The light was provided by 600 watt flood lights.

F. LASER DOPPLER VELOCIMETRY

When the multiline argon ion beam, created by the laser head, passes through the Bragg cell inside the colorburst multicolor beam separator, it is split into 3 pairs of shifted and unshifted beams; green (514.5 nm), blue (488 nm), and violet (476.5 nm). Ideally, each beam has the same intensity. The beams are then emitted from the fiberoptic probe. In the beam intersection area, fringes are created. The spacing between the fringes is $\delta = \frac{\lambda}{2 \sin(0.59)}$, where λ is the wave length. Blue beams, for example, with the half angle of 4.0856° create a fringe of spacing of 3.4247 micron.

When a particle passes through the measuring volume, it scatters light whose intensity varies according to the light intensity variations inside the bisector of the two beams. Therefore, it is important to achieve as high a power intensity as possible.

It is very important to have a large degree of beam overlap to ensure that the highest fringe visibility occurs. The photomultiplier then converts the detected light into an electric signal from which the frequency of the fringe crossings can be determined. The particle velocity is then the product of this frequency and the fringe spacing.

LDV measurements require seed particles that are moving with the flow. If these particles do not have the appropriate size and concentration distribution, the experiment may be adversely affected. However, water naturally carries enough particles and therefore no seeding was needed in the experiments.

Sample size is also important because the LDV calculation provides the average velocity. Sample size was set to 1000 in most of the experiments.

G. MATRIX OF EXPERIMENTS

Table 4.2 and 4.3 lists all the LDV experiments. Figures 5.1.1 through 5.2.9 refer to the single flapping airfoil experiments. Figures 5.3.1 through 5.4.26 refer to the backward-facing step experiments.

Figure No	Airfoil size(mm)	Frequency Hz	Amplitude H' (H/c)	Free Stream vel. Uo(m/s)
5.2.1	100	5	0.02	0, 0.05, 0.14
5.2.2	100	5	0.04	0, 0.05, 0.14
5.2.3	100	5	0.06	0, 0.05, 0.14
5.2.4	100	5	0.08	0, 0.05, 0.14
5.2.5	100	2.5	0.04	0, 0.05, 0.14
5.2.6	100	10	0.04	0, 0.05, 0.14
5.2.7	100	2.5, 5, 10	0.04	0
5.2.8	100	2.5, 5, 10	0.04	0.05
5.2.9	100	2.5, 5, 10	0.04	0.14

Table 4.2 LDV measurements of single airfoil flapping in the free stream flow

Figure	Airfoil (mm)	Frequency	Amplitude
No	location	Hz	H' (H/c)
5.3.1	3-D, short	no airfoil	
5.3.2	3-D, short, (1.83,0.2)	0	0
5.3.3	2-D, modified	no airfoil	
5.4.1	no airfoil	picture	picture
5.4.2	no airfoil	picture	picture
5.4.3	no airfoil	10	0.04
5.4.4	10, (1.83,0.2)	0	0
5.4.5	10, (1.83,0.6)	0	0
5.4.6	10, (1.83,0.9)	0	0
5.4.7	10, (1.83,1.3)	0	0
5.4.8	10, (1.83,0.2)	5	0.25
5.4.9	10, (1.83,0.2)	10	0.25
5.4.10	10, (1.83,0.2)	20	0.125
5.4.11	10, (1.83,0.9)	10	0.25
5.4.12	10, (1.83,0.9)	10	0.5
5.4.13	10, (1.83,2.5)	10	0.25
5.4.14	10, (1.83,2.5)	10	0.5
5.4.15	20, (1.83,0.2)	0	0
5.4.16	20, (1.83,0.2)	5	0.25
5.4.17	20, (1.83,0.2)	10	0.25
5.4.18	10, (1.83,0.6)	10	0.25
5.4.19	10, (1.83,1.3)	10	0.25
5.4.20(a)	x/c=1.83	0	0
5.4.20(b)	y/c=0.2,0.6,0.9,1.3	10	0.25
5.4.21(a)	x/c=2.5	0	0
5.4.21(b)	y/c=0.2,0.6,0.9,1.3	10	0.25
5.4.22(a)	x/c=4.0	0	0
5.4.22(b)	y/c=0.2,0.6,0.9,1.3	10	0.25
5.4.23(a)	x/c=2.5, y/c=0.9	10	0.125,0.25,0.5
5.4.23(b)	x/c=2.5, y/c=0.9	5,10,20	0.25
5.4.24	3-D, short, (1.83,0.2)	10	0.25
5.4.25	3-D, short, (1.83,0.2)	20	0.125
5.4.26	3-D, short, (1.83,0.2)	5	0.25

Table 4.3 LDV measurements of BSF

V. RESULTS

A. VISUALIZATION OF FLOW OVER FLAPPING AIRFOIL

Table 5.1 shows the range of parameters which were investigated in the dye flow visualizations of flow over a flapping airfoil.

Freq.(Hz)	Amp, H'	Chord (m)	U_o (m/s)	U_p (m/s)	U_e (m/s)	k_o	k_e	V_p
5.00	0.02	0.10	0.00	0.04	0.04	∞	70.71	1.41
5.00	0.04	0.10	0.00	0.09	0.09	∞	35.36	1.41
5.00	0.06	0.10	0.00	0.13	0.13	∞	23.57	1.41
5.00	0.08	0.10	0.00	0.18	0.18	∞	17.68	1.41
10.00	0.04	0.10	0.00	0.18	0.18	∞	35.36	1.41
2.50	0.04	0.10	0.00	0.04	0.04	∞	35.36	1.41
5.00	0.02	0.10	0.05	0.04	0.07	62.83	46.97	0.94
5.00	0.04	0.10	0.05	0.09	0.10	62.83	30.81	1.23
5.00	0.06	0.10	0.05	0.13	0.14	62.83	22.07	1.32
5.00	0.08	0.10	0.05	0.18	0.18	62.83	17.02	1.36
10.00	0.04	0.10	0.05	0.18	0.18	125.66	34.03	1.36
2.50	0.04	0.10	0.05	0.04	0.07	31.42	23.48	0.94
5.00	0.02	0.10	0.14	0.04	0.15	22.44	21.39	0.43
5.00	0.04	0.10	0.14	0.09	0.17	22.44	18.95	0.76
5.00	0.06	0.10	0.14	0.13	0.19	22.44	16.25	0.98
5.00	0.08	0.10	0.14	0.18	0.23	22.44	13.89	1.11
10.00	0.04	0.10	0.14	0.18	0.23	44.88	27.77	1.11
2.50	0.04	0.10	0.14	0.04	0.15	11.22	10.69	0.43

Table 5.1 List of Dye Flow Visualization

It was found by Dohring (1996) that the vortex wake behind a flapping airfoil is symmetric for values of the non-dimensional flapping velocity less than approximately one, but that it changes to an asymmetric wake as soon as the flapping velocity exceeds one. In the present experiments the free-stream velocity was set to zero or to very small values. This causes the product of the reduced frequency and the flapping velocity to be greater than one. Therefore, an asymmetric wake behavior was expected to occur. This is indeed the case as can be seen from the photos, shown in Figures 5.1.1 through 5.1.6 for the NACA0012 airfoil of 100 mm chord.

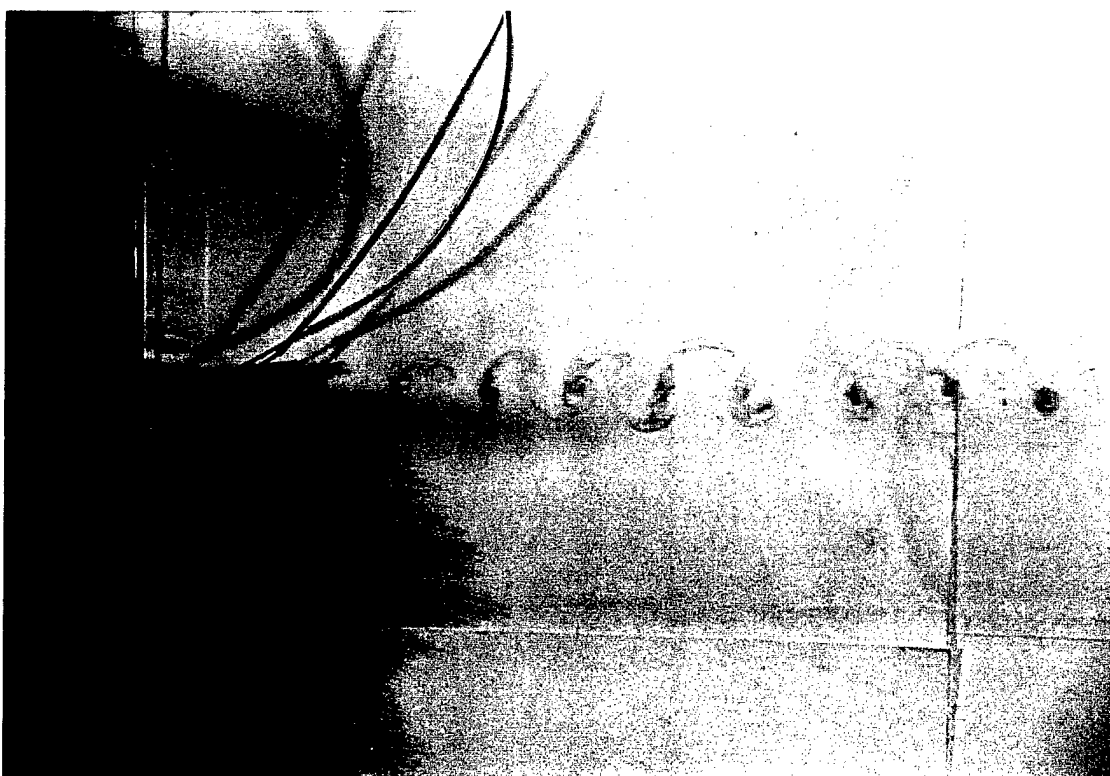


Figure 5.1.1 $U_0=0.14$ m/s, no flapping case.

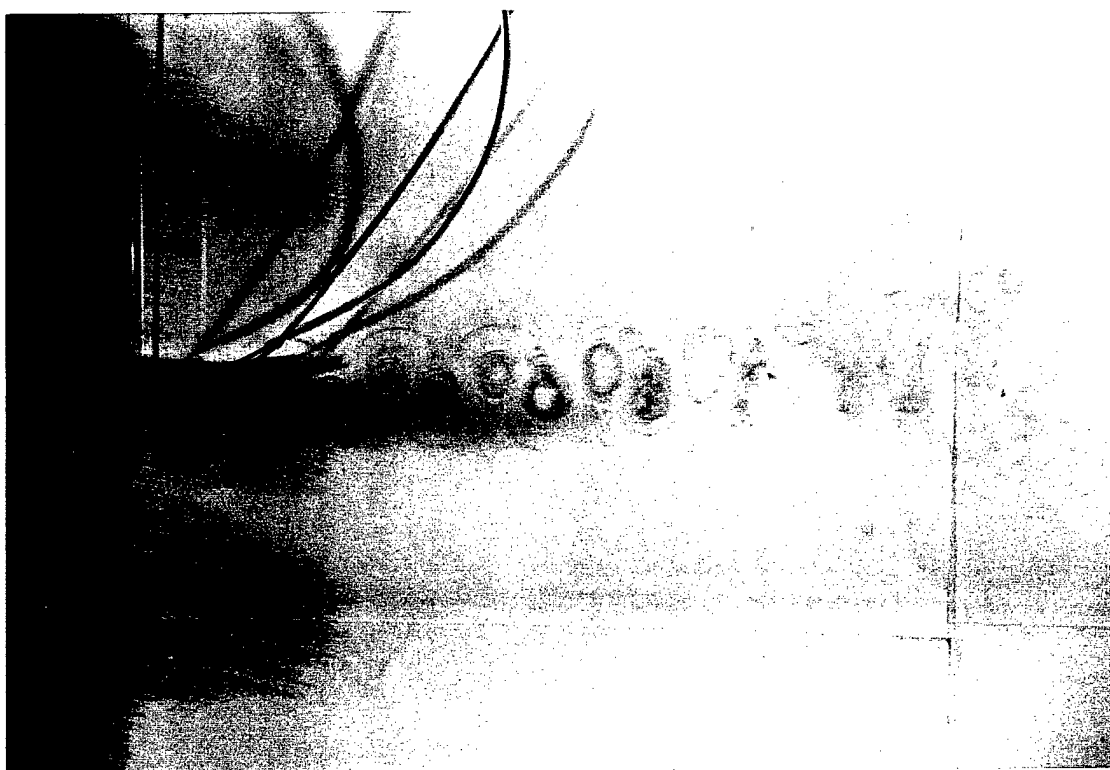


Figure 5.1.2 $U_0=0.14$ m/s, $f=5$ Hz, $H'=0.02$, $V_p=0.43$.

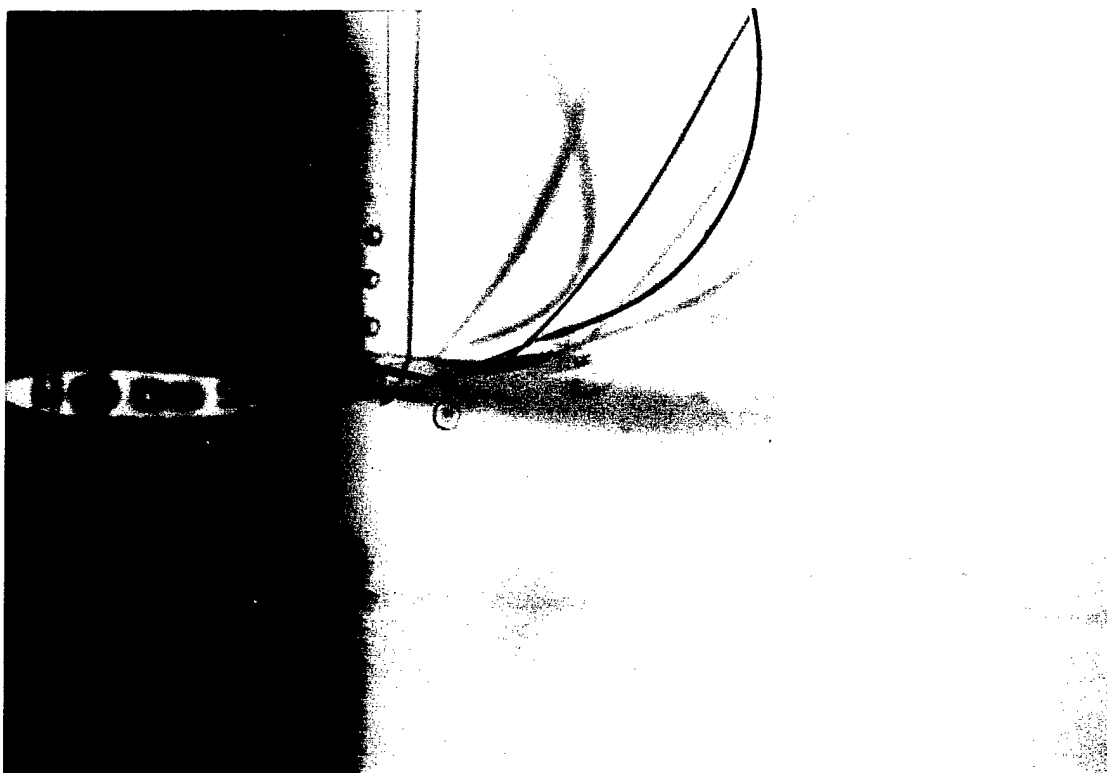


Figure 5.1.3 $U_0=0.14$ m/s, $f=5$ Hz, $H'=0.04$, $V_p=0.76$.

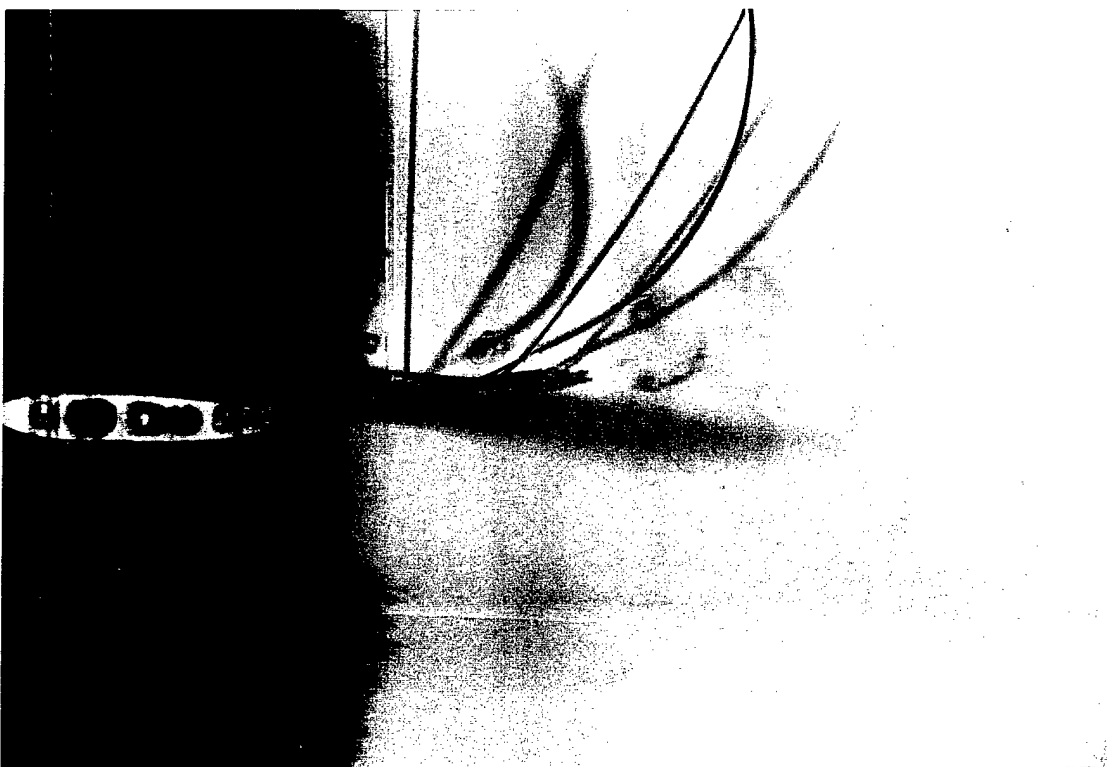


Figure 5.1.4 $U_0=0.14$ m/s, $f=5$ Hz, $H'=0.06$, $V_p=0.98$

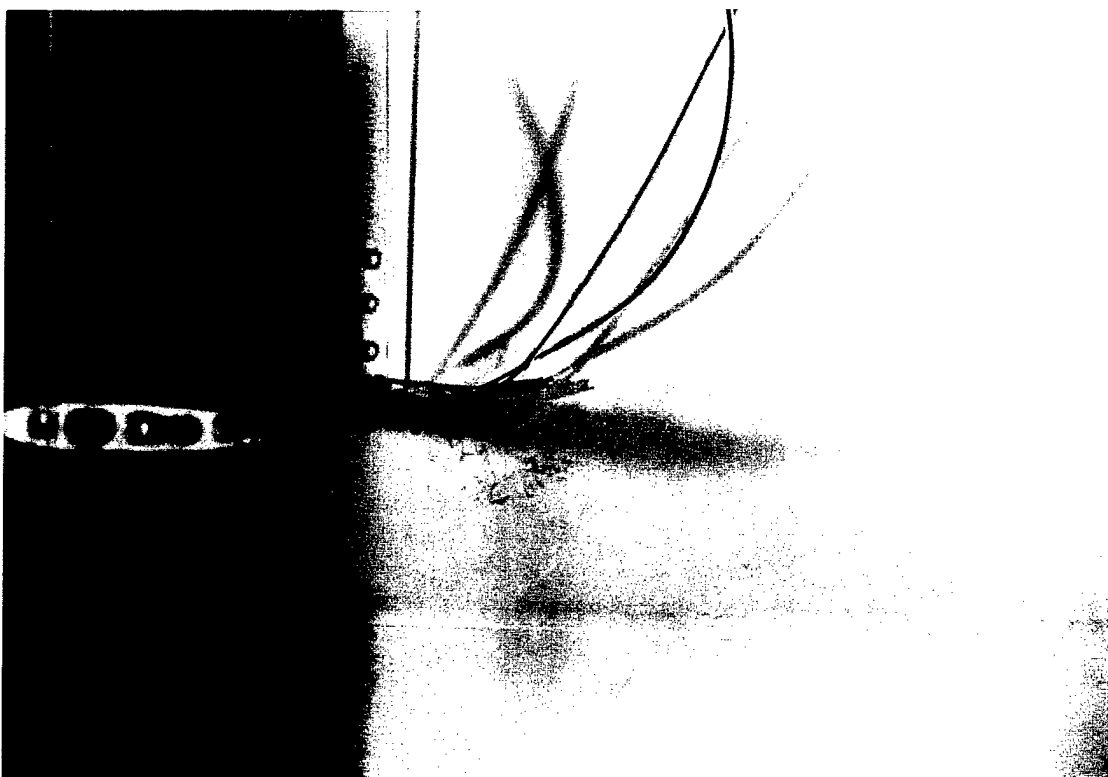


Figure 5.1.5 $U_0=0.05$ m/s, $f=5$ Hz, $H'=0.04$, $V_p=1.23$.

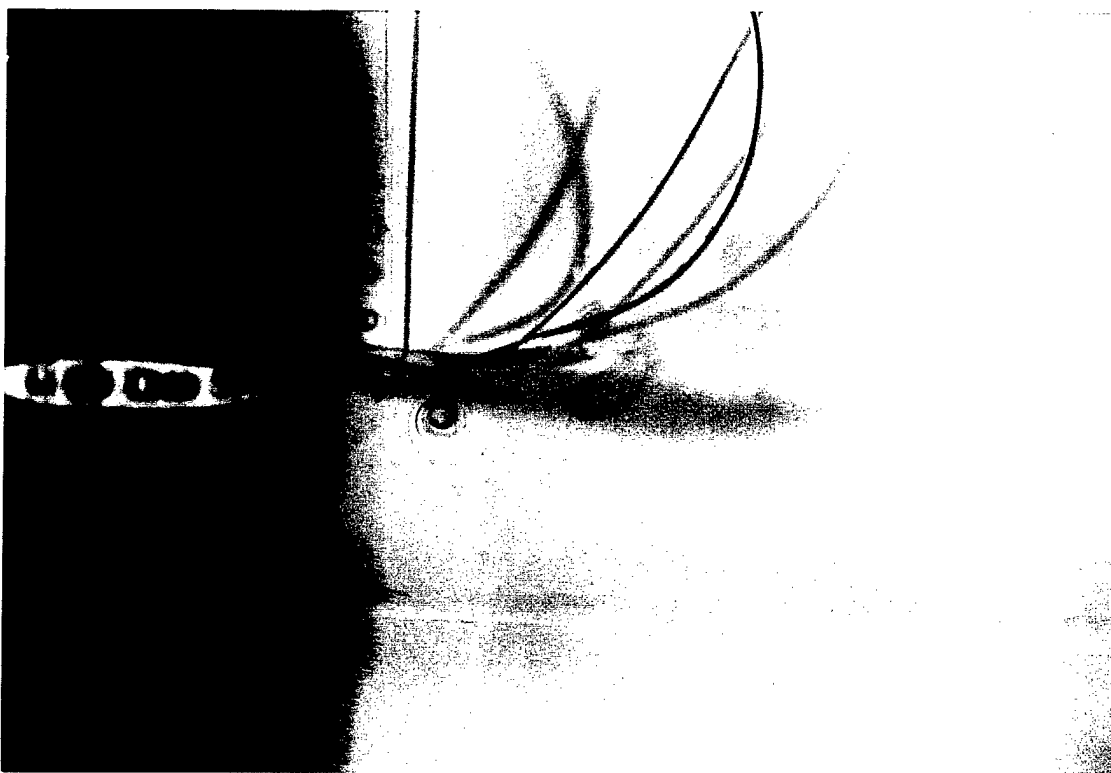


Figure 5.1.6 $U_0=0$ m/s, $f=5$ Hz, $H'=0.06$, $V_p=1.41$.

B. LDV MEASUREMENT OF FLOW OVER FLAPPING AIRFOIL

Figures 5.2.1 through 5.2.9 present LDV measurements of the velocity distributions induced by a flapping airfoil. The measurements were taken at two streamwise locations, 15% of chord upstream of the leading edge and 41% of chord downstream of the trailing edge. It is seen that airfoil flapping induces a flow in the downstream direction which increases with increasing frequency and amplitude of oscillation. Note that the velocities are made non-dimensional with the plunge velocity U_p rather than with the free stream velocity U_o so that the special case of zero free-stream velocity could be included. Therefore, also note that airfoil flapping at zero free-stream velocity still induces a flow in the downstream direction. Also, it is seen that the velocity profiles at three different free stream speeds are quite similar as shown in Figures 5.2.7, 5.2.8 and 5.2.9, respectively, for three different frequencies $f=2.5, 5, 10$ Hz but constant amplitude at $H'=0.04$, where $H'=H/c$.

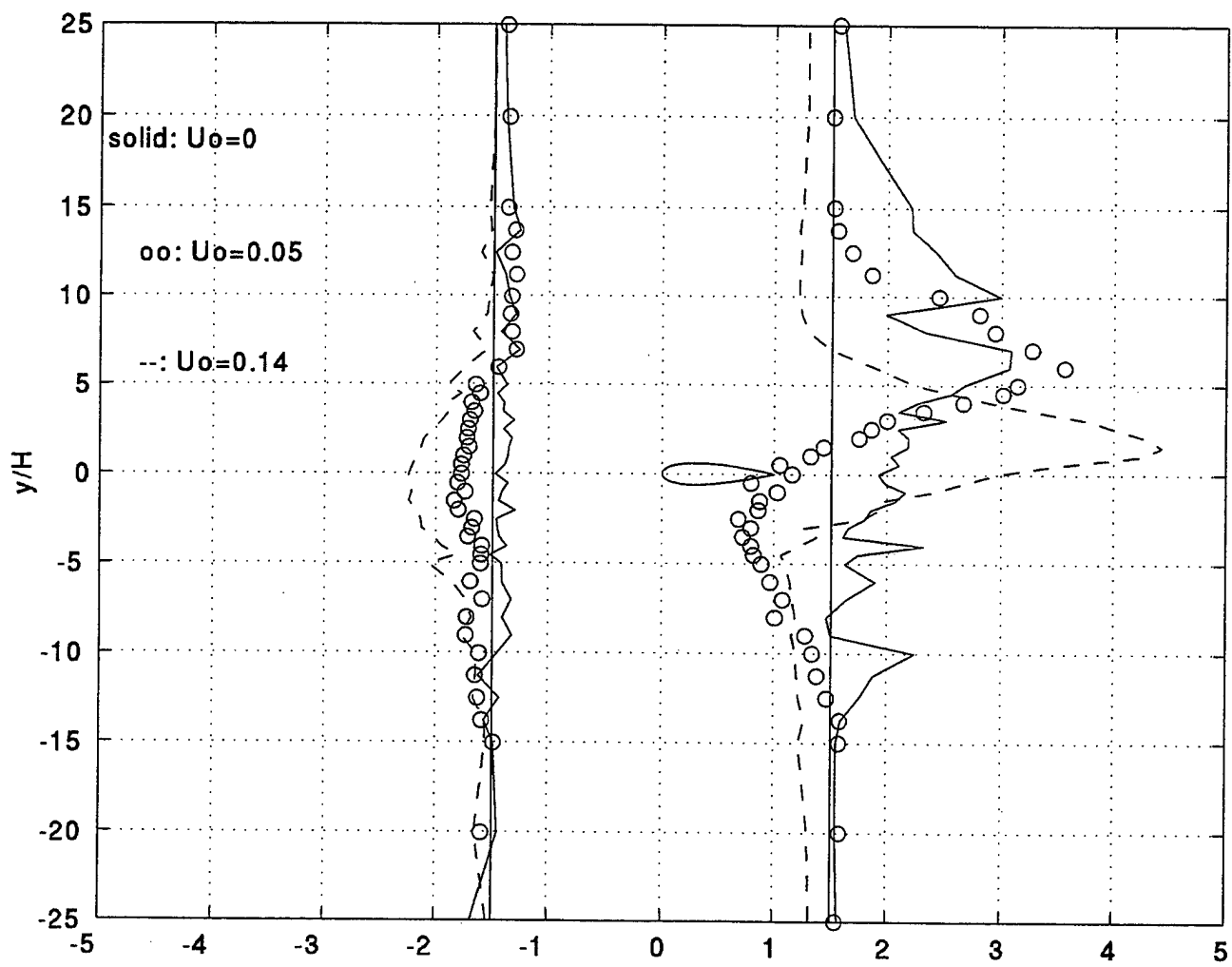


Figure 5.2.1 $(U-U_0)/U_p$, $f = 5$ Hz, $h = 0.02$

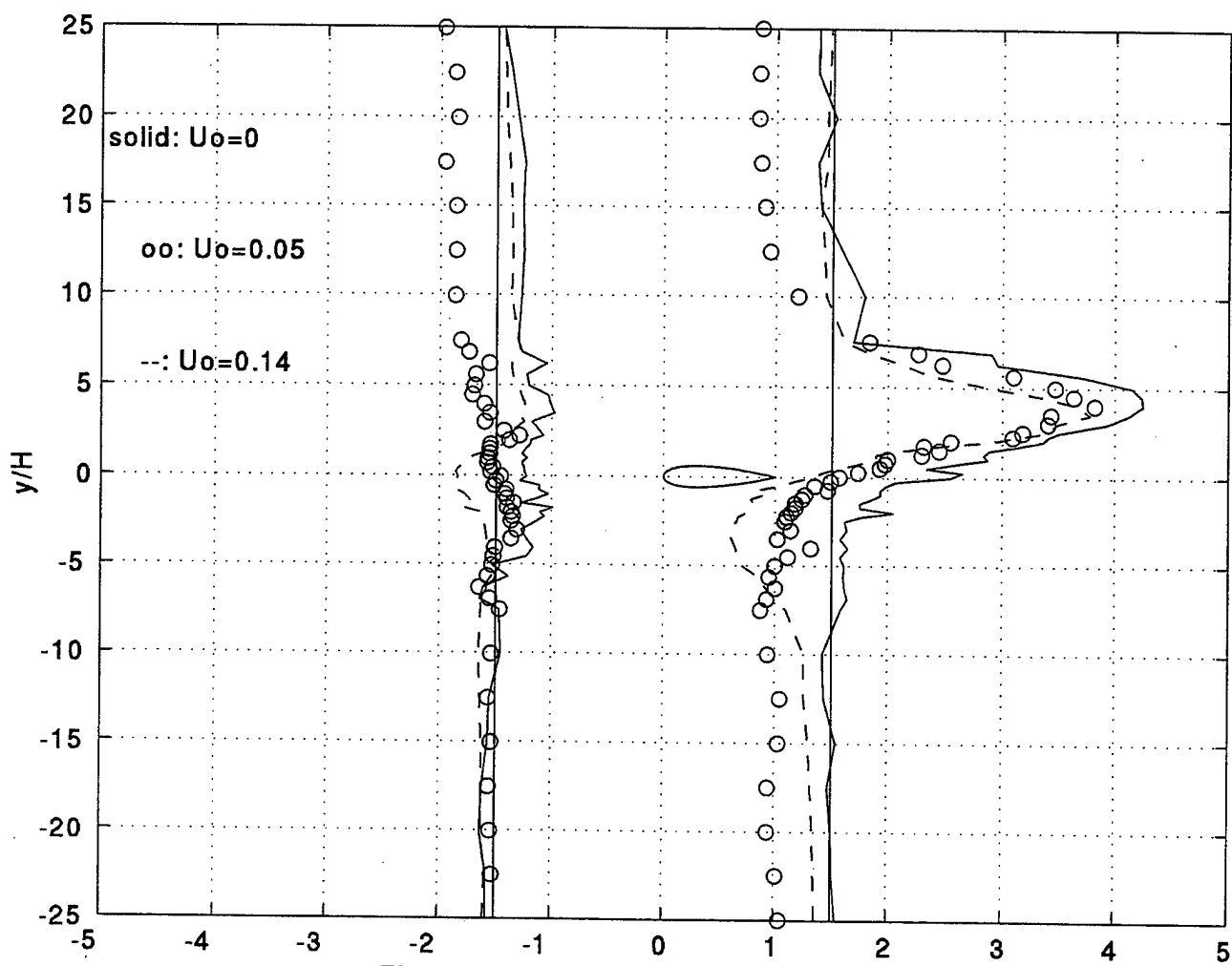


Figure 5.2.2 $(U-U_0)/U_p$, $f = 5$ Hz, $h = 0.04$

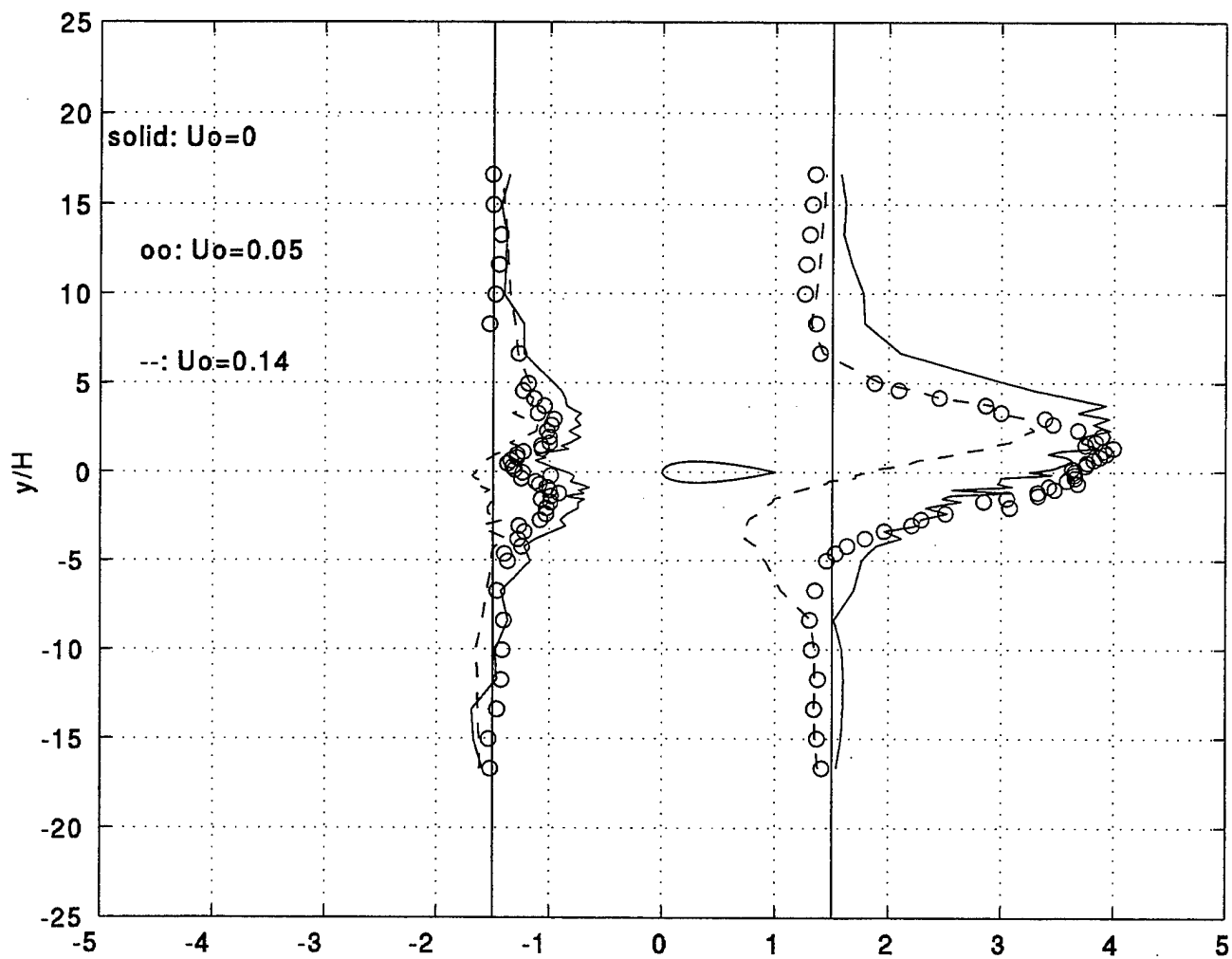


Figure 5.2.3 $(U-U_0)/U_p$, $f = 5$ Hz, $h = 0.06$

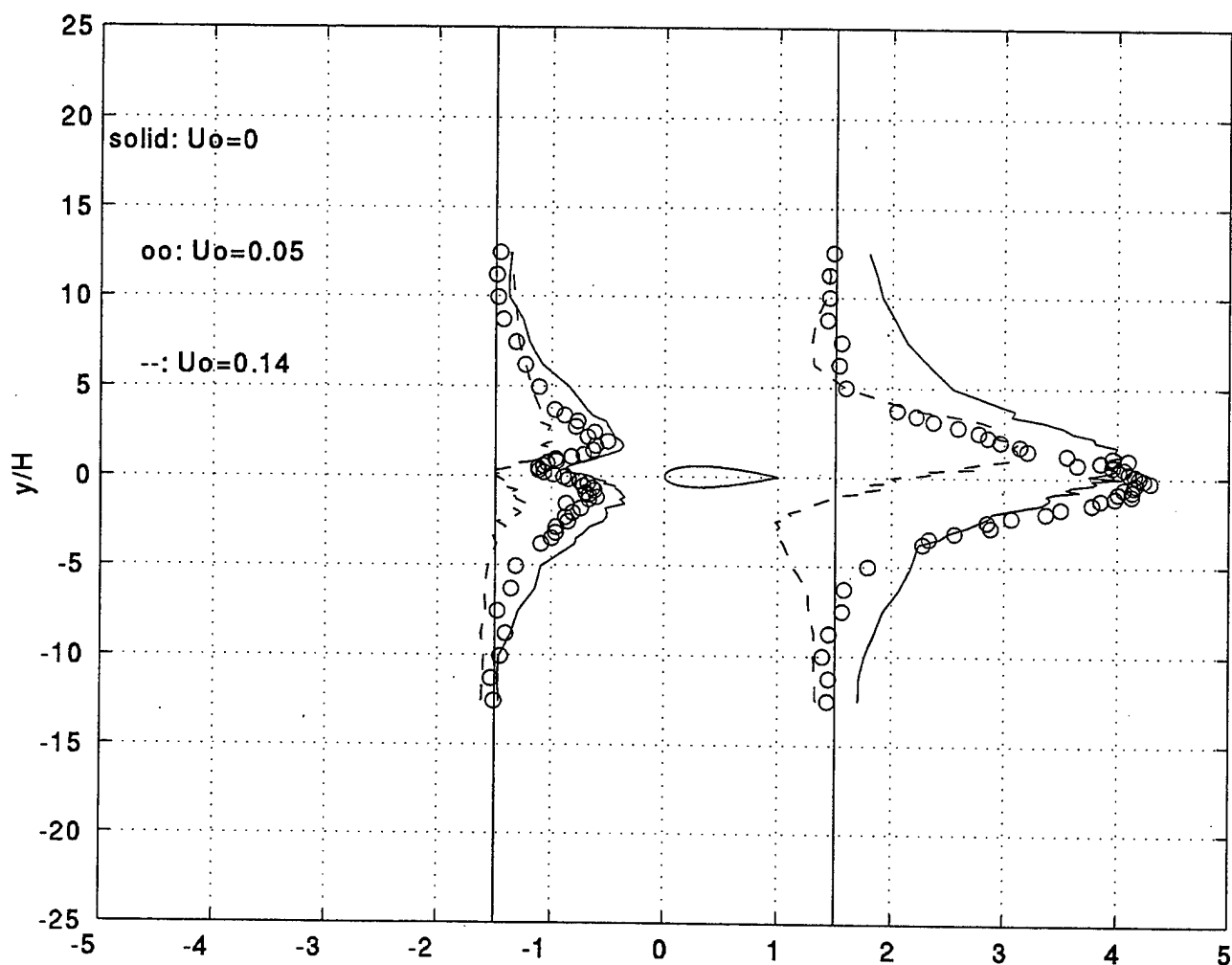


Figure 5.2.4 $(U-U_o)/U_p$, $f = 5$ Hz, $h = 0.08$

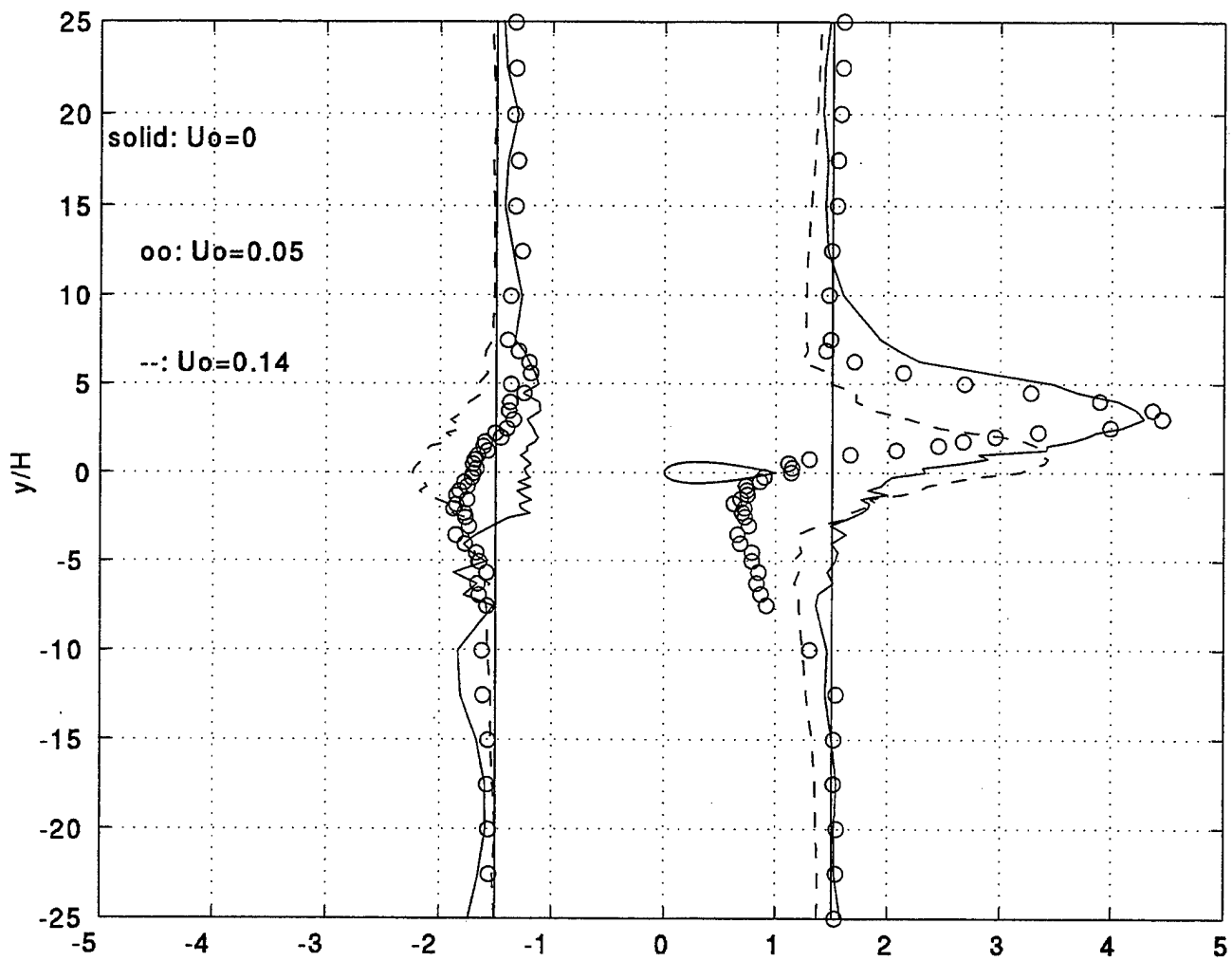


Figure 5.2.5 $(U-U_0)/U_p$, $f = 2.5$ Hz, $h = 0.04$

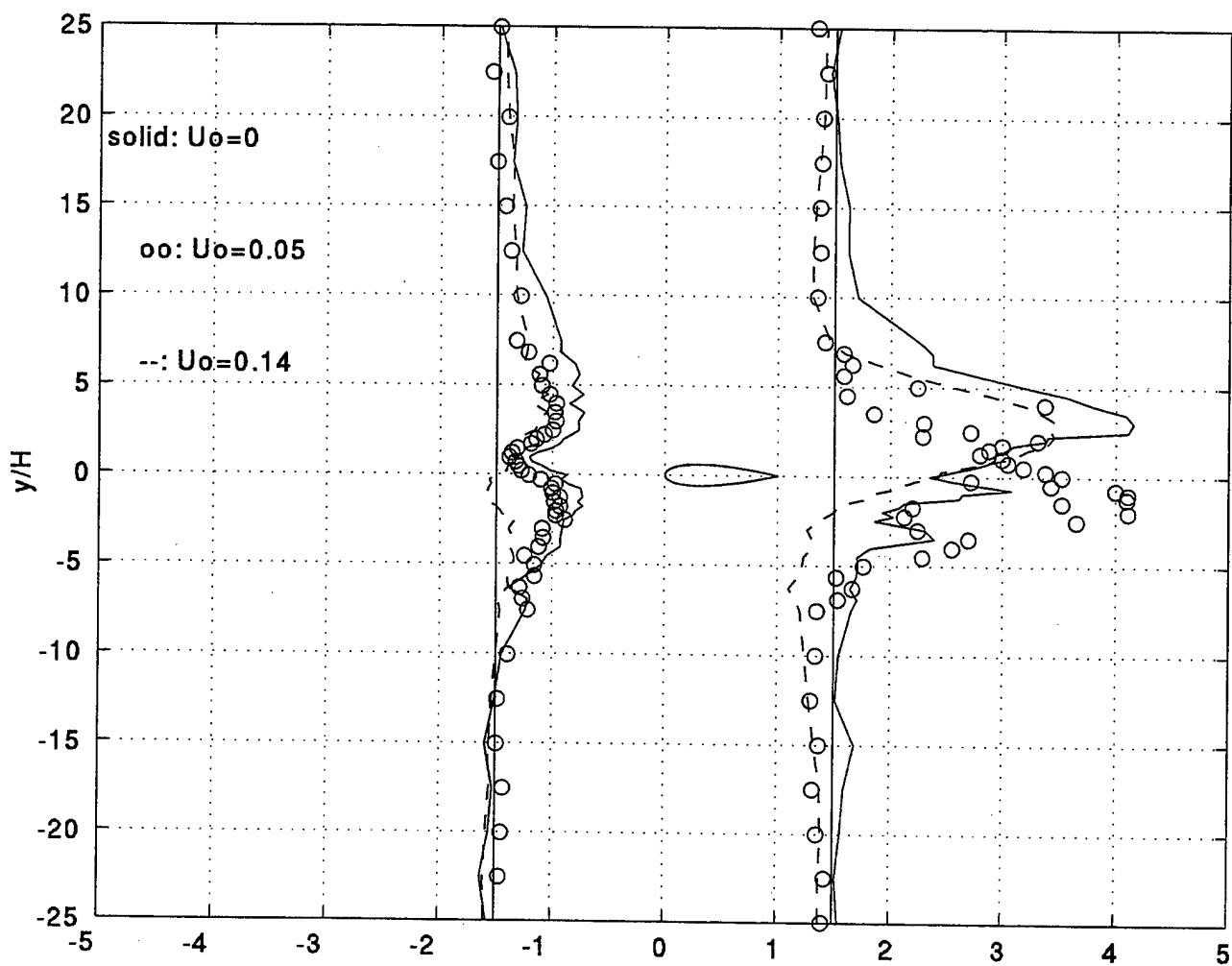


Figure 5.2.6 $(U-U_0)/U_p$, $f = 10$ Hz, $h = 0.04$

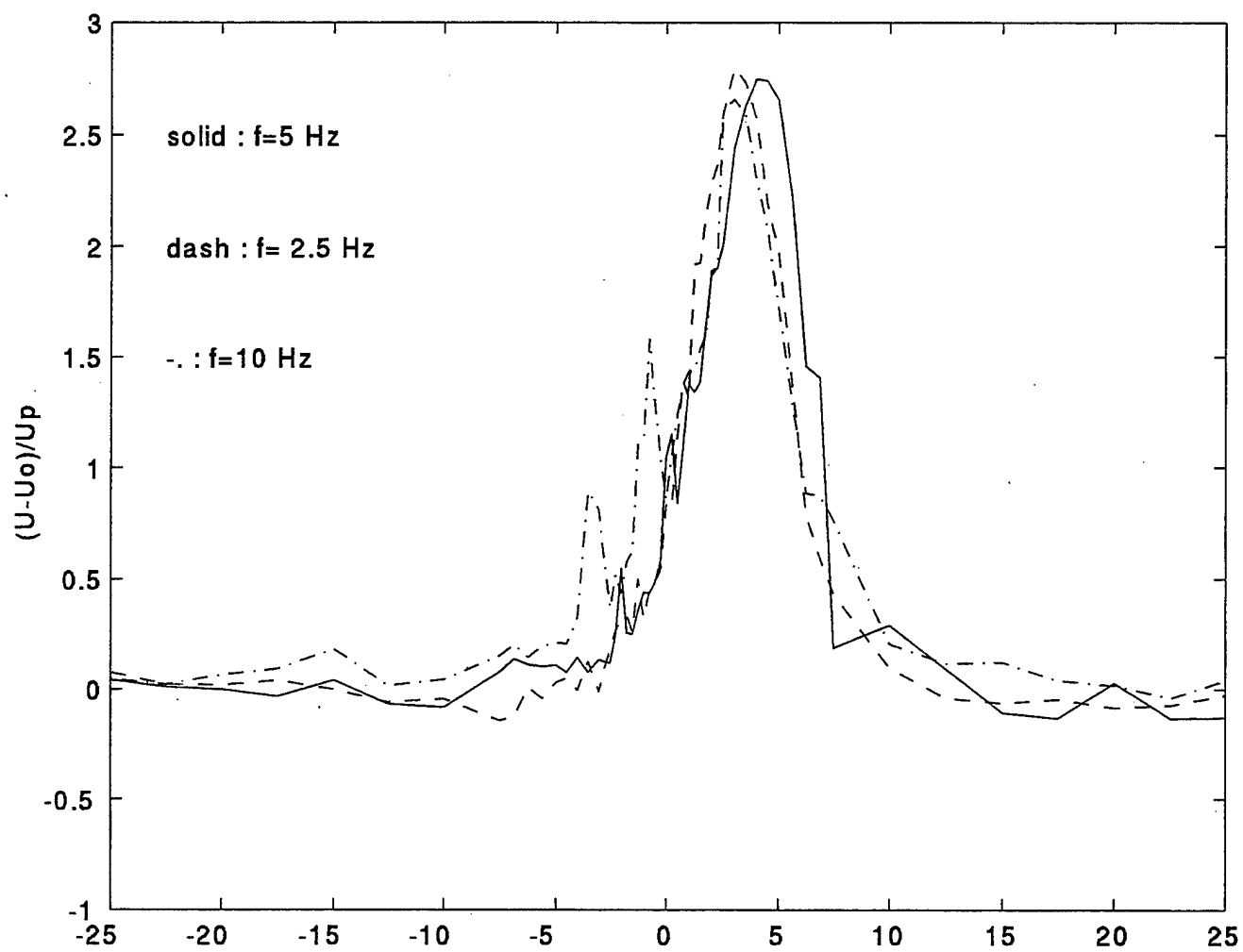
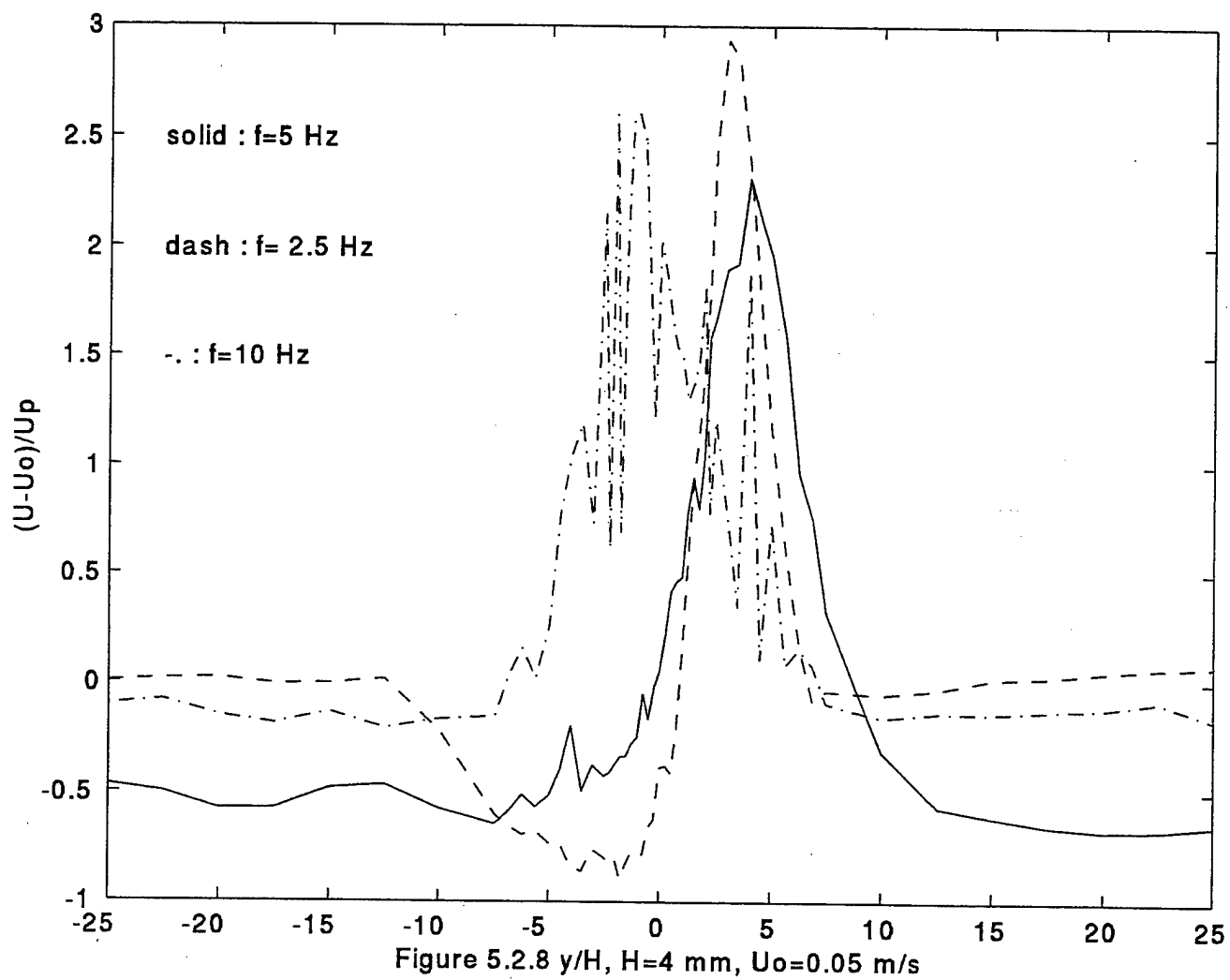
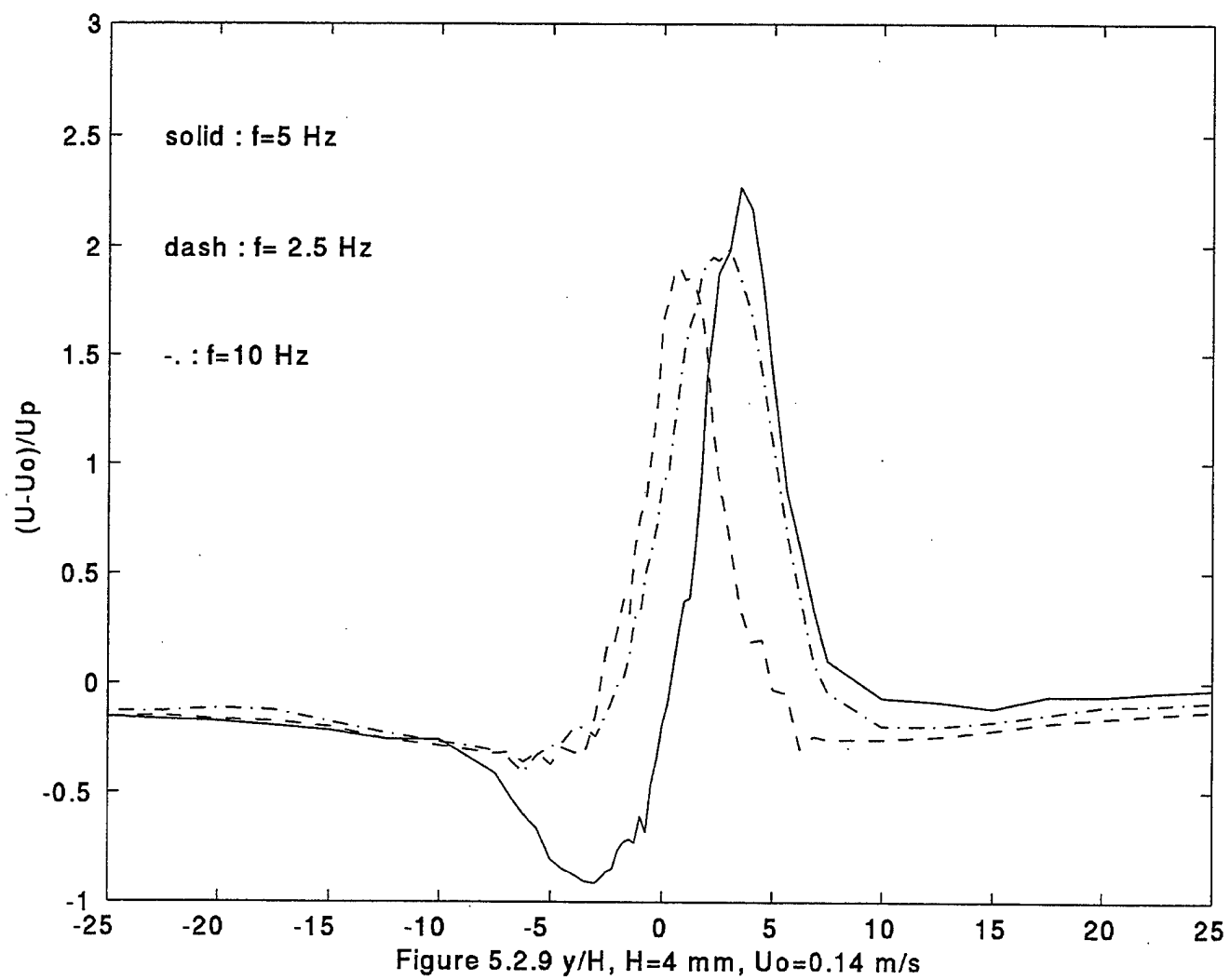


Figure 5.2.7 y/H , $H=4$ mm, $U_0=0$ m/s





C. BACKWARD-FACING STEP FLOW

The investigation of the backward-facing step flow was also conducted in the water tunnel facility, described in section III.A, using the model described in section III.D. Figure 3.2 shows the set-up of the backward-facing step. Note the distances H_o and H_i . The free surface is 272 mm (H_o) and 242 mm (H_i) above the plate and the step respectively, thus giving an expansion ratio of 1.12. The free stream velocity was 0.33m/s, giving a Reynolds number Re_h based on the step height of 10,000. At first, a short plate with a blunt leading edge was installed upstream of the step. Figure 5.3.1(a) shows that the spanwise variation of the mean streamwise velocity at $y/h=2$ and at the edge of the step is about 40% variation. This indicates that the flow at separation is strongly three-dimensional due to the short plate length and due to the blunt leading edge. The mean streamwise velocity profiles at the edge of the step in Figure 5.3.1(b) for $z/h=-1.33, 0$ and 1.33 document the conditions of three-dimensionality for this set-up. Figure 5.3.2 displays profiles of mean streamwise velocity and turbulence intensity and contours of mean non-dimensional streamlines. It can be seen that the recirculation zone which is indicated by a negative mean streamwise velocity is much smaller than that expected from a two-dimensional upstream flow condition. By integrating the mean streamwise velocity profiles, contours of normalized streamline are obtained and displayed in Figure 5.3.2(c). The reattachment length is estimated to be about three step heights which is substantially smaller than the range of 4.9 through 8.2 step heights given by Eaton and Johnston (1981) for two-dimensional backward-facing step flow. This substantial reduction in reattachment length due to three-dimensionality in upstream condition has not been fully documented in the literature. By $x/h=3.5$ which is downstream of the reattachment zone, the mean streamwise velocity profiles for $z/h=-1.33, 0, 1.33$ at $x/h=3.5$ indicate that the flow is still three-dimensional.

In order to achieve two-dimensional flow upstream of the separation point, the plate upstream of the step was extended and the leading edge was modified to be sharp as shown in Figure 3.2. As shown in Figure 5.3.3(a), the variation of mean streamwise velocity at the edge of the step and $y/h=2$ over the central $4h$ (120 mm) is less than 5%,

thus indicating two-dimensionality. The mean streamwise velocity profiles at the separation edge for $z/h = -1.33, 0, 1.33$ in Figure 5.3.3(b) show that they agree with each other within 5% and follow the $1/7$ power law, thus indicating that the separating shear layer is fully turbulent at the edge. The mean streamwise velocities and turbulence intensity profiles and mean normalized streamlines are displayed on Figure 5.4.3. The reattachment length is 5.2 step heights, slightly different from the published reattachment length of 6.0 for most two dimensional BSF studies. It compares well with the value of 4.9 step heights determined by Etheridge and Kemp (1978) using LDV under similar conditions in a water tunnel with a free surface. A corner eddy is also visible within one step height which is due to the secondary separation and has been observed by Abbot and Kline (1962) and Kasagi and Matsunaga (1995). By six step heights which is downstream of the reattachment zone, the mean streamwise velocity profiles for $z/h = -1.33, 0, 1.33$ in Figure 5.3.4 indicate that the flow is still two-dimensional, which is to be expected because the aspect ratio of the flow apparatus is 12.33, larger than the value of 10 which de Brederode and Bradshaw (1981) recommended to ensure two-dimensionality for the reattaching flow.

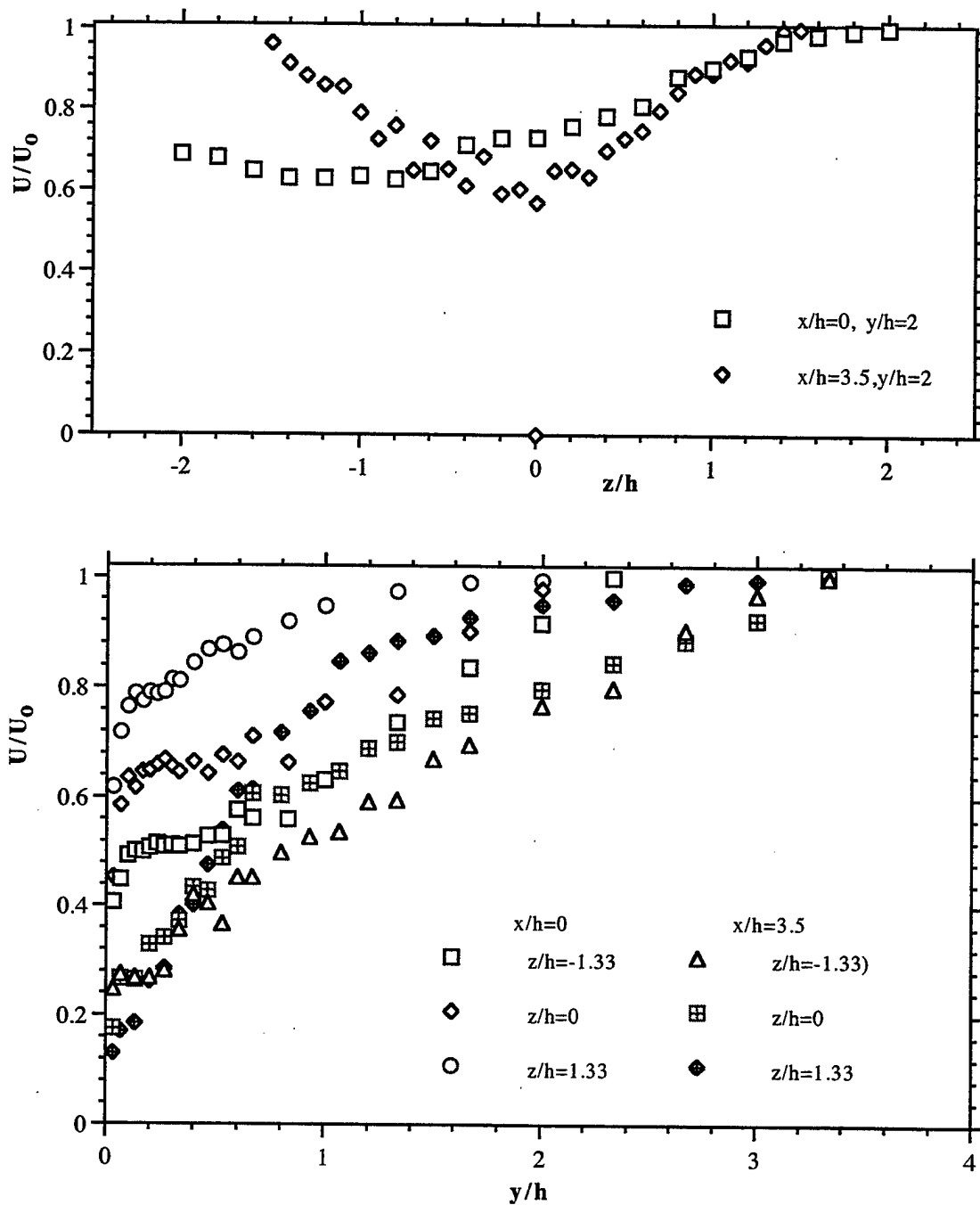


Figure 5.3.1 Three dimensionality of the short blunt plate.
(a) Spanwise traverse, (b) Vertical traverses.

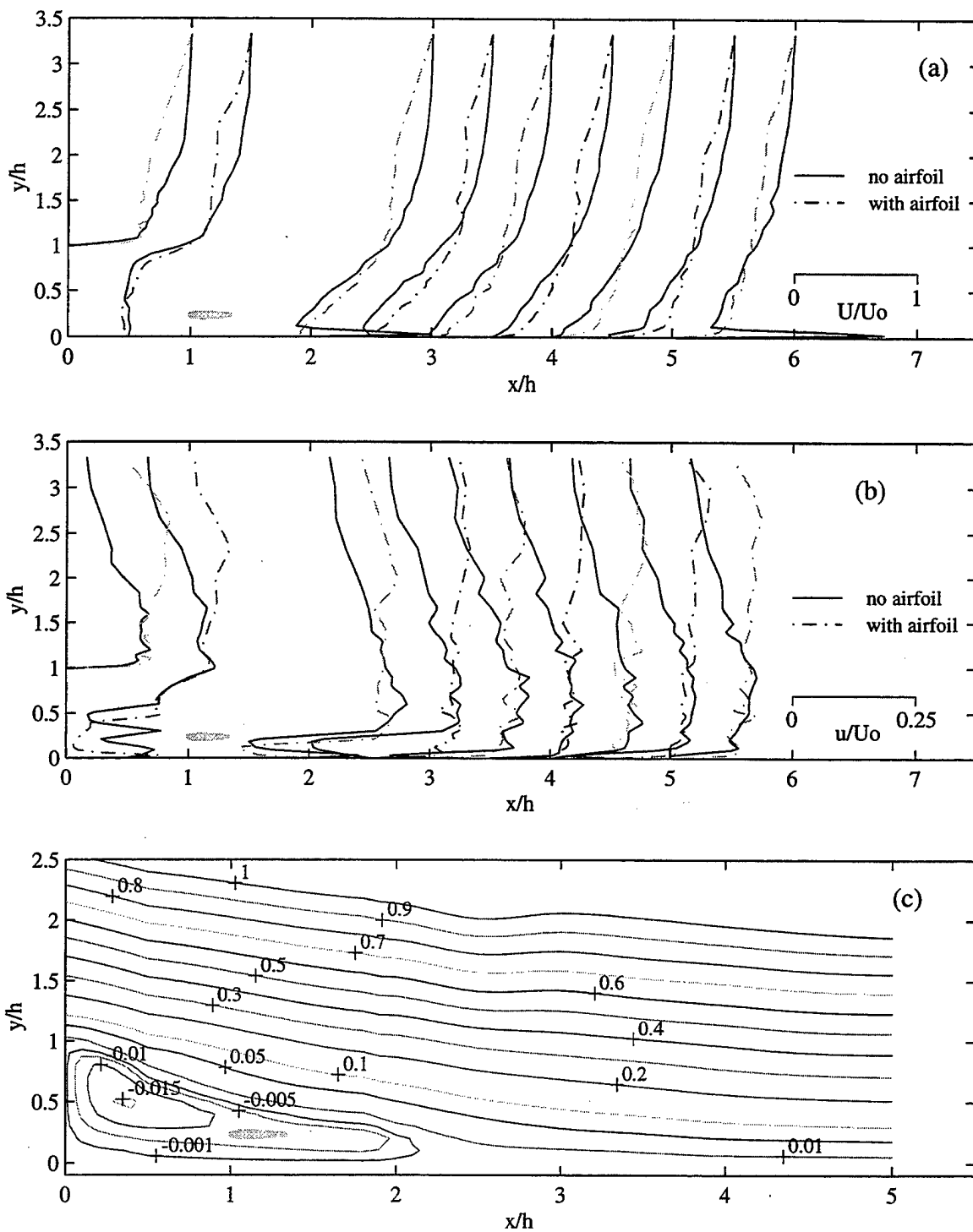


Figure 5.3.2 (a) velocity, (b) turbulence intensity, (c) streamlines of the backward-facing step. 10mm airfoil at $(1.83h, 0.2h)$, stationary. short blunt leading edge upstream plate

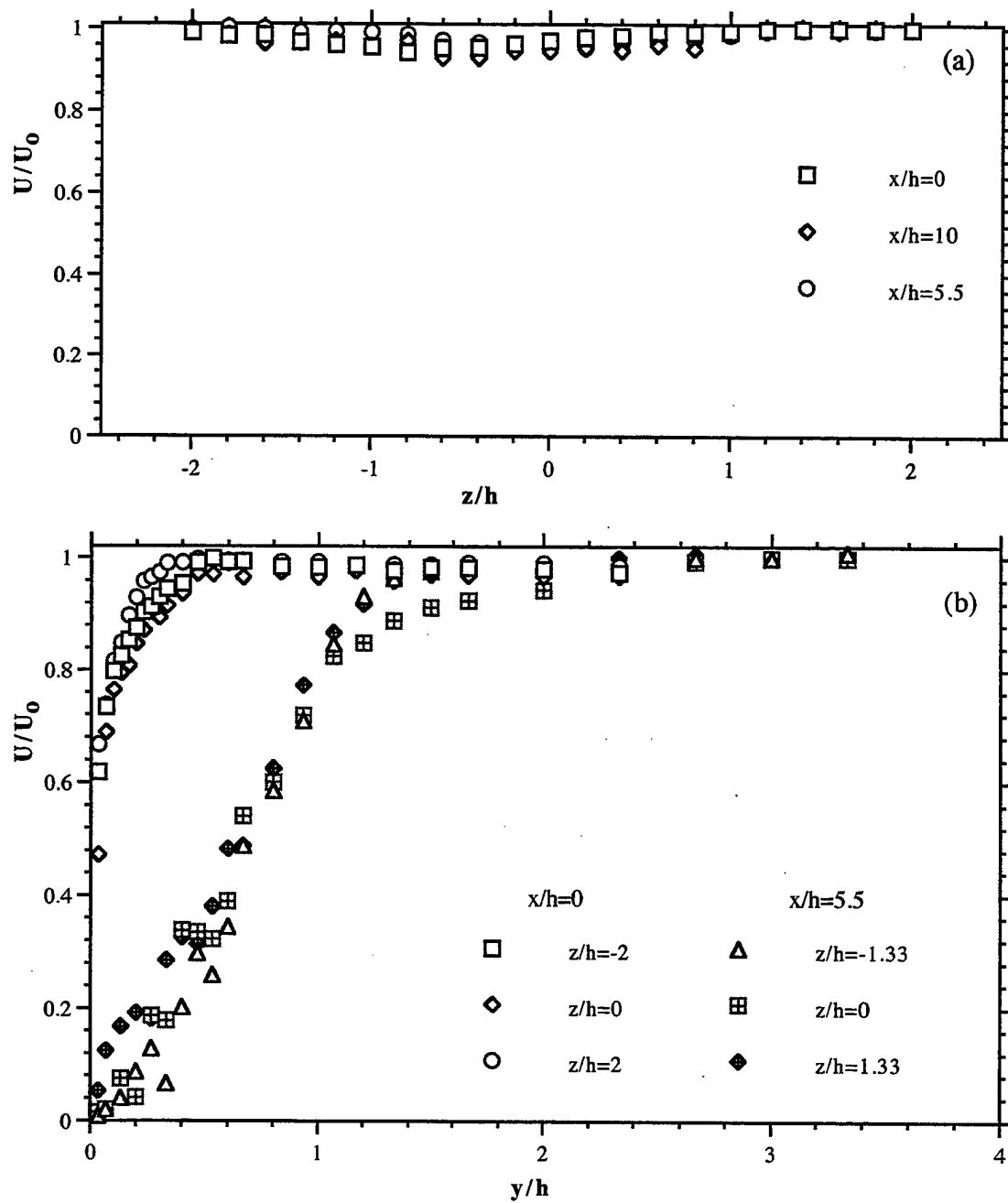


Figure 5.3.3 Two dimensionality of the modified sharp leading edge plate.
(a) Spanwise traverse, (b) Vertical traverses.

D. CONTROL OF BACKWARD-FACING STEP FLOW WITH A FLAPPING AIRFOIL

1. Flow Visualization

Before detailed LDV measurements were made, flow visualization using dye injection at $x/h=3.5, 4.5, 5.5$ and 7 was conducted for various locations of a 10 mm NACA0012 airfoil and various frequencies and amplitudes of oscillation. Three different frequencies were used, namely, 5 Hz, 10 Hz and 20 Hz with an amplitude of either $0.25c$ or $0.125c$. Table 5.2 summarizes the effect of airfoil location and oscillation on the flow near the dye injection holes. It is quite clear from Table 5.2 that for a given frequency and amplitude, it is more effective to locate the airfoil closer to the wall and the step. In order to quantify this observation, LDV measurements of mean streamwise velocity were made at $y/h=0.066$ for various locations and oscillations of the airfoil. As an example, the effect of oscillating a small airfoil in plunge on the reattachment length can be seen from Figure 5.4.1. In Figure 5.4.1(a) for a stationary airfoil located at $(1.833h, 0.2h)$, the dyes injected at $x/h=3.5$ and 4.5 were seen to be moving upstream towards the step; when the airfoil was oscillated in plunge at 10 Hz with an amplitude of $0.25c$ in Figure 5.4.1(b), these dyes could be seen to be moving downstream (indicating forward flow). As shown in Figure 5.4.2, for a given location of the airfoil, reattachment length reduces as the frequency and amplitude of oscillation increase.

2. LDV Measurements

Based on the flow visualization studies and the preliminary LDV traverses, the following locations of the airfoil, $(1.83h, 0.2h)$, $(1.83h, 0.6h)$, $(1.83h, 0.9h)$, $(1.83h, 1.3h)$, $(2.5h, 0.9h)$ and $(2.5h, 1.3h)$, were chosen for detailed LDV measurements of mean streamwise velocity and turbulence intensity distributions. The streamwise position of $1.83h$ was chosen so that it was close enough to the step and still allowed a few transverse traverses to be made upstream of the airfoil. The streamwise position of $2.5h$ was chosen because it was about half the reattachment length. Vertical position of $0.2h$ was chosen so that it was the closest location near the wall that allowed a sufficiently large amplitude of plunge to be executed. The location of $(1.83h, 0.6h)$ is approximately the center of the

recirculation flow region, $y=0.9h$ is within the separated shear layer while $y=1.3h$ is outside the separated shear layer. Results of 0 Hz and 10 Hz were reported for all locations of the airfoil. For some locations and frequencies of 5 Hz and 20 Hz, a larger airfoil (20 mm NACA0015) was also used. Generally, the amplitude of plunge was 0.25c but 0.125c and 0.5c was also used for some cases. Table 5.2 lists the conditions for all the test cases. Figure 5.4.3 shows the mean streamwise velocity and turbulence intensity profiles and the mean normalized streamlines of the backward-facing step without an airfoil.

x/h	f(Hz)/h(Volt)	ended time	at $y=7.2\text{mm}$
1	0/0	0:37	reversed flow
1	5/2	0:51	No effect
1	10/2	1:13	9 & 11 holes forward
1	20/1	1:55	9 & 11 holes forward
1.5	0/0	2:14	reversed flow
1.5	0/0	2:30	reversed flow
1.5	5/2	2:48	reversed flow
1.5	10/2	3:10	9 reversed & 11 forward
1.5	20/1	3:53	9 reversed & 11 forward
2.5	0/0	4:38	reversed flow
2.5	5/2	4:53	No effect
2.5	10/2	5:40	9 & 11 holes forward
2.5	20/1	6:23	9 & 11 holes forward
3.5	0/0	6:59	reversed flow
3.5	5/2	7:22	No effect
3.5	10/2	7:43	9 & 11 holes forward
3.5	20/1	8:06	9 & 11 holes forward

x/h	f(Hz)/h(Volt)	ended time	at $y=14\text{mm}$
3.5	5/2	8:34	No effect
3.5	10/2	8:53	reversed flow
3.5	20/1	9:13	reversed flow
2.5	0/0	9:26	reversed flow
2.5	5/2	9:53	worse than 0 Hz
2.5	10/2	10:19	better than 0 Hz
2.5	20/1	10:40	worse than 0 Hz
1.5	0/0	10:55	reversed flow
1.5	0/0	11:18	reversed flow
1.5	5/2	11:48	slightly better
1.5	10/2	12:18	good
1	0/0	12:30	reversed flow
1	5/2	12:45	No effect
1	10/2	13:07	better
1	20/1	13:28	9 & 11 holes forward

x/h	f(Hz)/h(Volt)	ended time	at y = 20mm
1	0/0	13:36	reversed flow
1	5/2	13:48	reversed flow
1	10/2	14:12	9 & 11 holes forward
1	20/1	14:28	9 & 11 holes forward
1.5	0/0	14:36	reversed flow
1.5	5/2	14:48	reversed flow
1.5	10/2	15:02	reversed flow
1.5	20/1	15:19	reversed flow
2.5	0/0	15:39	reversed flow
2.5	5/2	15:56	reversed flow
2.5	10/2	16:20	reversed flow
2.5	20/1	16:36	reversed flow
3.5	0/0	16:52	reversed flow
3.5	5/2	17:02	reversed flow
3.5	10/2	17:11	reversed flow
3.5	20/1	17:33	reversed flow

Table 5.2(a) Dye injection visualization of BSF using a blunt leading upstream plate.

y=0.2h			dye injection at, x/h				6/26/96
x/h	f/Volt	End time	3.5	4.5	5.5	7	Comments
No airfoil	0, 0	18:15					-1 means 100% backward
1	0	18:29	-1	-1	0	1	1 is 100% forward
1	5, 2	18:42	-1	-1	0		start from 18:00
1	10, 2	18:54	-1	1	1		$X_R=3.5-4.5$
1	20, 1	19:08	1	1	1		$X_R<3.5$
2.5	0	19:22	-1	-1	0		$X_R=5.2$
2.5	5, 2	19:32	-1	-1	0		$X_R=5.2$
2.5	10, 2	19:45	0	1	1		$X_R=3.5$
2.5	20, 1	19:55	1	1	1		$X_R<3.5$
4	0	20:05	-1	-1	0		$X_R=5.2$
4	5, 2	20:15	-1	-1	0		$X_R=5.2$
4	10, 2	20:25	-1	-1	1		$X_R=4.5-5.5$
4	20, 1	20:40	-1	-1	1		$X_R=4.5-5.5$
6	0	20:50		-1	0	1	$X_R=5.2$
6	5, 2	21:00		-1	0	1	$X_R=4.5-5.5$
6	10, 2	21:10		0	1	1	$X_R=5.2$
6	20, 1	21:20		-1	0	1	$X_R=5.2$
y=0.5h			dye injection at, x/h				
x/h	f/Volt	End time	3.5	4.5	5.5	7	
6	0	21:30		-1	0	1	$X_R=5.2$
6	5, 2	21:40		-1	0	1	$X_R=5.2$
6	10, 2	21:50		-1	0	1	$X_R=5.2$
6	20, 1	22:00		-1	0	1	$X_R=5.2$
4	0	22:10	-1	-1	0		$X_R=5.2$
4	5, 2	22:20	-1	-1	0		$X_R=5.2$
4	10, 2	22:30	-1	-1	0		$X_R=5.2$
4	20, 1	22:40	-1	-1	0		$X_R=5.2$
2.5	0	22:50	-1	-1	0		$X_R=5.2$
2.5	5, 2	23:00	-1	-1	1		$X_R=4.5-5.5$
2.5	10, 2	23:12	0	0.2	1		$X_R=3.5-4.5$
2.5	20, 1	23:23	-1	1	1		$X_R=3.5-4.5$
1	0	23:32	-1	-1	0		$X_R=5.2$
1	5, 2	23:41	-1	0.2	1		$X_R=3.5-4.5$
1	10, 2	23:50	-1	0.2	1		$X_R=3.5-4.5$
1	20, 1	24:00	1	1	1		$X_R<3.5$

y=0.9h			dye injection at, x/h				
x/h	f/Volt	End time	3.5	4.5	5.5	7	
1	0	24:10	-1	-1	0		$X_R=5.2$
1	5, 2	24:22	-1	0.2	1		$X_R=3.5-4.5$
1	10, 2	24:30	-1	0	1		$X_R=4.5$
1	20, 1	24:40	0	1	1		$X_R<4.5$
2.5	0	24:50	1	1	1		$X_R<3.5$
2.5	5, 2	25:00	-1	0	0		$X_R=3.5-4.5$
2.5	10, 2	25:10	-1	-1	0		$X_R=5.2$
2.5	20, 1	25:20	-1	-1	-0.2		$X_R=5.2$
4	0	25:30	-1	0	1		$X_R=3.5-4.5$
4	5, 2	25:43	-1	0	1		$X_R=3.5-4.5$
4	10, 2	25:52	-1	0	1		$X_R=3.5-4.5$
4	20, 1	26:00	-1	0	1		$X_R=3.5-4.5$
6	0	26:10		-1	0	1	$X_R=5.2$
6	5, 2	26:20		-1	0	1	$X_R=5.2$
6	10, 2	26:30		-1	0.2	1	$X_R=5.2$
6	20, 1	26:43		-1	-0.2	1	$X_R=5.2$
y=1.3h			dye injection at, x/h				
x/h	f/Volt	End time	3.5	4.5	5.5	7	
6	0	26:50		-1	0	1	$X_R=5.2$
6	5, 2	27:00		-1	0	1	$X_R=5.2$
6	10, 2	27:19		-1	0.2	1	$X_R=5.2$
6	20, 1	27:30		-1	0	1	$X_R=5.2$
4	0	27:40	-1	-0.2	0		$X_R=4.5-5.5$
4	5, 2	27:50	-1	-0.2	0.2		$X_R=4.5-5.5$
4	10, 2	28:00	-1	-0.2	0.2		$X_R=4.5-5.5$
4	20, 1	28:10	-1	-0.2	0.2		$X_R=4.5-5.5$
2.5	0	28:20	-1	-0.2	1		$X_R=4.5-5.5$
2.5	5, 2	28:30	-1	-0.2	1		$X_R=4.5-5.5$
2.5	10, 2	28:40	-1	-0.2	1		$X_R=4.5-5.5$
2.5	20, 1	28:50	-1	-0.2	1		$X_R=4.5-5.5$
1	0	29:00	-1	-0.2	1		$X_R=4.5-5.5$
1	5, 2	29:10	-1	0	1		$X_R=4.0-5.0$
1	10, 2	29:20	0	0.2	1		$X_R=3.5-4.5$
1	20, 1	29:40	-1	1	1		$X_R=3.5-4.5$
y=-0.3h			dye injection at, x/h				
x/h	f/Volt	End time	3.5	4.5	5.5	7	
-0.33	0	29:00	-1	-0.2	1		$X_R=4.0-5.0$
-0.33	5, 2	30:00	-1	0	1		$X_R=4.0-5.0$
-0.33	10, 2	30:20	-0.2	0	1		$X_R=4.0-5.0$
-0.33	20, 1	30:30	0	1	1		$X_R=3.0-4.0$

Table 5.2(b) Dye injection visualization of BSF using a sharp extended leading upstream plate

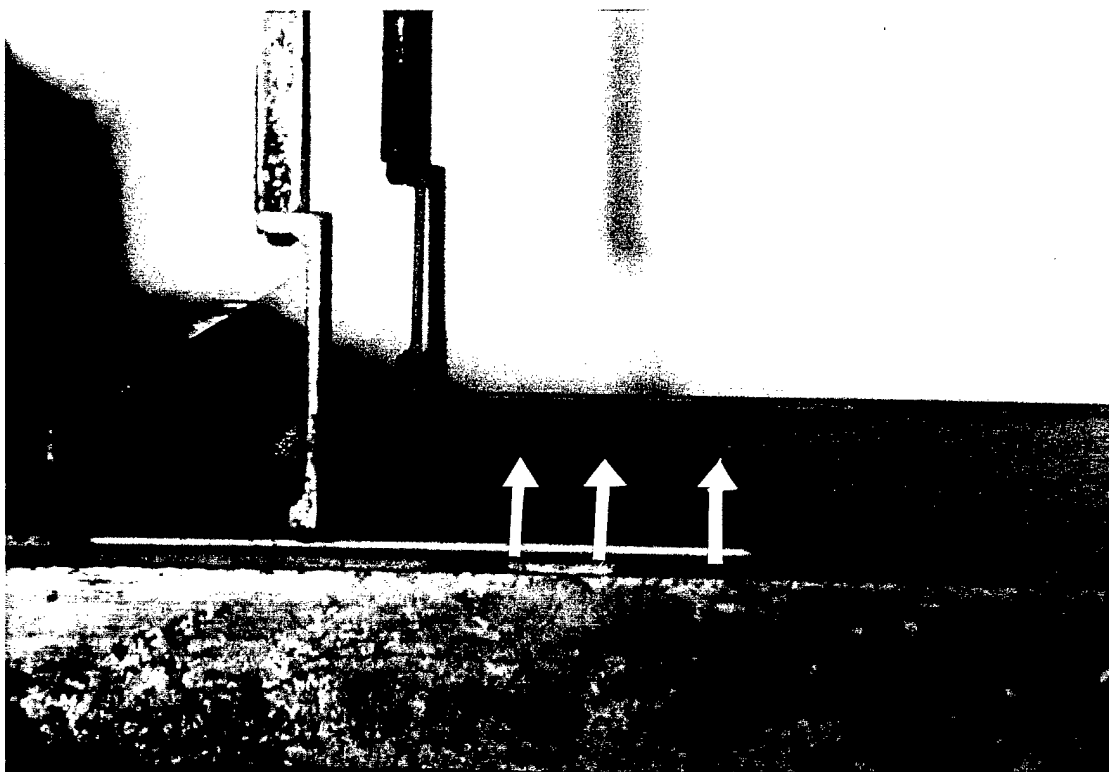


Figure 5.4.1(a) $Re_h=10,000$, airfoil at $(1.83h, 0.2h)$, stationary.

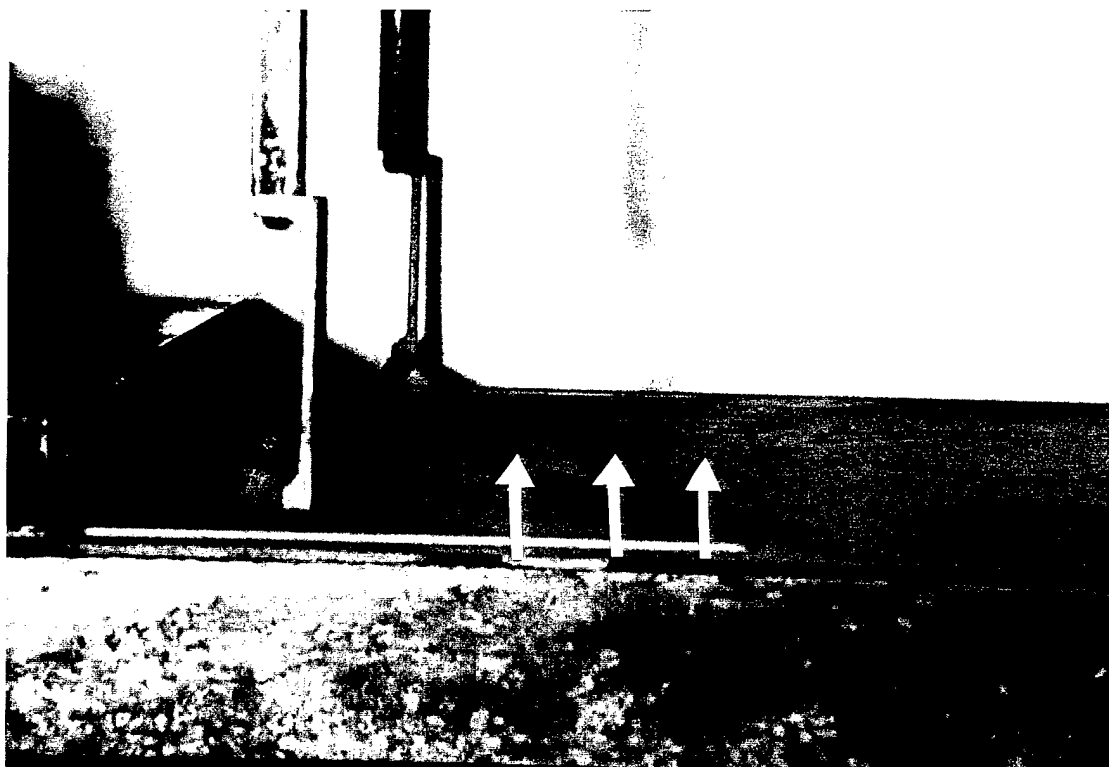


Figure 5.4.1(b) $Re_h=10,000$, airfoil at $(1.83h, 0.2h)$, $f=5$ Hz, $H'=0.25$.

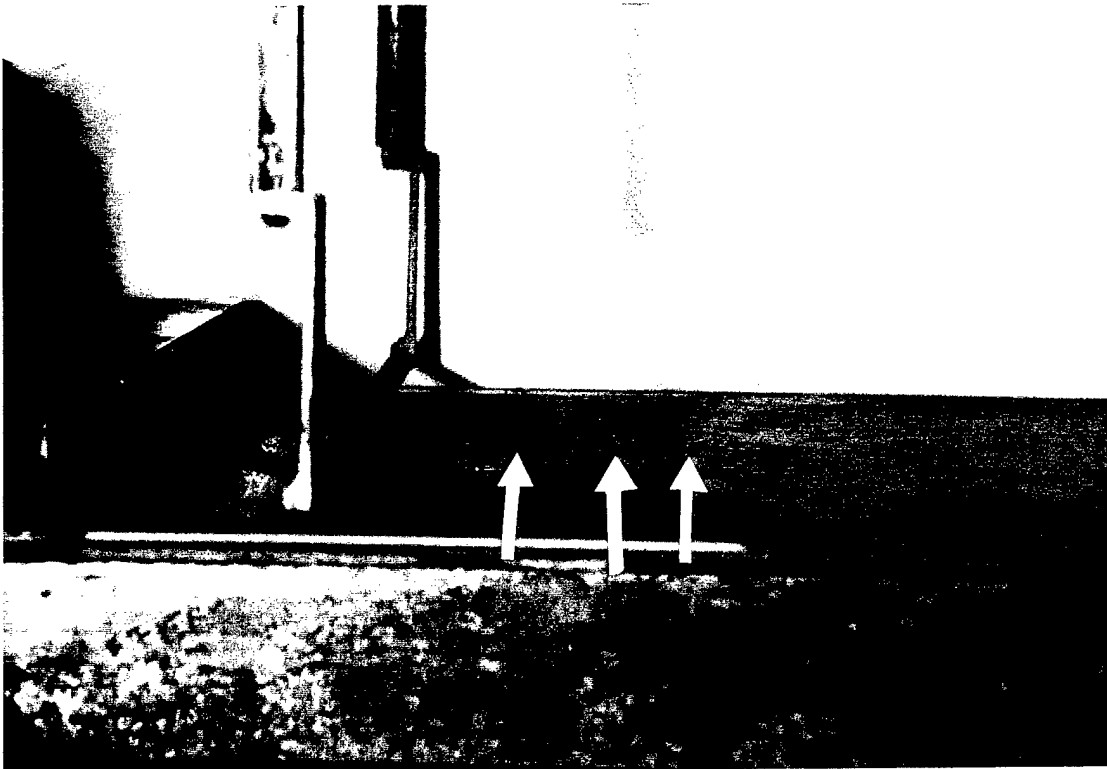


Figure 5.4.2(a) $Re_h=10,000$, airfoil at $(1.83h, 0.2h)$, $f=10$ Hz, $H'=0.25$.

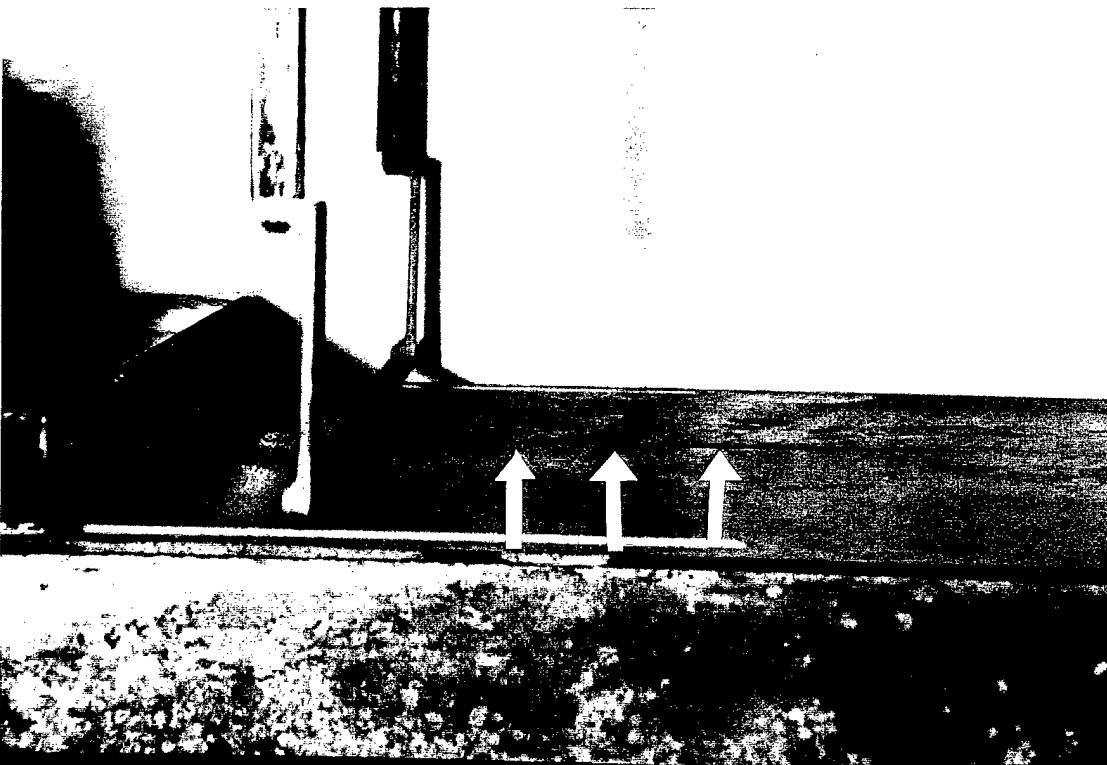


Figure 5.4.2(b) $Re_h=10,000$, airfoil at $(1.83h, 0.2h)$, $f=20$ Hz, $H'=0.125$.

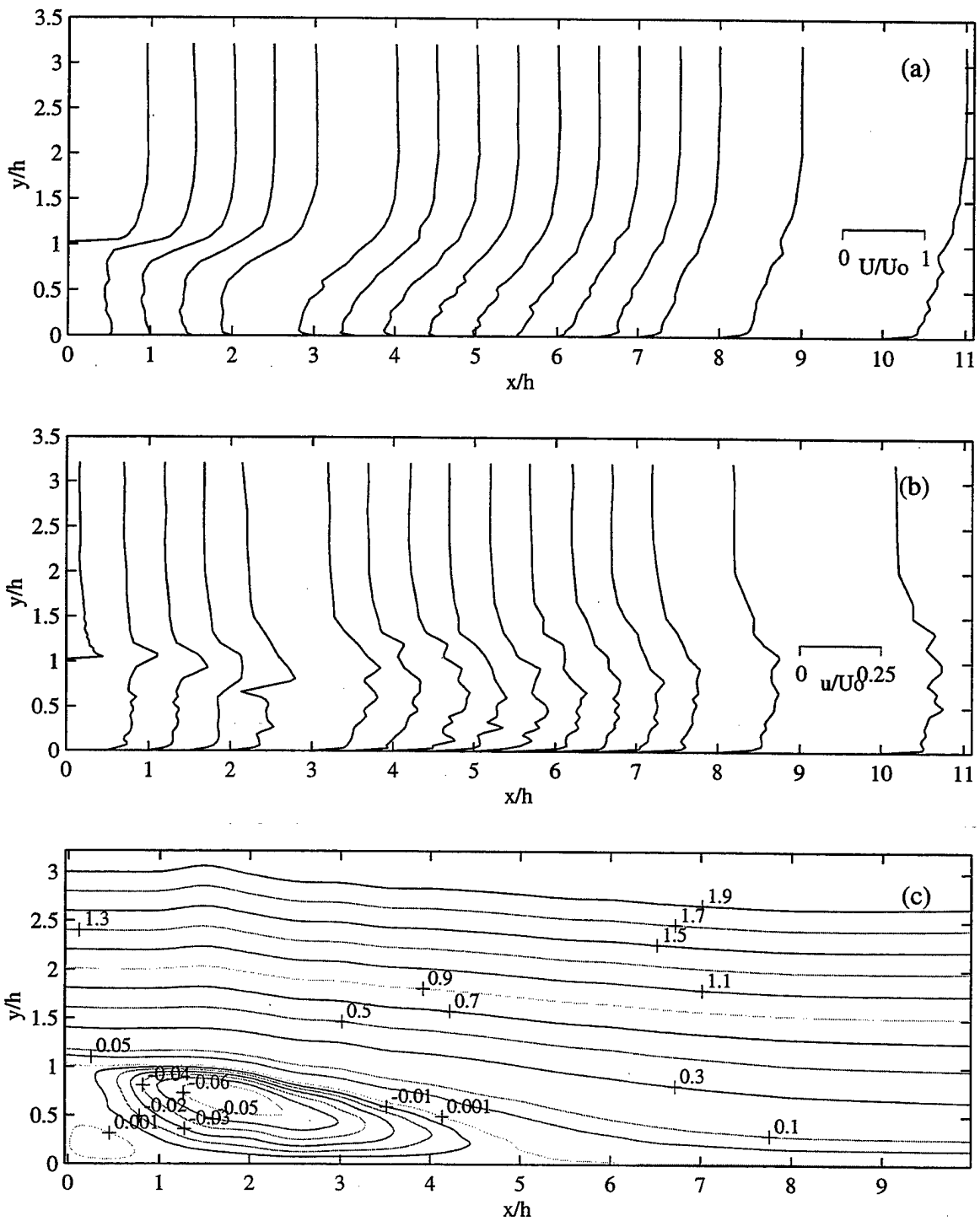


Figure 5.4.3 (a) velocity, (b) turbulence intensity, (c) streamlines of the backward-facing step. no airfoil

3. Effect of Stationary Airfoil

The mean streamwise velocity and turbulence intensity profiles and the normalized streamlines with a stationary 10 mm NACA0012 airfoil, installed at four locations i.e. (1.83h, 0.2h), (1.83h, 0.6h), (1.83h, 0.9h) and (1.83h, 1.3h), are compared with those without an airfoil in Figures 5.4.4, 5.4.5, 5.4.6, and 5.4.7, respectively. The mean flow profiles upstream of the airfoil do not seem to be significantly affected by the existence of the airfoil at these four locations. While there are some subtle differences between flow profiles with an airfoil installed and those without an airfoil, the stationary airfoil is not perceived to have a significant impact on the dynamics of the flow. This is indeed supported by the mean streamline profiles for the four test locations. Although there is some slight variation of the size of the recirculation flow region, the reattachment length appears to be virtually not affected and remains at 5.2 step heights. Furthermore, the corner eddy is present in all four cases.

4. Effect of Frequency of Oscillation

The mean streamwise velocity and turbulence intensity profiles and the normalized streamlines of the airfoil, oscillating at (1.83h, 0.2h) with three different conditions (5 Hz, 0.25c), (10 Hz, 0.25c) and (20 Hz, 0.125c), are compared with those without an airfoil in Figures 5.4.8, 5.4.9 and 5.4.10, respectively. The mean flow profiles near the edge of the separation point do not seem to be significantly affected by the motion of the airfoil for all three frequencies. With the exception of 5 Hz, the mean flow profiles in the neighborhood of the airfoil are dramatically changed for 10 Hz and 20 Hz. In particular, the streamwise turbulence intensity near the wall is significantly higher. With the increase in streamwise turbulence intensity for 10 Hz and 20 Hz, it would be expected that the separated shear layer grows faster and reattaches sooner. The velocity profiles indicate that indeed the region of the reversed flow is significantly reduced for 10 Hz and 20 Hz. The mean streamwise turbulence intensities for these three frequencies reveal much higher levels in the separated shear layer and recirculation zone compared with those for a stationary airfoil. The mean non-dimensional streamlines show that the reattachment length X_R has been altered from 5.2 to 5.0, 4.2 and 1.5 step heights for the

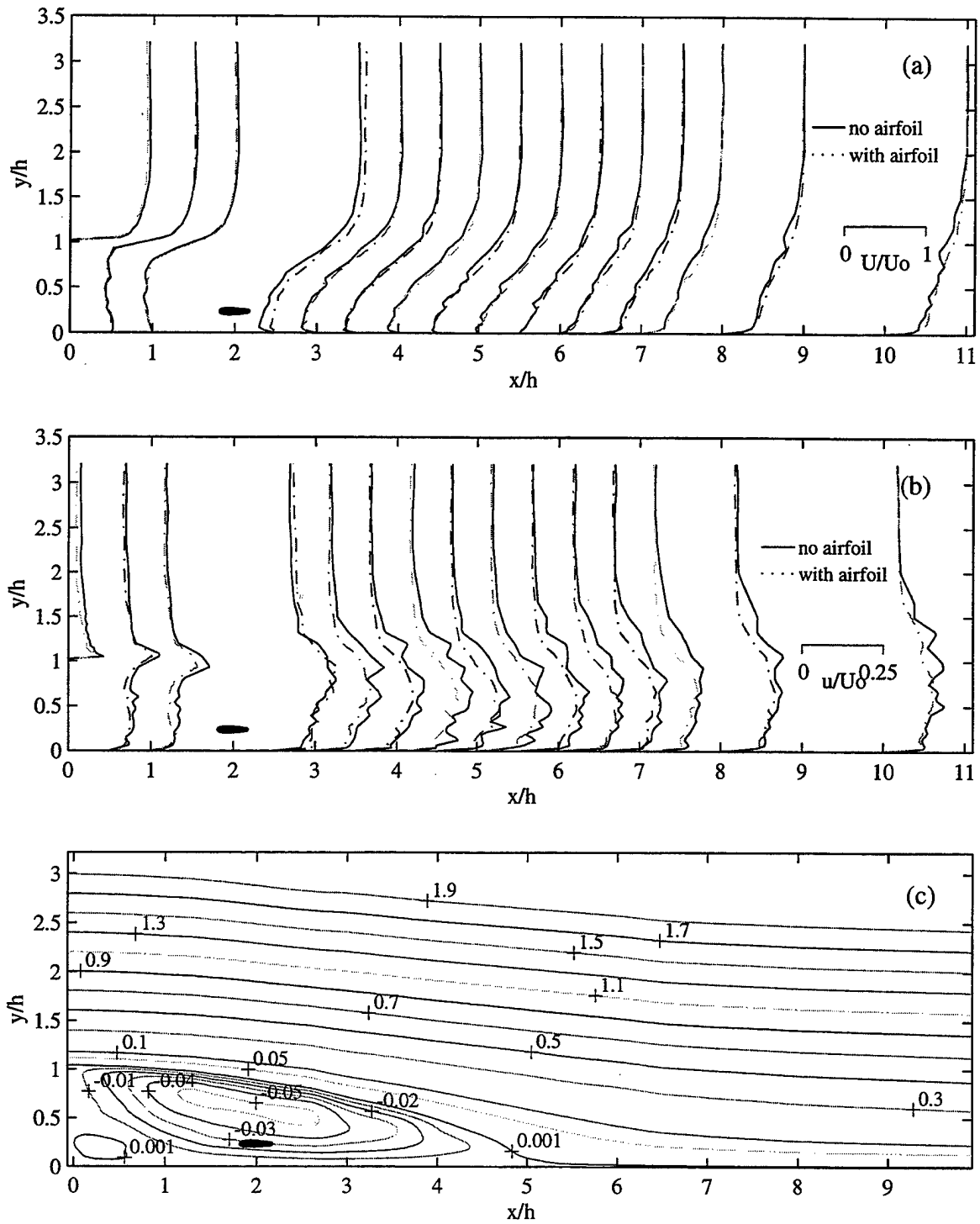


Figure 5.4.4 (a) velocity, (b) turbulence intensity, (c) streamlines of the backward-facing step. 10 mm airfoil at $(1.83h, 0.2h)$, stationary.

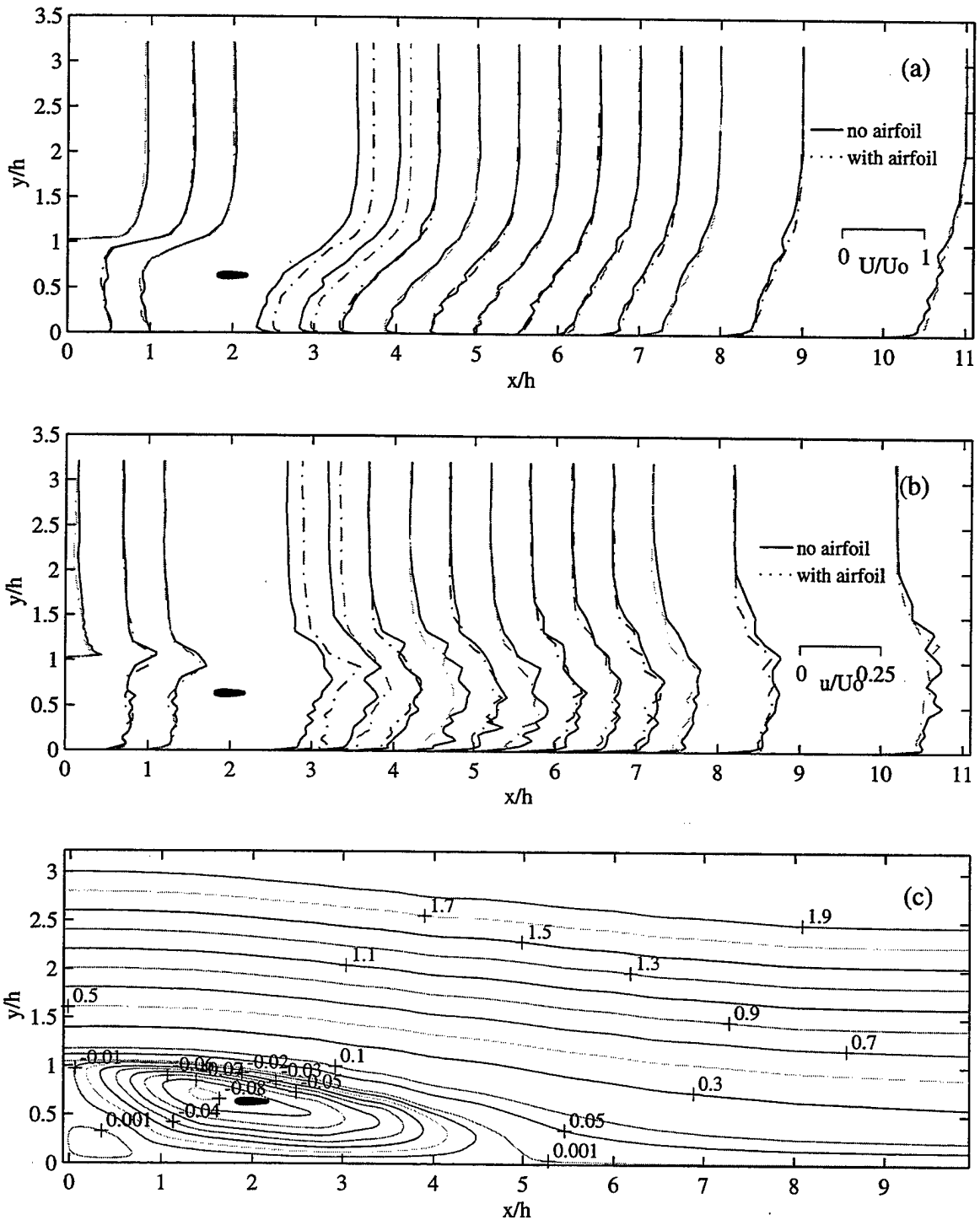


Figure 5.4.5 (a) velocity, (b) turbulence intensity, (c) streamlines of the backward-facing step. 10 mm airfoil at (1.83h, 0.6h), stationary.

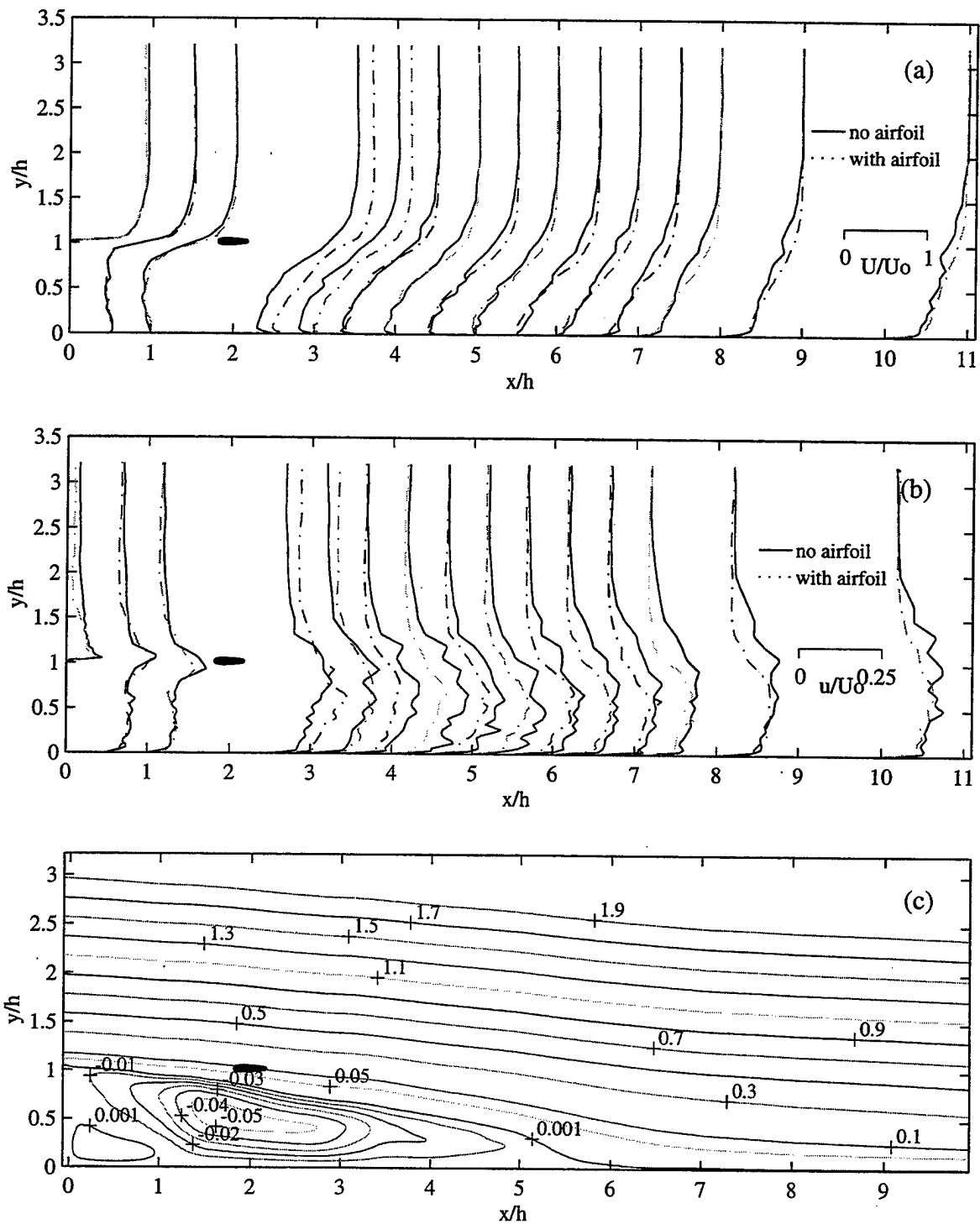


Figure 5.4.6 (a) velocity, (b) turbulence intensity, (c) streamlines of the backward-facing step. 10 mm airfoil at (1.83h, 1.0h), stationary.

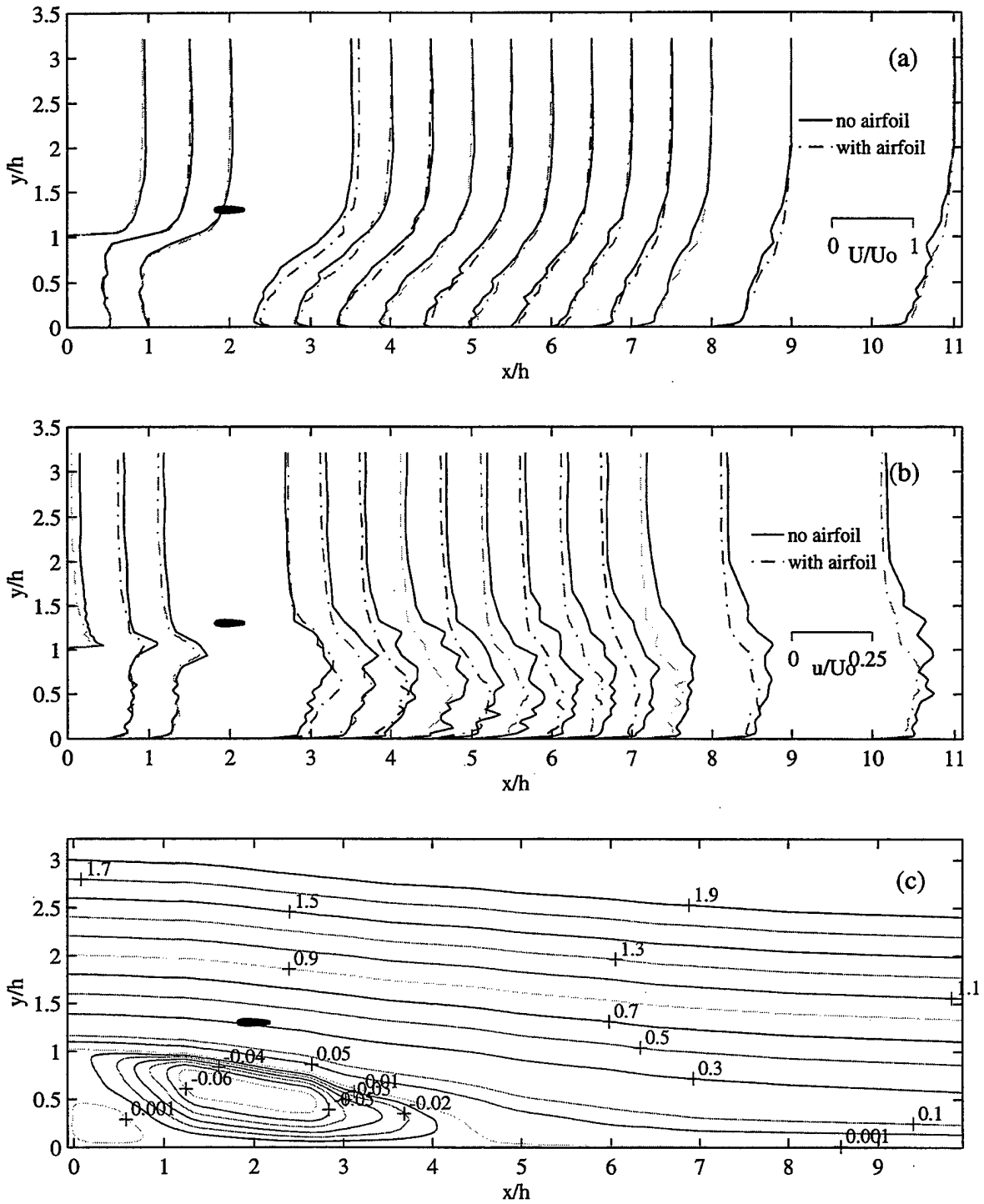


Figure 5.4.7 (a) velocity, (b) turbulence intensity, (c) streamlines of the backward-facing step. 10 mm airfoil at (1.83h, 1.3h), stationary

three conditions, respectively. In particular, the separated shear layer reattaches upstream of the leading edge of the airfoil for 20 Hz. The behavior for 10 Hz is slightly more complex. It seems that the shear layer reattaches at 2.0 step heights and separates again at 2.9 step heights before finally reattaching to the wall at 4.5 step heights. It should be noted that while the maximum value of the mean non-dimensional streamline in the recirculation zone is approximately -0.01 for both 5 Hz and 10 Hz, that for 20 Hz is at least 10 times higher. The exact cause of this phenomenon is not clear at this stage.

5. Effect of Amplitude of Oscillation

The effects of the oscillation amplitude of the 10 mm airfoil, oscillating at (1.83h, 0.9h) with two different conditions (10 Hz, 0.25c) and (10 Hz, 0.5c), on the mean streamwise velocity and turbulence intensity profiles and the normalized streamlines are compared with those without an airfoil in Figures 5.4.11, and 5.4.12, respectively. It should again be noted that the mean flow profiles near the edge of the separation point ($x/h=0.066$) are hardly different from those for a backward-facing step flow without an airfoil. However, the streamwise turbulence intensity near the wall and in the separated shear layer region is also significantly higher and it increases as the plunge amplitude is increased from 0.25c to 0.5c. The mean streamlines reveal that the region of the reversed flow has been significantly reduced for both cases. As expected, the streamwise turbulence intensities reveal much higher levels in the separated shear layer and recirculation zone for both plunge amplitudes compared with those for a stationary airfoil. The mean normalized streamlines show that the reattachment length has been reduced from 5.2 to 3.5 and 2.6 step heights for a plunge amplitude of 0.25c and 0.5c, respectively.

Similar results are obtained when the airfoil is moved to (2.5h, 0.9h). Figures 5.4.13 and 5.4.14 show that the reattachment lengths are changed from 5.2 to 3.9 and 2.9 step heights for flapping amplitudes at 0.25c and 0.5c, respectively.

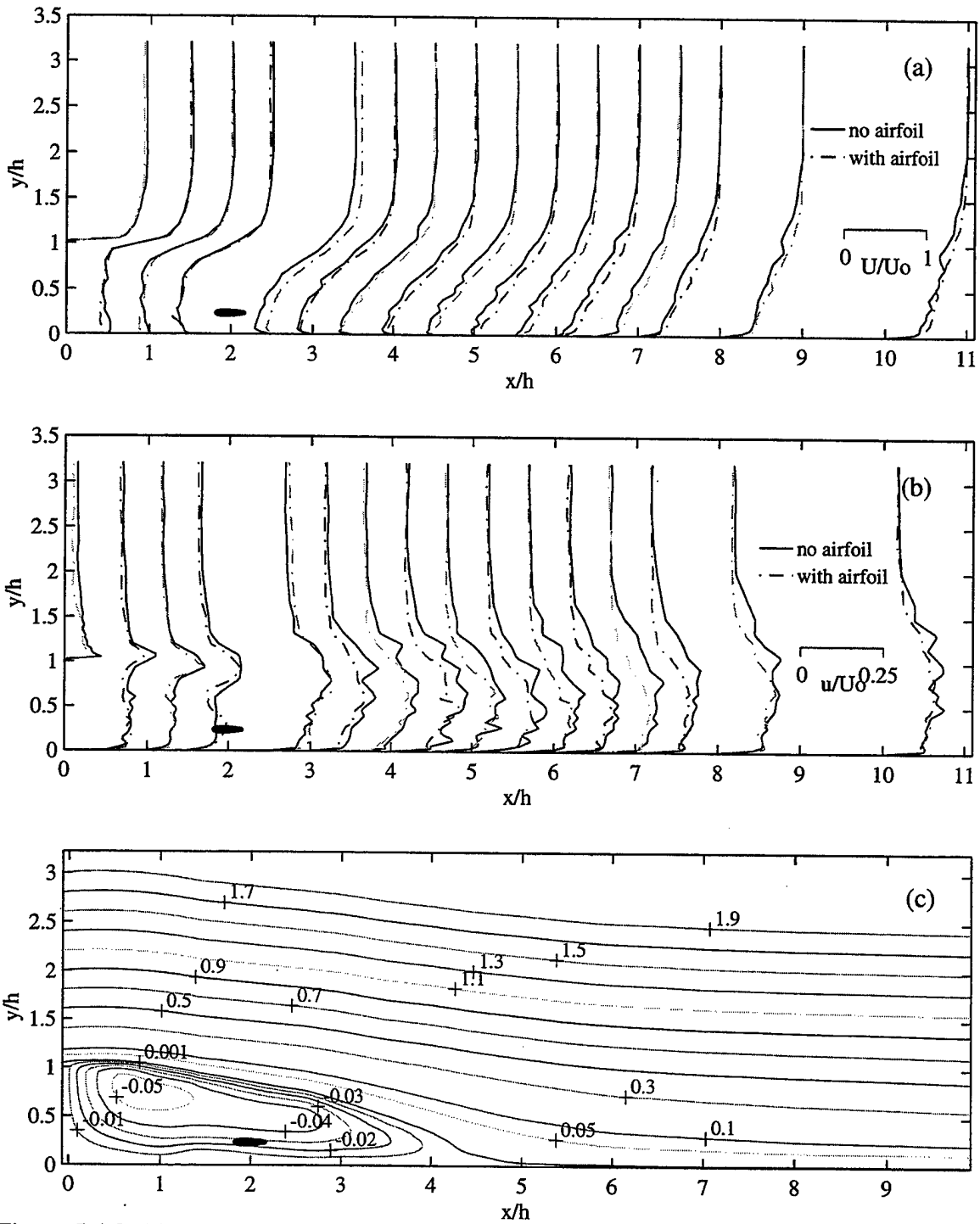


Figure 5.4.8 (a) velocity, (b) turbulence intensity, (c) streamlines of the backward-facing step. 10 mm airfoil at $(1.83h, 0.2h)$, oscillation frequency $f = 5$ Hz, amplitude $H' = 0.25$.

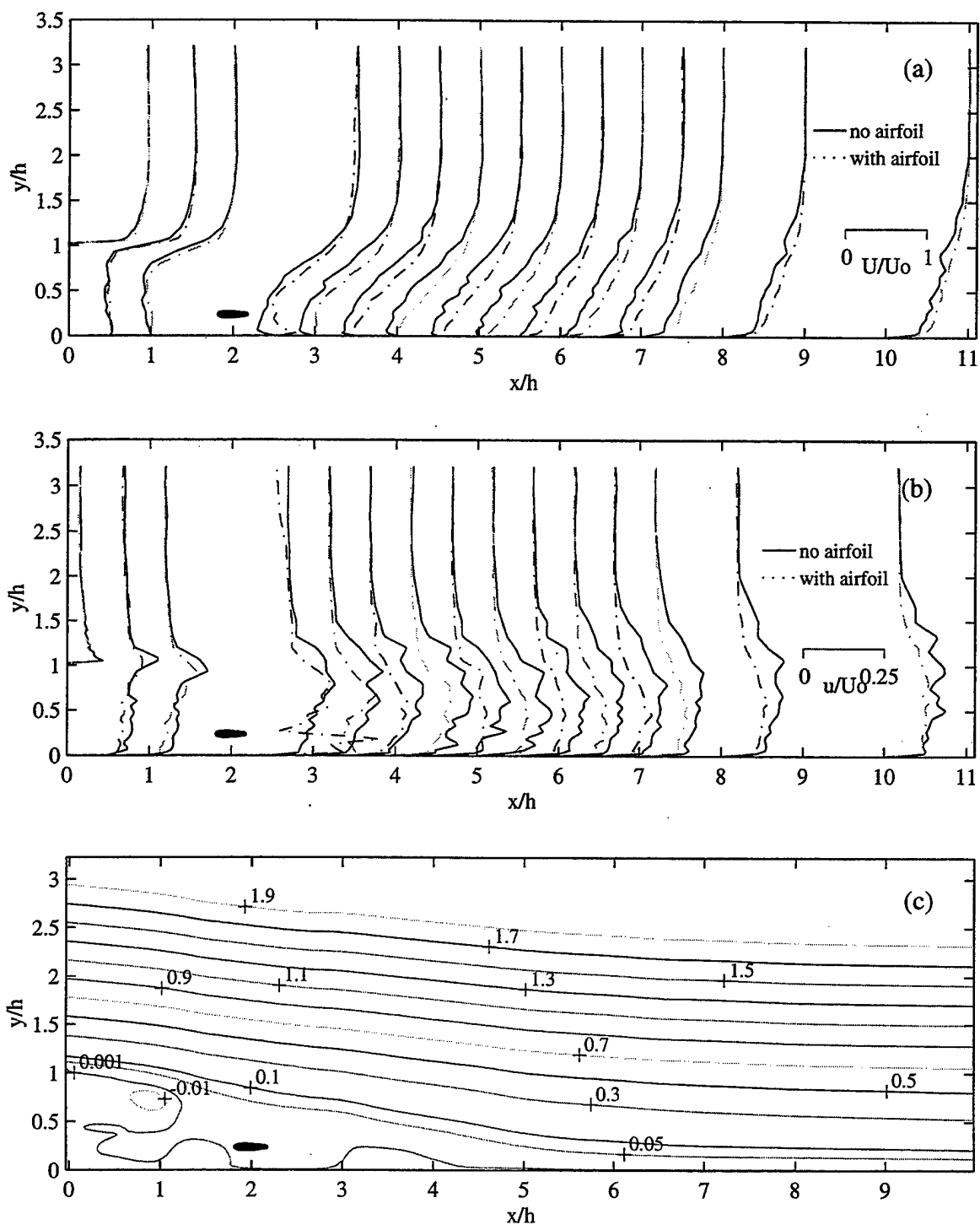


Figure 5.4.9 (a) velocity, (b) turbulence intensity, (c) streamlines of the backward-facing step. 10 mm airfoil at $(1.83h, 0.2h)$, oscillation frequency $f=10$ Hz, amplitude $H'=0.25$.

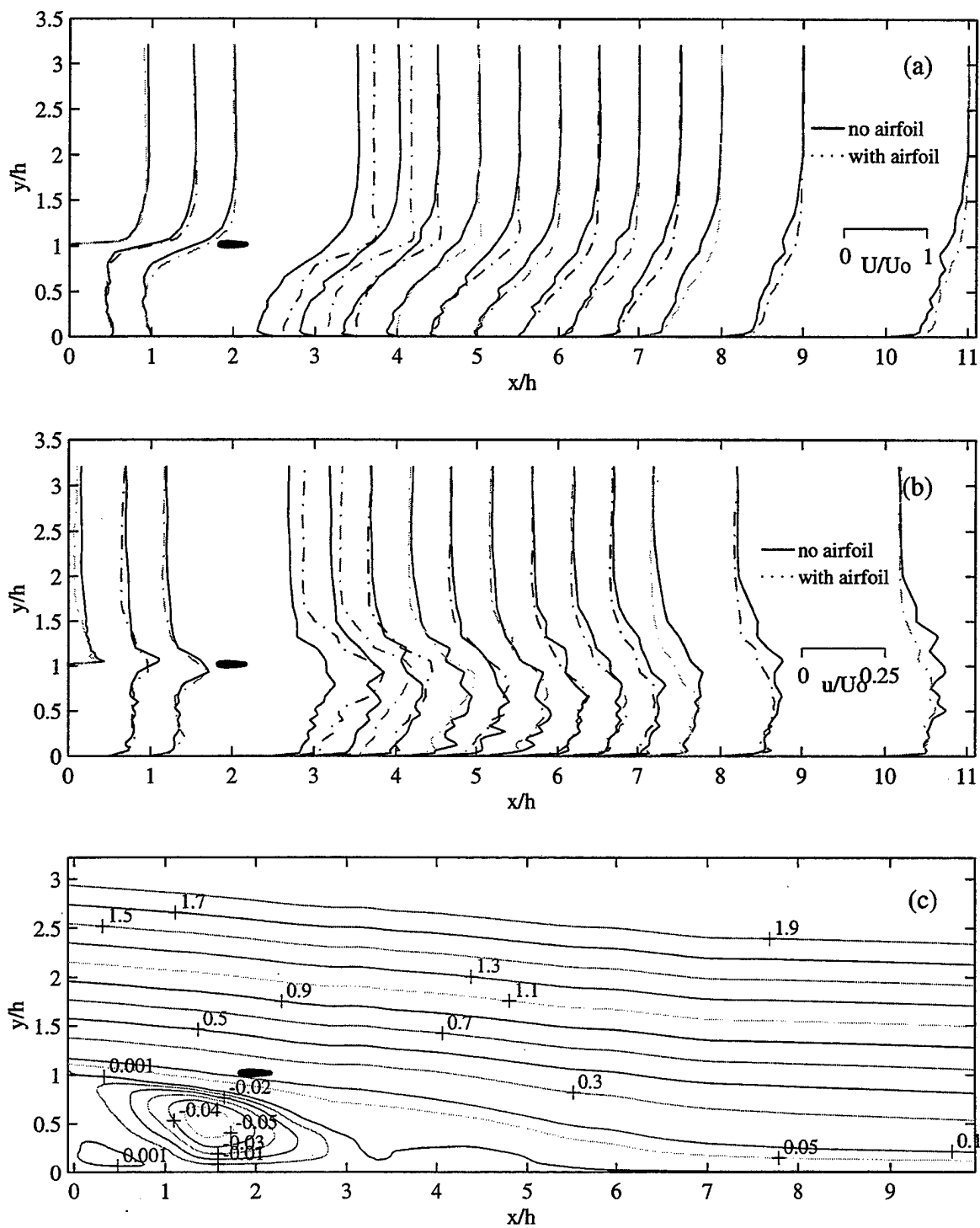


Figure 5.4.11 (a) velocity, (b) turbulence intensity, (c) streamlines of the backward-facing step. 10 mm airfoil at (1.83h, 1.0h), oscillation frequency $f=10$ Hz, amplitude $H'=0.25$.

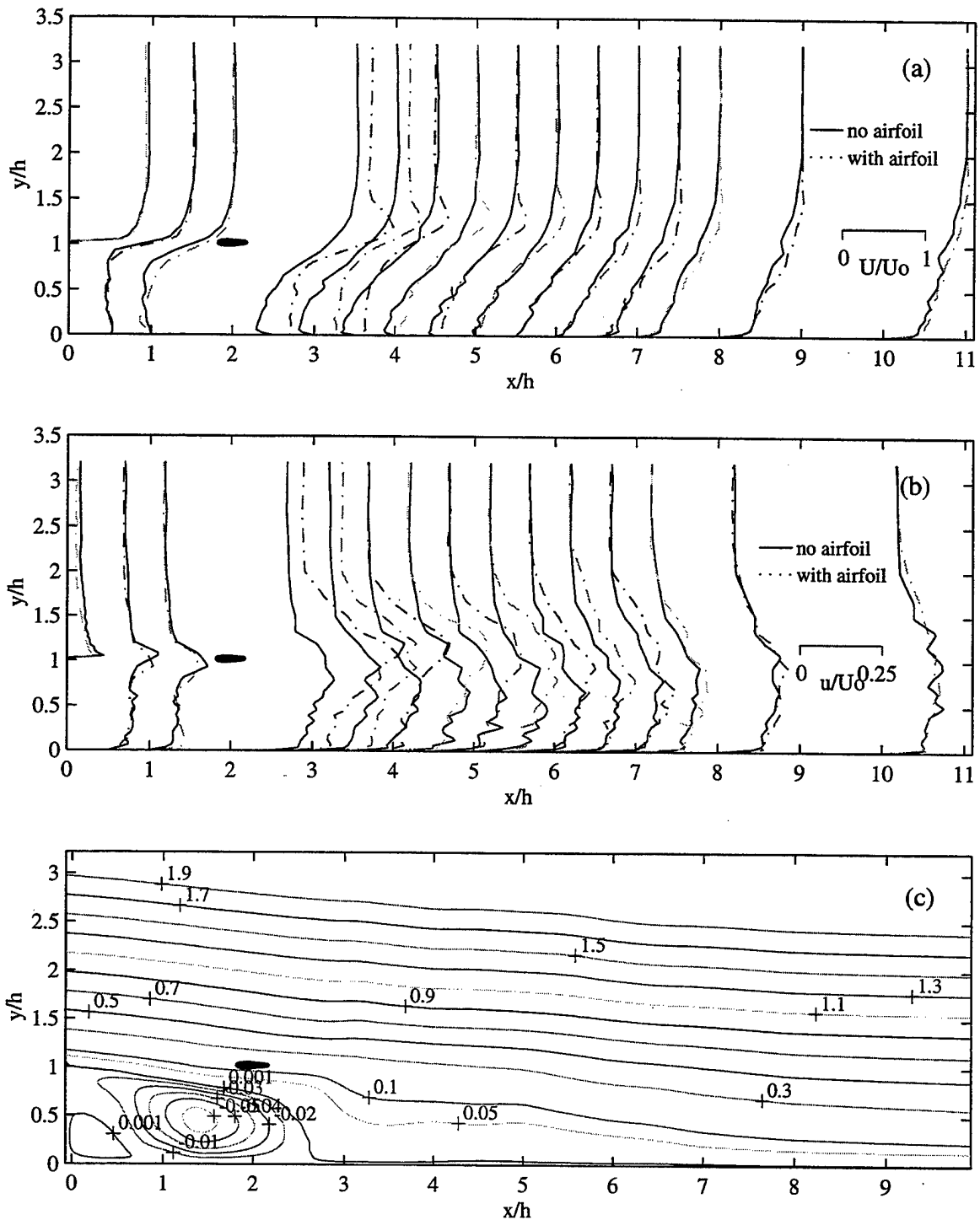


Figure 5.4.12 (a) velocity, (b) turbulence intensity, (c) streamlines of the backward-facing step. 10 mm airfoil at (1.83h, 1.0h), oscillation frequency $f=10$ Hz, amplitude $H'=0.5$.

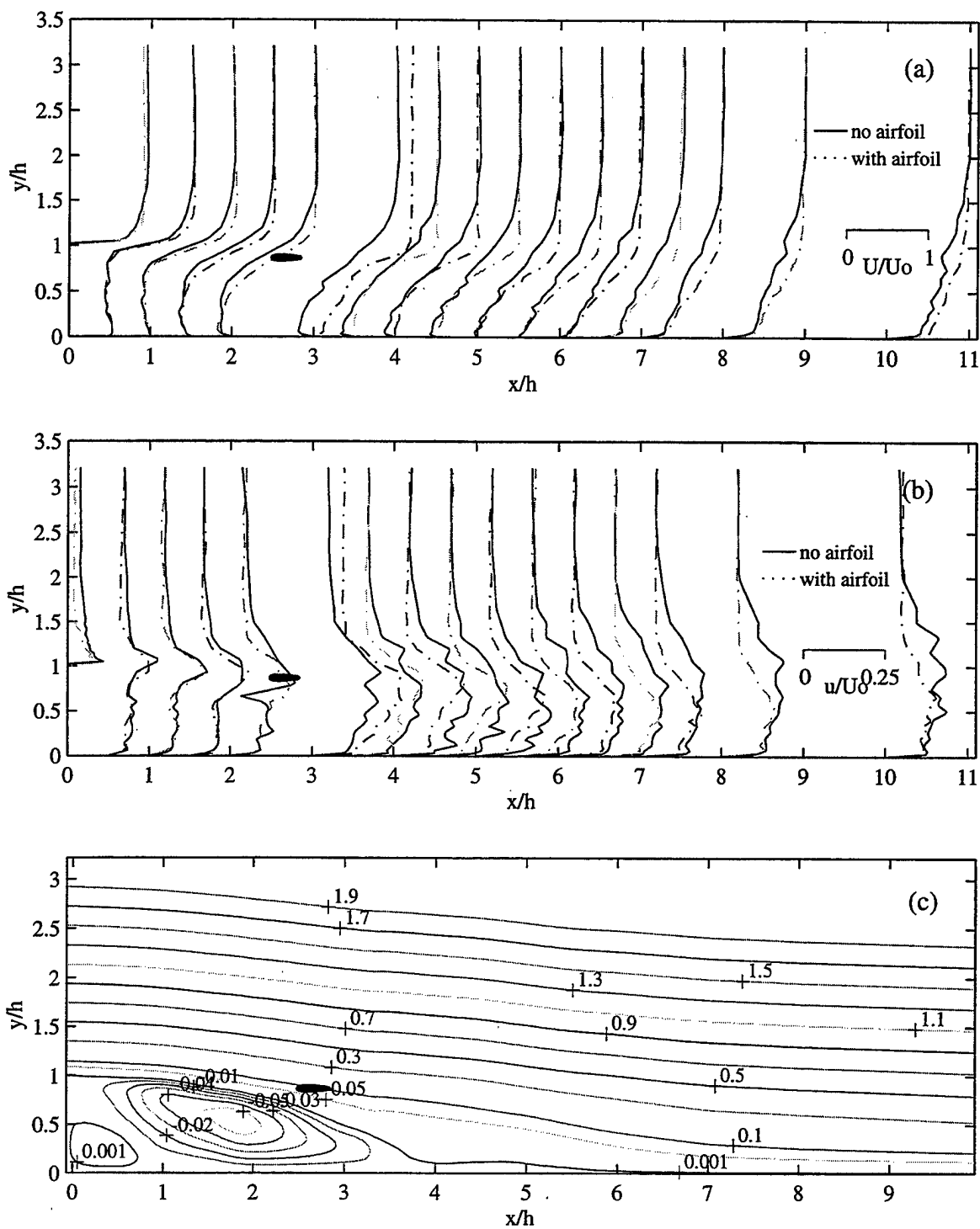


Figure 5.4.13 (a) velocity, (b) turbulence intensity, (c) streamlines of the backward-facing step. 10 mm airfoil at (2.5h, 0.9h), oscillation frequency $f=10$ Hz, amplitude $H'=0.25$.

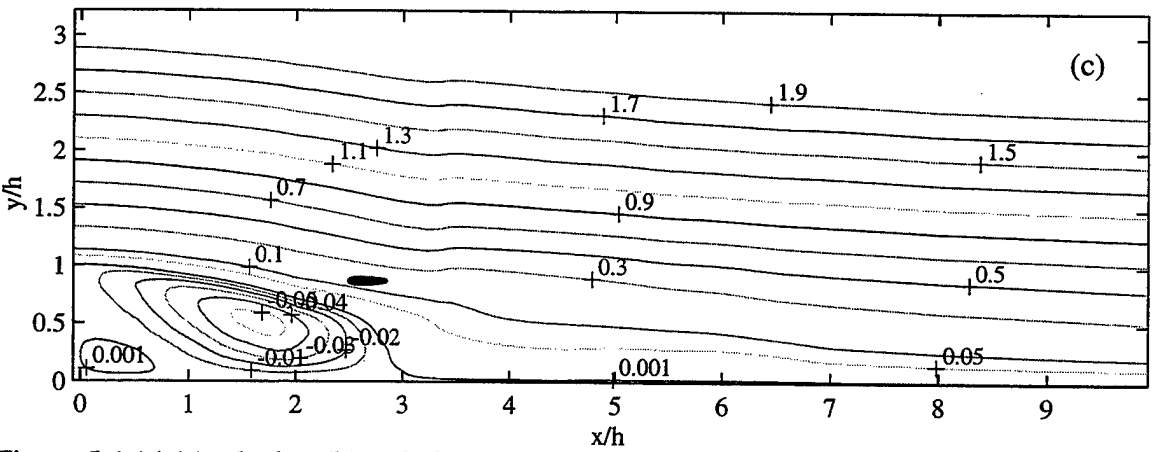
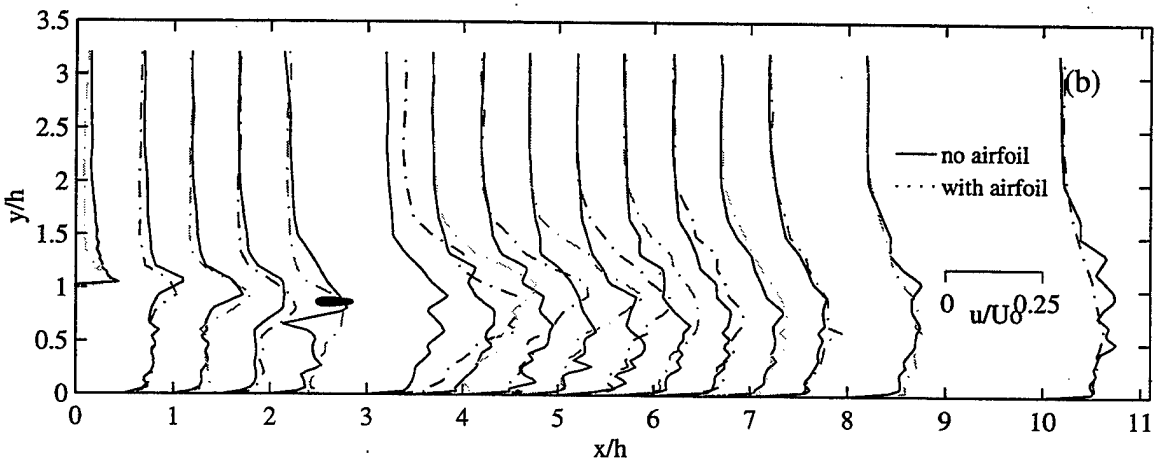
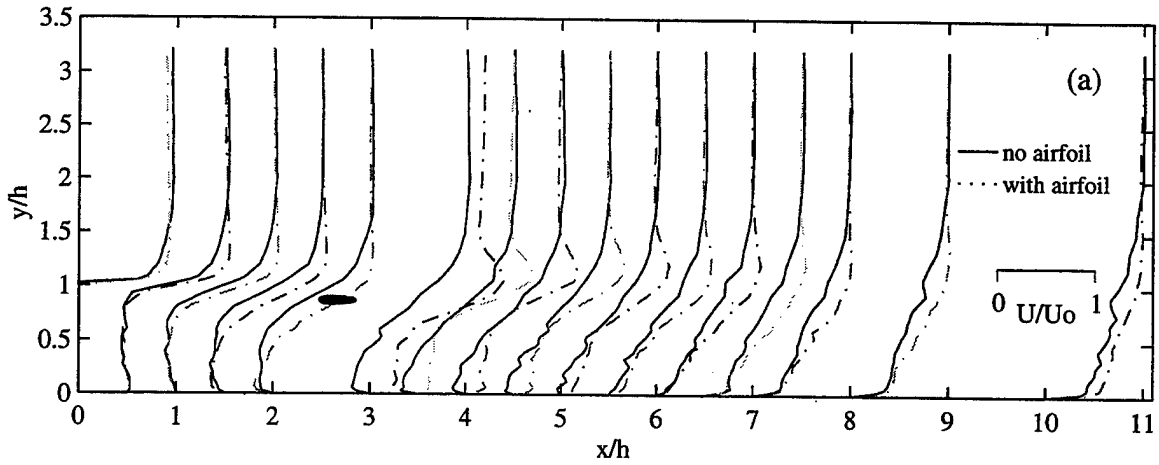


Figure 5.4.14 (a) velocity, (b) turbulence intensity, (c) streamlines of the backward-facing step. 10 mm airfoil at (2.5h,0.9h), oscillation frequency $f=10$ Hz, amplitude $H'=0.5$.

6. Effect of Airfoil Size

The effect of the size of the 20 mm airfoil, located at $(1.83h, 0.2h)$ with the three flapping conditions $(0, 0)$, $(5 \text{ Hz}, 0.25c)$ and $(10 \text{ Hz}, 0.25c)$, is shown in Figures 5.4.15, 5.4.16 and 5.4.17, respectively. It should be pointed out that the 20 mm airfoil does not have a sharp trailing edge and the trailing edge thickness is 1.27 mm. The results are similar to those obtained with the 10 mm airfoil. When the 20 mm airfoil is stationary, the mean flow profiles do not seem to be affected, and the reattachment length still remains at 5.2 step heights. On the other hand, when the 20 mm airfoil is flapping at 5 Hz and 0.25c, the mean nondimensional streamlines show that they are similar to those for the 10 mm airfoil (Figure 5.4.8(c)) except that there are two maxima within the recirculation zone. The reattachment length is slightly higher at 4.3 step heights compared with 4.2 step heights for the 10 mm airfoil. With 10 Hz oscillation, the reattachment length has been reduced to 2.1 step heights for the 20 mm airfoil. There is no reattachment and second reattachment further downstream as observed for the 10 mm airfoil. Furthermore, it can be seen that the streamlines upstream of the airfoil are pulled in towards the wall due to the action of the plunging airfoil. This phenomenon has not been observed for the 10 mm airfoil. These results seem to indicate that the action of a larger airfoil is stronger than that of a smaller airfoil. However, the improvement by using a larger airfoil is less than linear.

7. Effect of Airfoil Location

In order to examine the effect of the location of a plunging airfoil on the recirculation zone, four different locations of $(1.83h, 0.2h)$, $(1.83h, 0.6h)$, $(1.83h, 0.9h)$ and $(1.83h, 1.3h)$ for the airfoil were chosen. These four locations correspond respectively to a position closest to the wall within the geometry constraints of oscillating the airfoil, vortex center in the recirculation zone without the installation of the airfoil, a position within the separated shear layer and a position outside the separated shear layer. The airfoil was oscillated in plunge at 10 Hz with an amplitude of 0.25c. Mean streamwise velocity and turbulence intensity profiles in Figures 5.4.9, 5.4.18, 5.4.11 and 5.4.19 show that while they are relatively unperturbed by the airfoil near the edge of

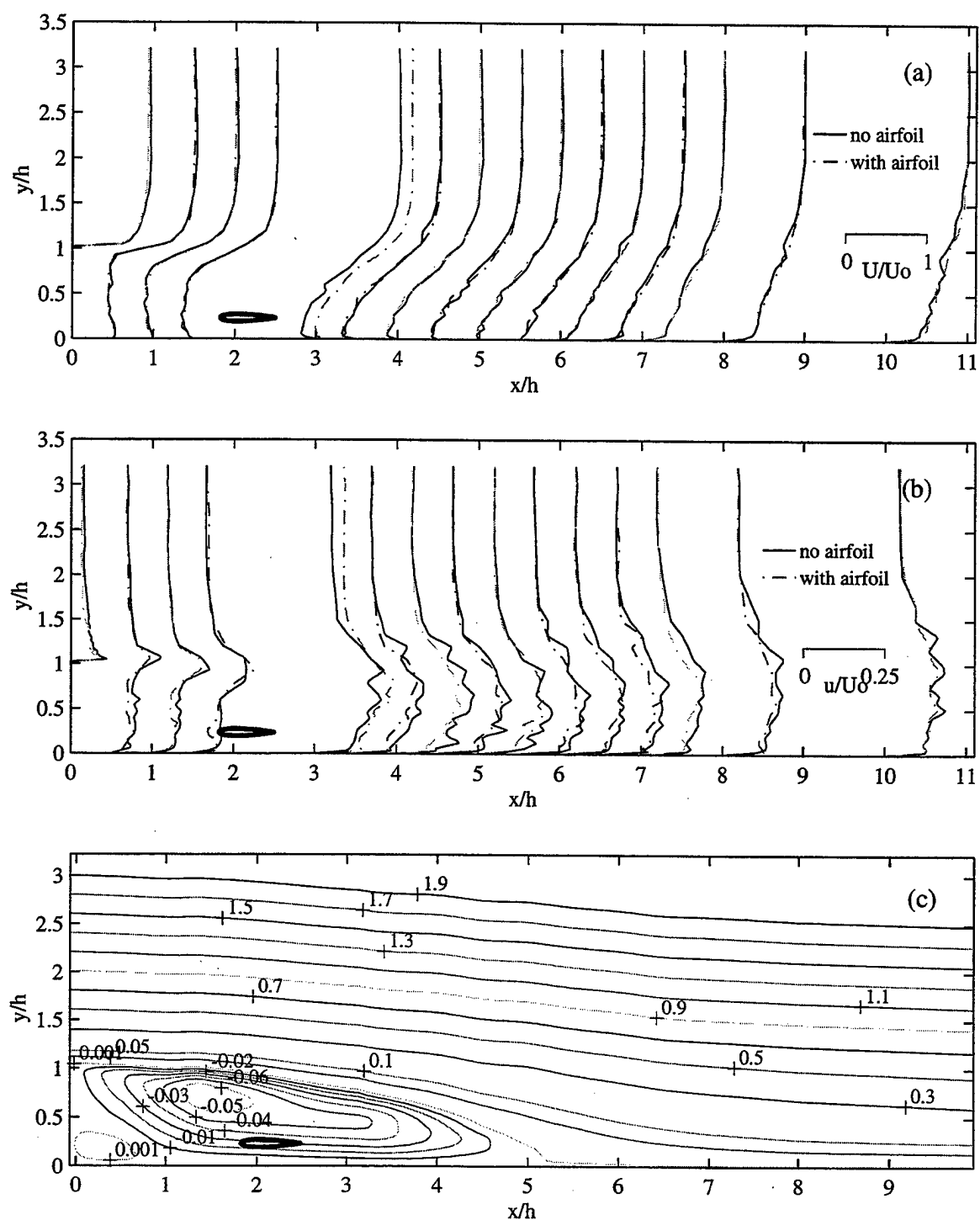


Figure 5.4.15 (a) velocity, (b) turbulence intensity, (c) streamlines of the backward-facing step. 20mm airfoil at $(1.83h, 0.2h)$, stationary.

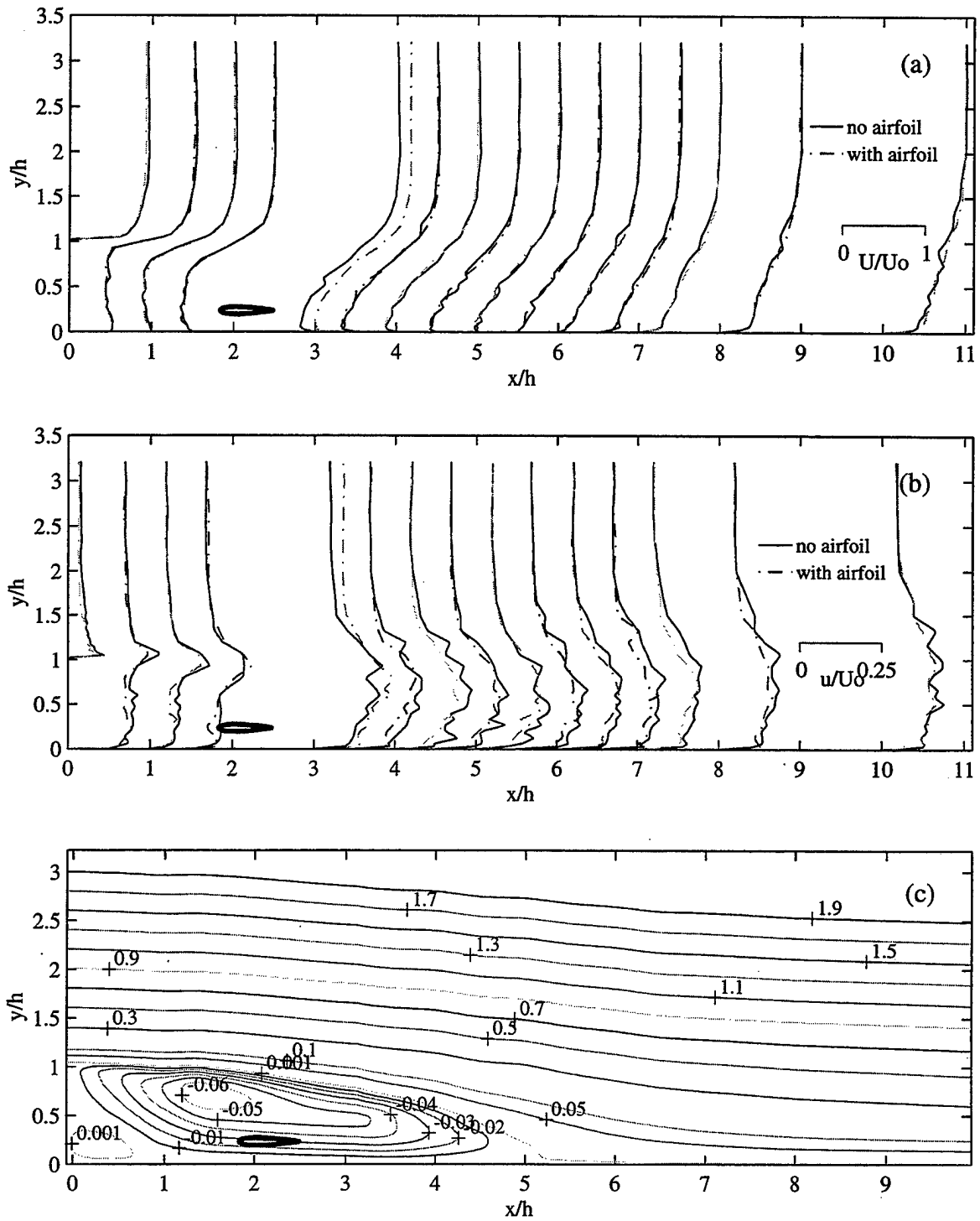


Figure 5.4.16 (a) velocity, (b) turbulence intensity, (c) streamlines of the backward-facing step. 20mm airfoil at $(1.83h, 0.2h)$, oscillation frequency $f=5$ Hz, amplitude $H'=0.25$.

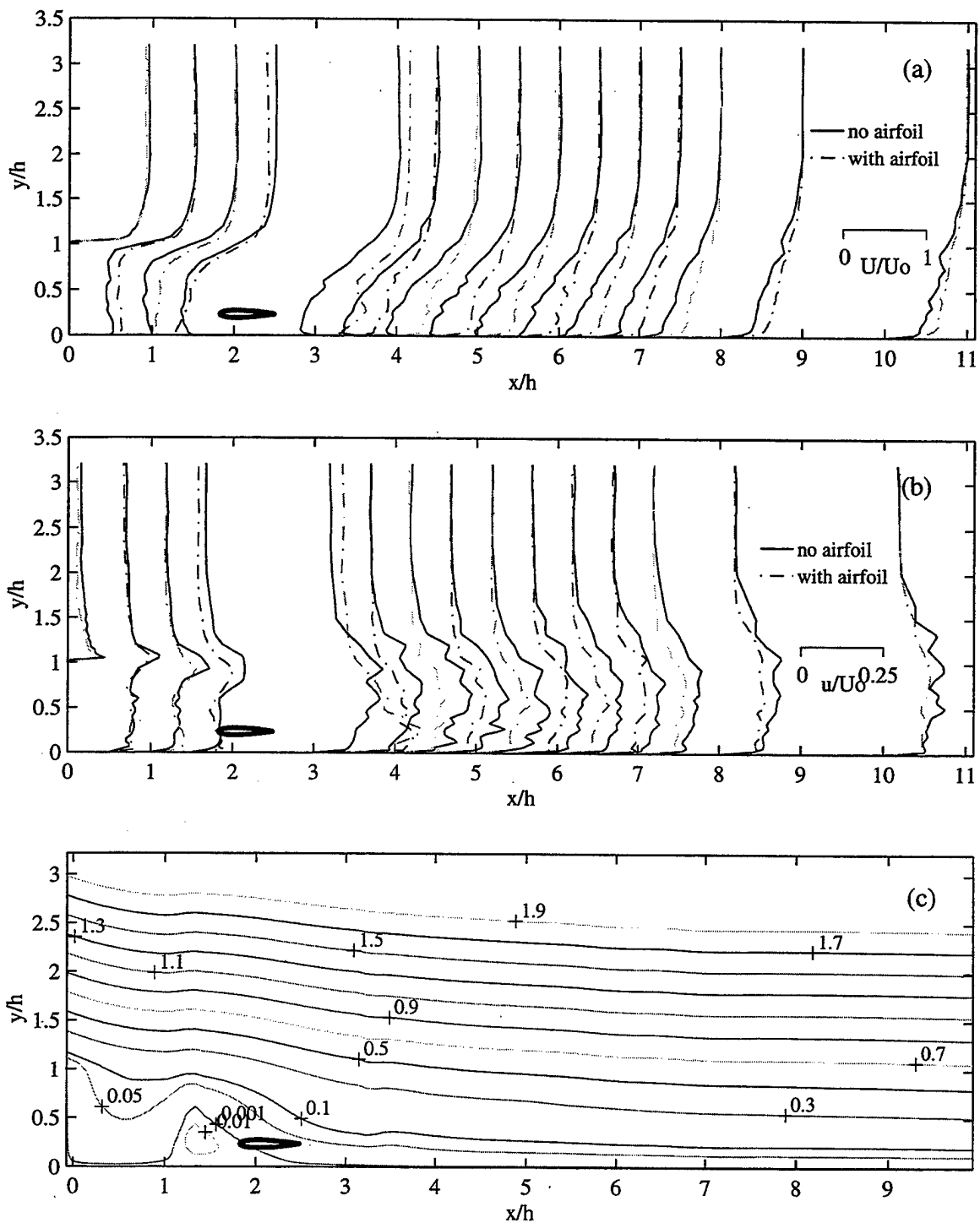


Figure 5.4.17 (a) velocity, (b) turbulence intensity, (c) streamlines of the backward-facing step. 20mm airfoil at $(1.83h, 0.2h)$, oscillation frequency $f=10$ Hz, amplitude $H'=0.25$.

separation, they are all significantly altered near the airfoil. In particular, the effect is the strongest for the airfoil located near the wall, followed by the airfoil at separated shear layer, the vortex center and outside the separated shear layer respectively. This observation is supported by the measured flow profiles. The streamlines show that the size of the separation bubble is most reduced when the airfoil is closest to the wall, followed by that located within the separated shear layer, at the standing vortex center in the absence of the airfoil and outside the separated shear layer. Results here indicate that the plunging airfoil is most effective when it is located closest to the wall.

The streamwise velocity distributions along the center line 2 mm above the wall with the 10 mm airfoil, both stationary and flapping at 10 Hz and $0.25c$, located at three streamwise sections $1.83h$, $2.5h$ and $4h$, are presented in Figures 5.4.20, 5.4.21 and 5.4.22, respectively. When the stationary airfoil is located in the vicinity of the separated shear layer, corresponding to $(1.83h, 0.9h)$ at the first streamwise section, Figure 5.4.20(a) shows that the reattachment is changed significantly. A similar effect is observed if the flapping airfoil is put at a height of $0.2h$, as shown in Figure 5.4.20(b), or if the airfoil is moved further downstream, as shown in Figures 5.4.2 and 5.4.22.

The frequency and amplitude effects of the 10 mm airfoil at $(2.5h, 0.9h)$ on the streamwise velocity are shown in Figure 5.4.23. The reattachment length is dramatically reduced by higher frequency or amplitude as described in the earlier sections.

8. Effect of Three-Dimensionality of Upstream Flow

The above results indicate that a plunging airfoil is very effective in reducing the size of the separation bubble in a two-dimensional backward-facing step flow. The effectiveness of a plunging airfoil under three-dimensional upstream condition is being explored here. A 10 mm NACA0012 airfoil was placed at $(1h, 0.2h)$ and oscillated in plunge at 5 Hz, 10 Hz and 20 Hz, respectively. The plunge amplitude for both 5 Hz and 10 Hz was $0.25c$ while that for 20 Hz was only 0.125 . All LDV measurements were made at the center plane. The mean streamwise velocity distributions in Figure 5.3.2

indicate that the region of the reversed flow does not appear to be significantly affected by a stationary airfoil, but is significantly reduced when the airfoil is oscillated at 10 Hz and 20 Hz. The mean streamwise turbulence intensities in Figures 5.4.24 and 5.4.25 show a much higher turbulence level in the recirculation zone and shear layer for 10 Hz and 20 Hz. With higher turbulence levels, it is expected that the separated shear layer will grow faster and therefore reattach to the wall closer to the step. This is indeed supported by the mean streamlines. When the airfoil is stationary or when it is oscillated at 5 Hz, Figure 5.4.26 shows that the size of the separation bubble is slightly smaller when compared with that in the absence of an airfoil. The separation bubble is found to be substantially reduced when the airfoil is oscillated at 10 Hz and 20 Hz. In particular, for both 10 Hz and 20 Hz, the separated shear layer reattaches to the wall upstream of the airfoil. These results indicate that a plunging airfoil is just as effective in reducing the size of the separation bubble in a backward-facing step flow under three-dimensional upstream flow condition as that under two-dimensional flow condition.

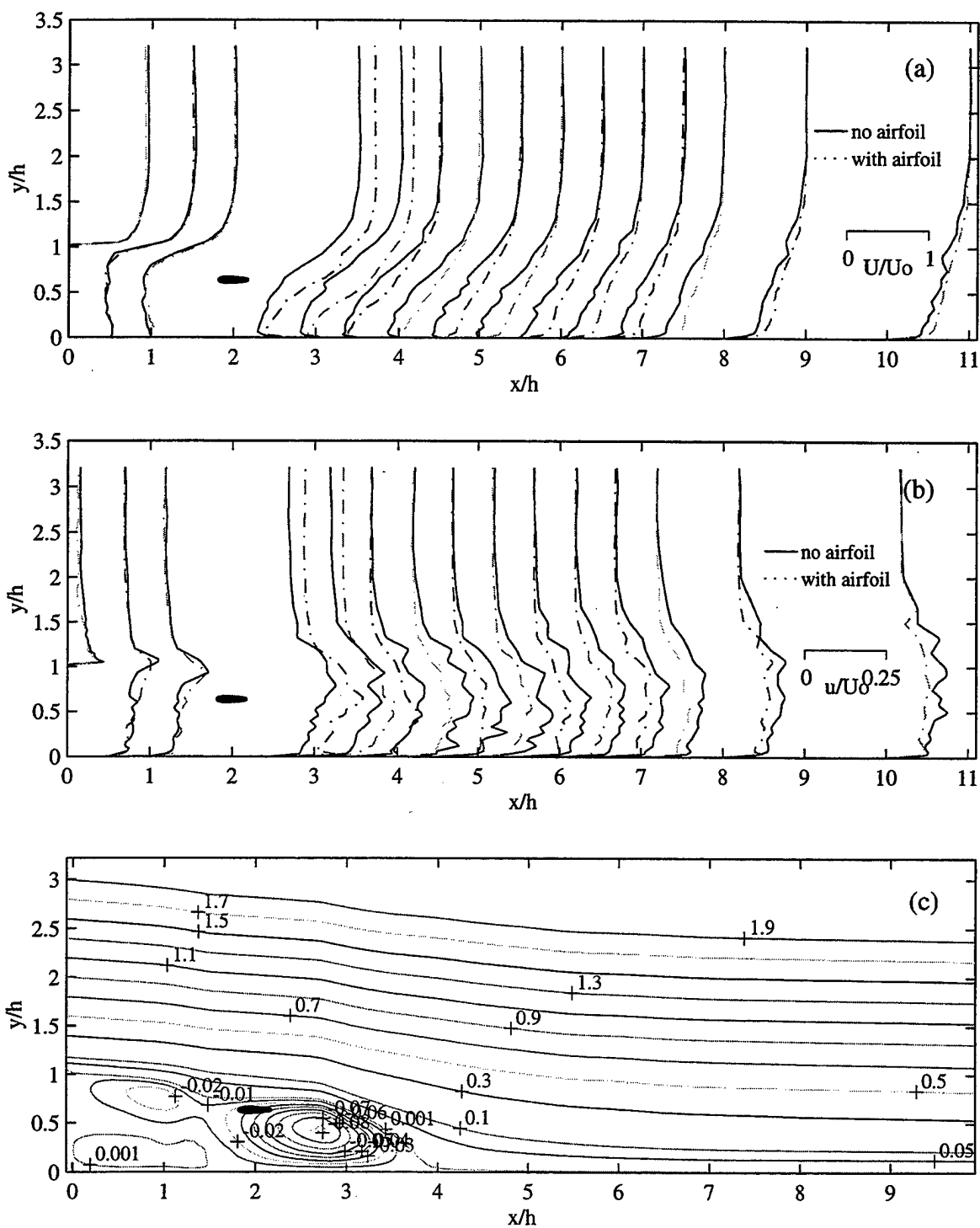


Figure 5.4.18 (a) velocity, (b) turbulence intensity, (c) streamlines of the backward-facing step. 10 mm airfoil at $(1.83h, 0.6h)$, oscillation frequency $f=10$ Hz, amplitude $H'=0.25$.

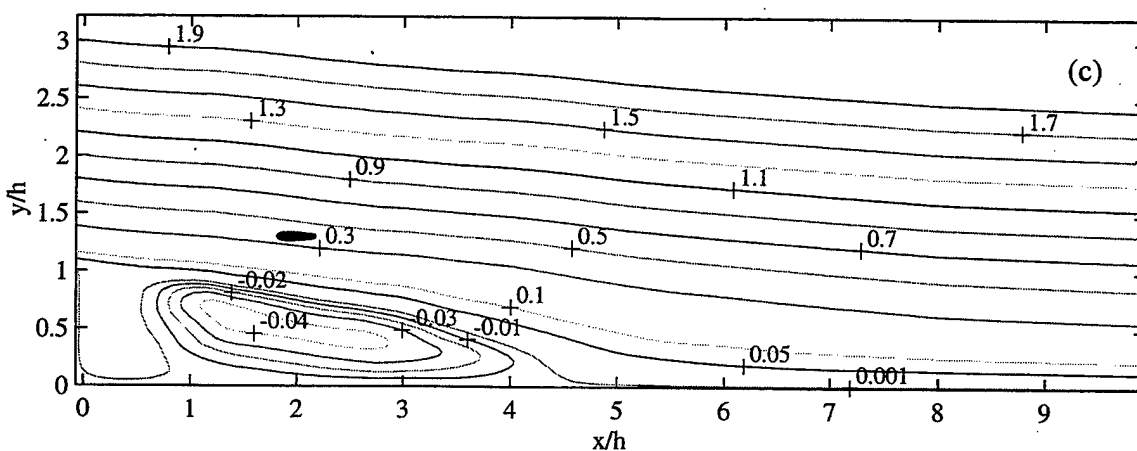
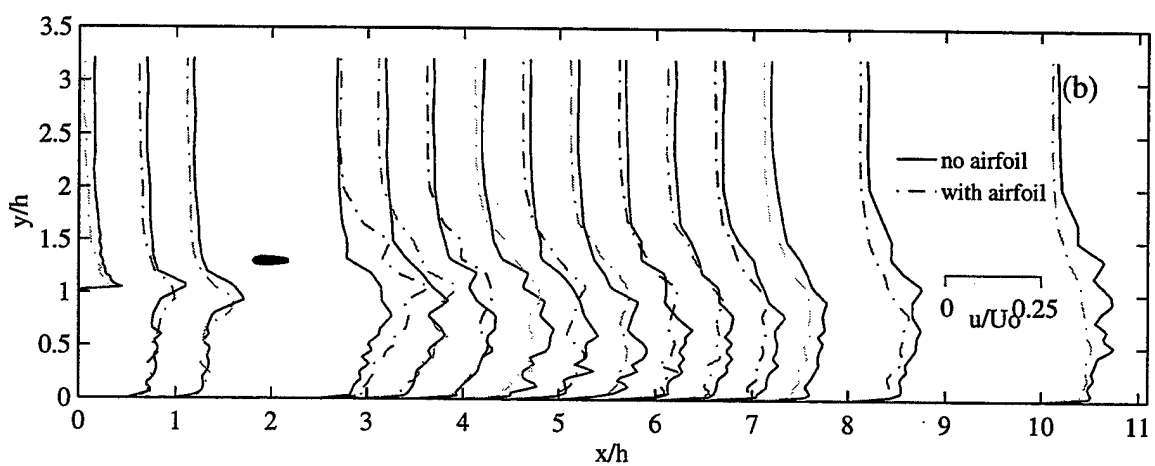
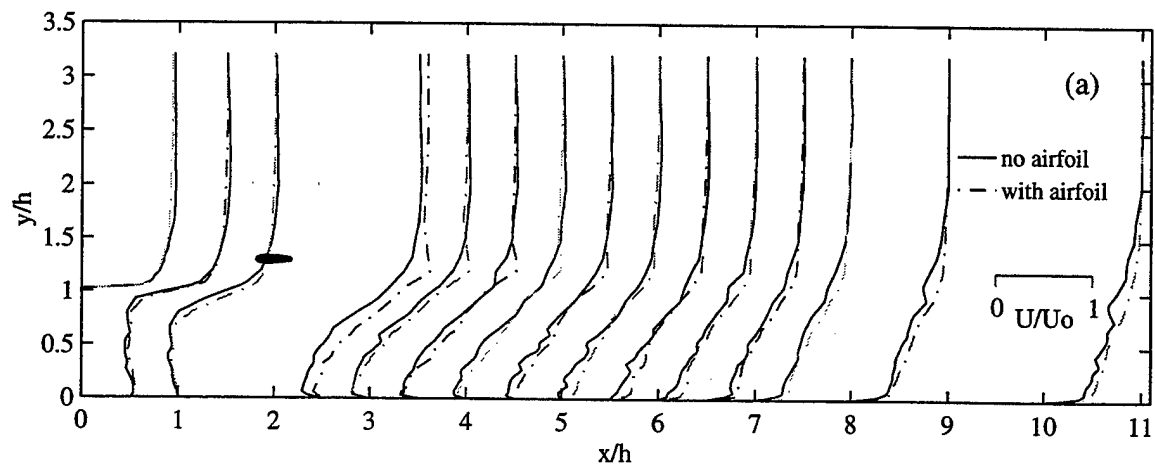


Figure 5.4.19 (a) velocity, (b) turbulence intensity, (c) streamlines of the backward-facing step. 10 mm airfoil at $(1.83h, 1.3h)$, oscillation frequency $f=10$ Hz, amplitude $H'=0.25$.

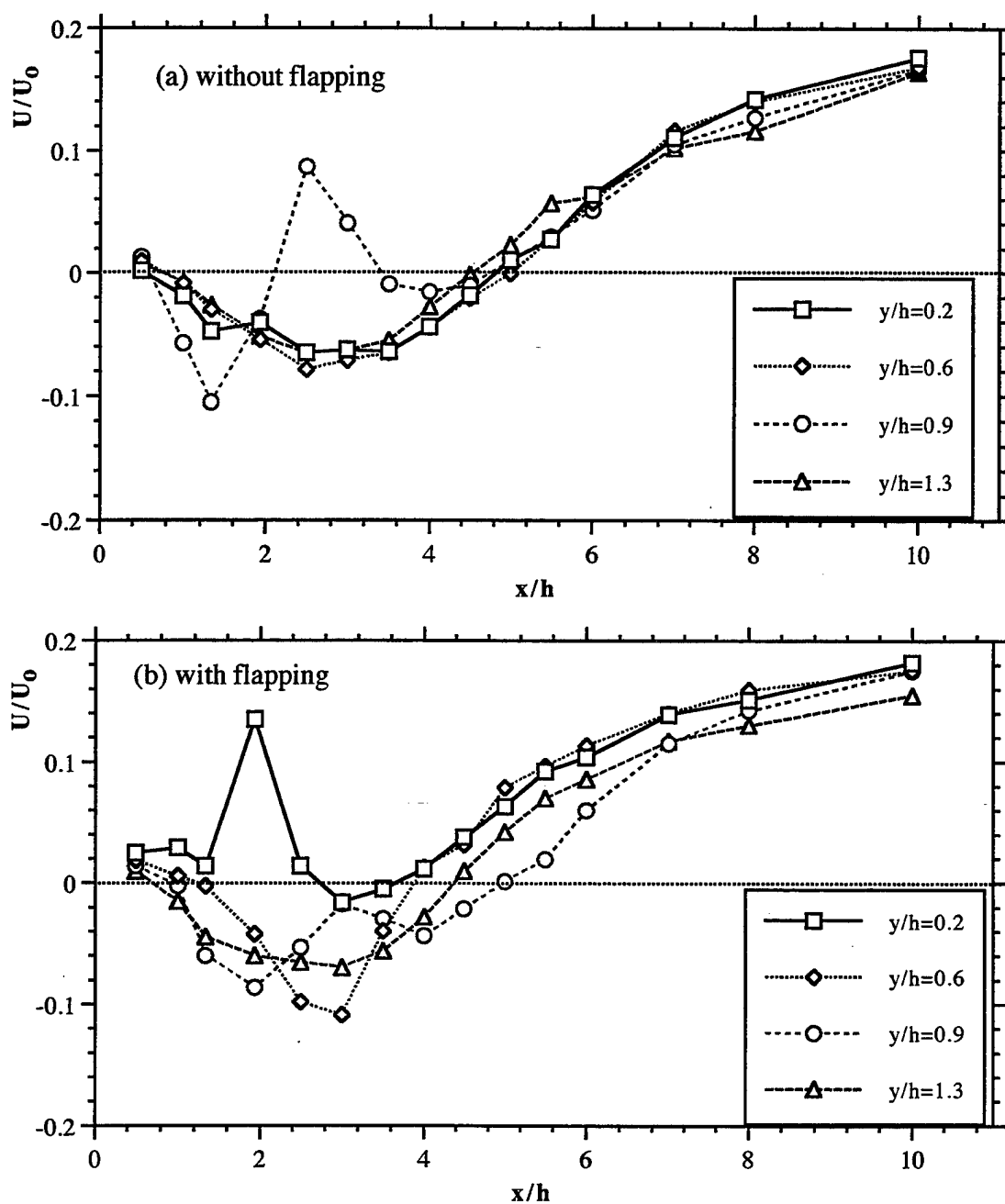


Figure 5.4.20 The streamwise velocity profile 2 mm above the plate, airfoil at the location $x/h=1.83$. (a) stationary, (b) flapping at $f=10\text{Hz}$, $H=0.25$

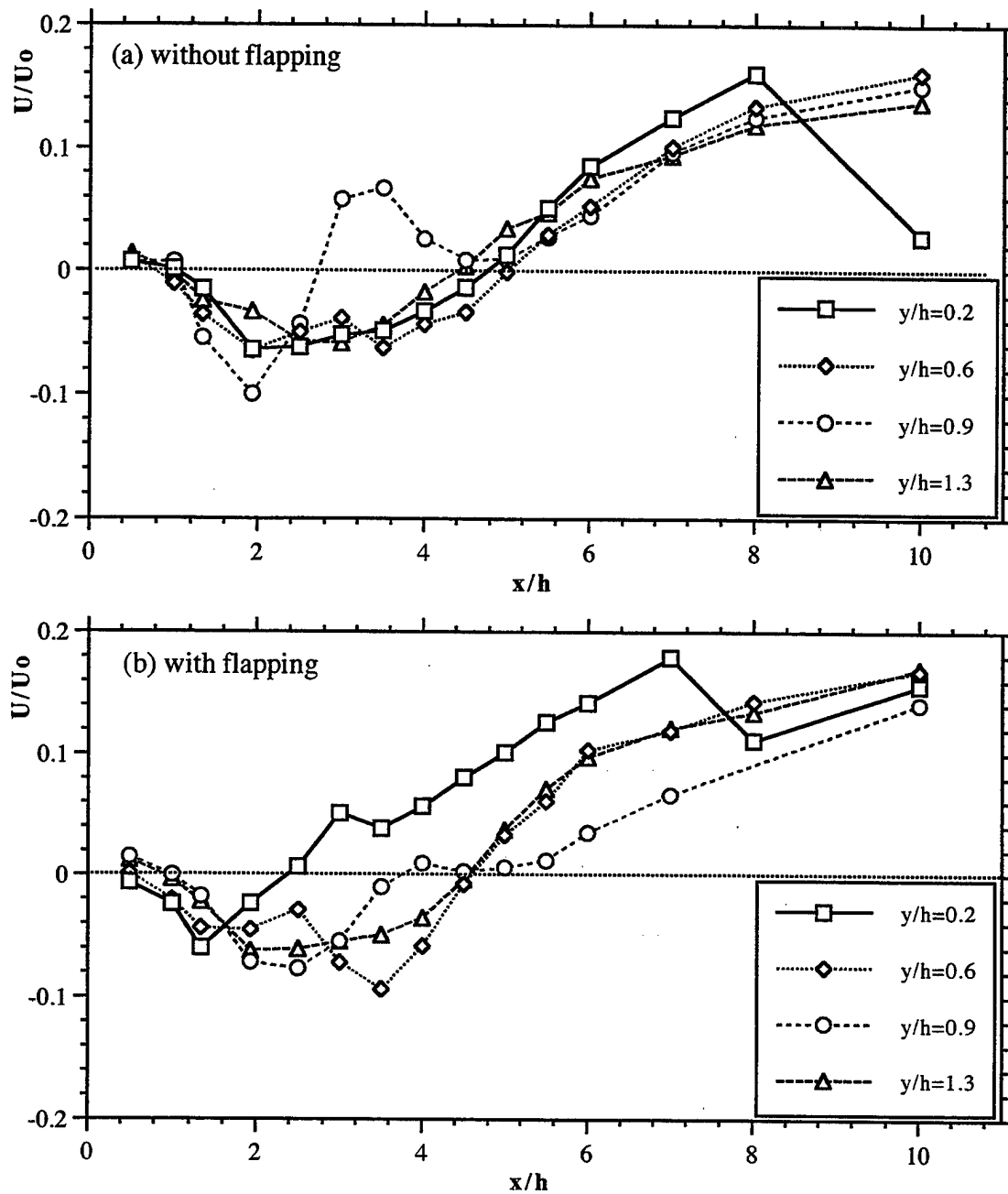


Figure 5.4.21 The streamwise velocity profile 2 mm above the plate, airfoil at the location $x/h=2.5$. (a) stationary, (b) flapping at $f=10\text{Hz}$, $H=0.25$

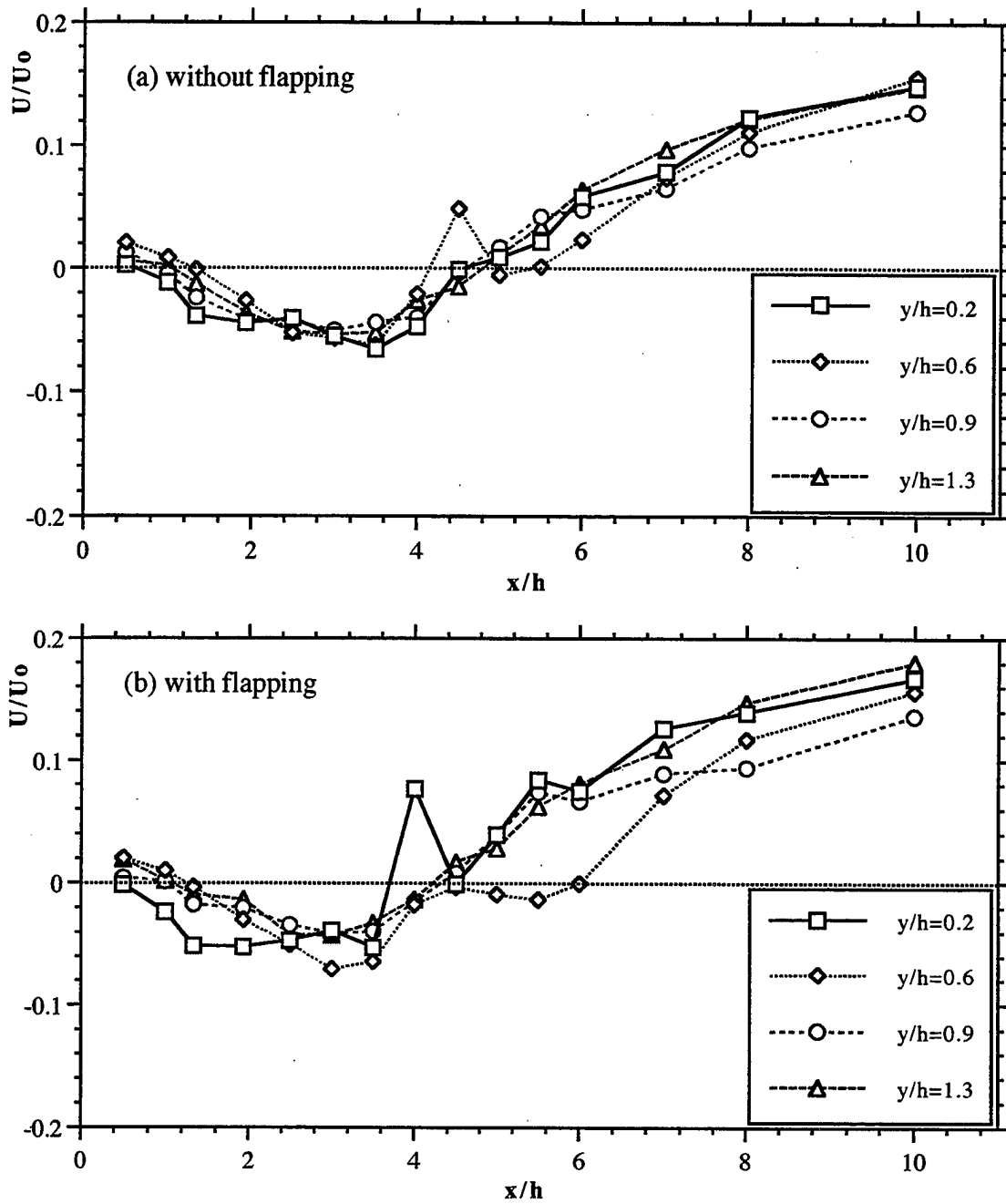


Figure 5.4.22 The streamwise velocity profile 2 mm above the plate, airfoil at the location $x/h=4.0$. (a) stationary, (b) flapping at $f=10\text{Hz}$, $H=0.25$

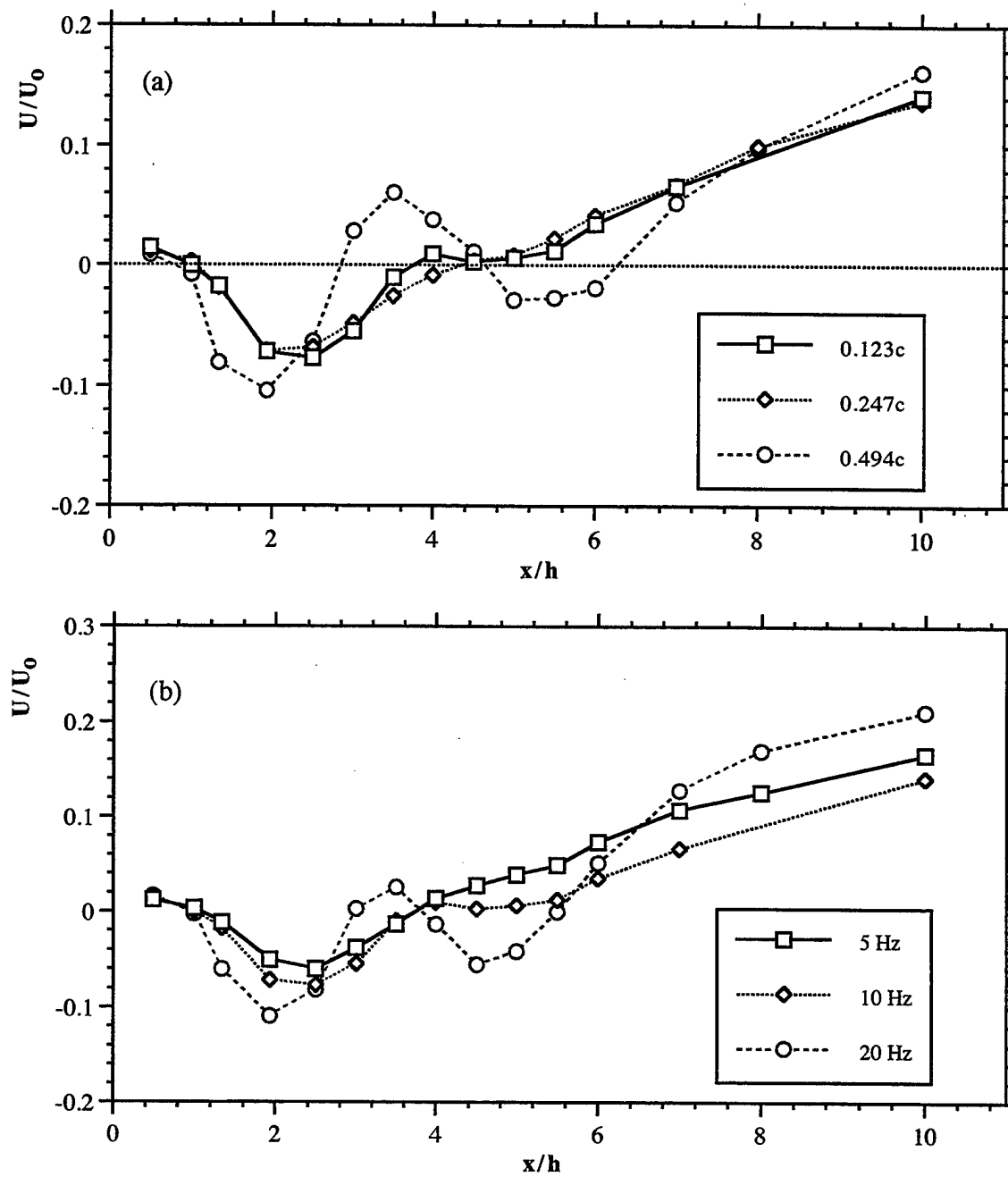


Figure 5.4.23 The streamwise velocity profile 2 mm above the plate, airfoil at the location $x/h=2.5$. (a) flapping at same frequency, $f=10$ Hz, (b) flapping at same amplitude, $h=0.25$

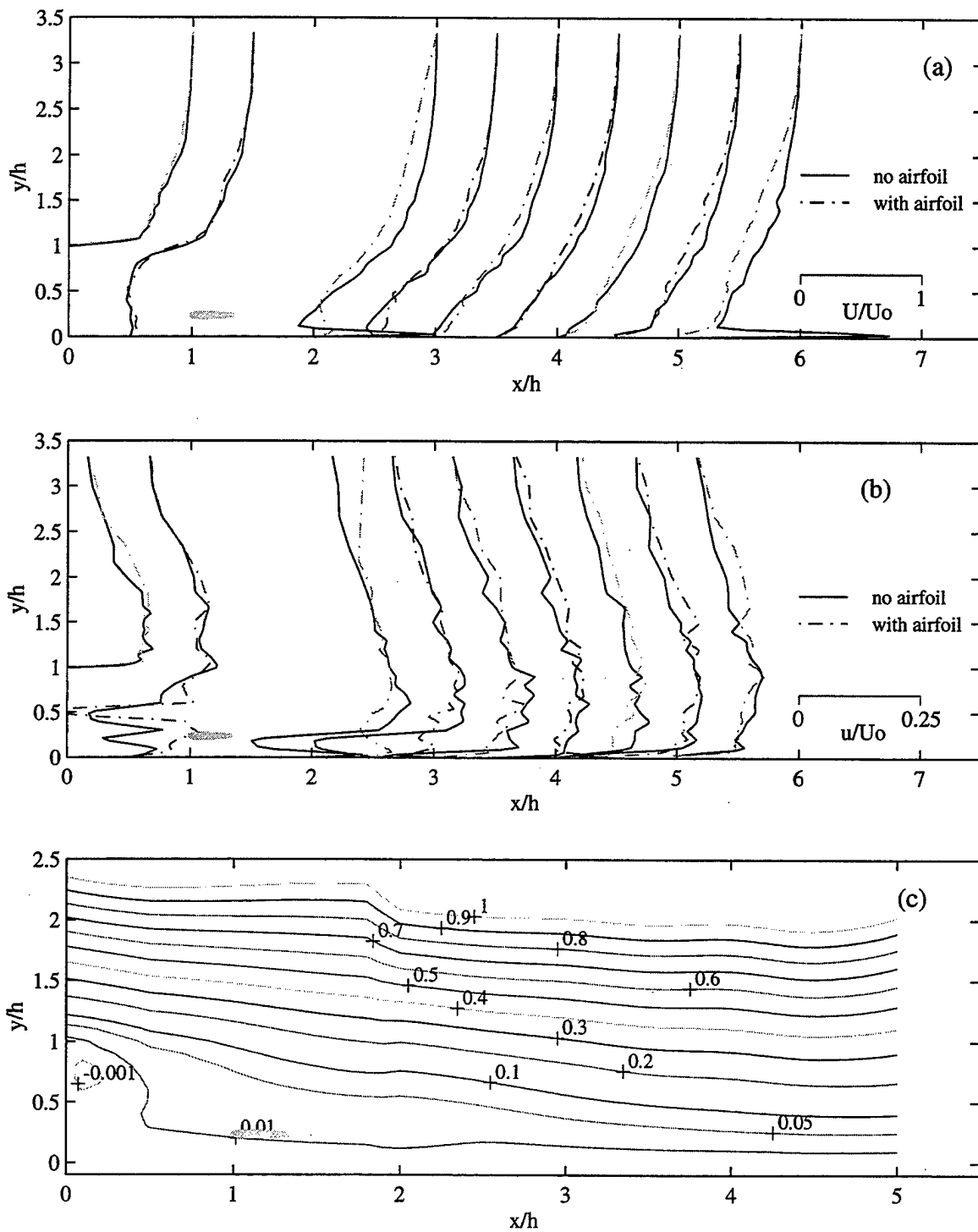


Figure 5.4.24 (a) velocity, (b) turbulence intensity, (c) streamlines of the backward-facing step. 10mm airfoil installed at $(1.83h, 0.2h)$, oscillation frequency $f=10$ Hz, amplitude $H'=0.25$. Short, blunt leading edge upstream plate.

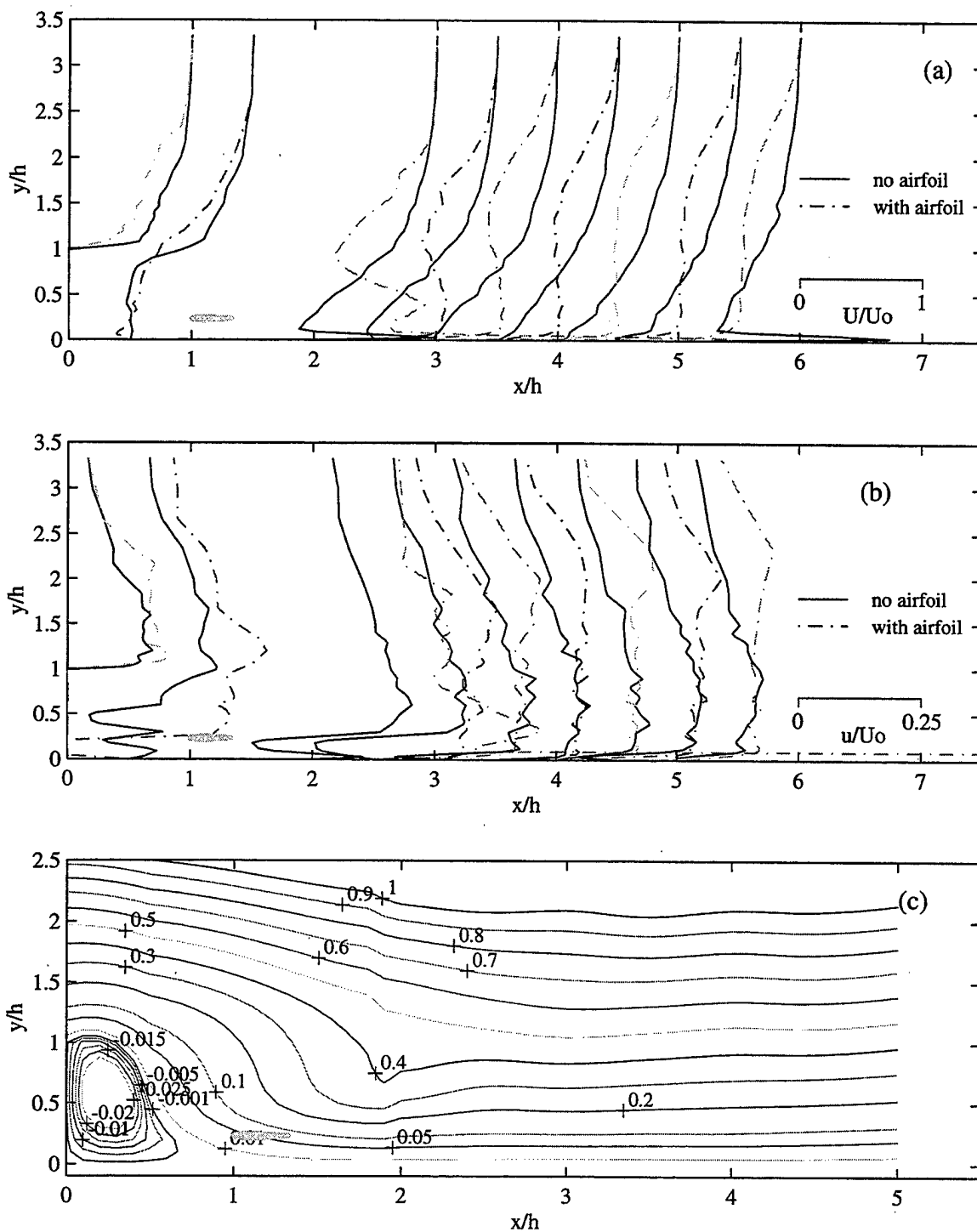


Figure 5.4.25 (a) velocity, (b) turbulence intensity, (c) streamlines of the backward-facing step. 10mm airfoil installed at $(1.83h, 0.2h)$, oscillation frequency $f=20$ Hz, amplitude $H'=0.125$. Short, blunt leading edge upstream plate.

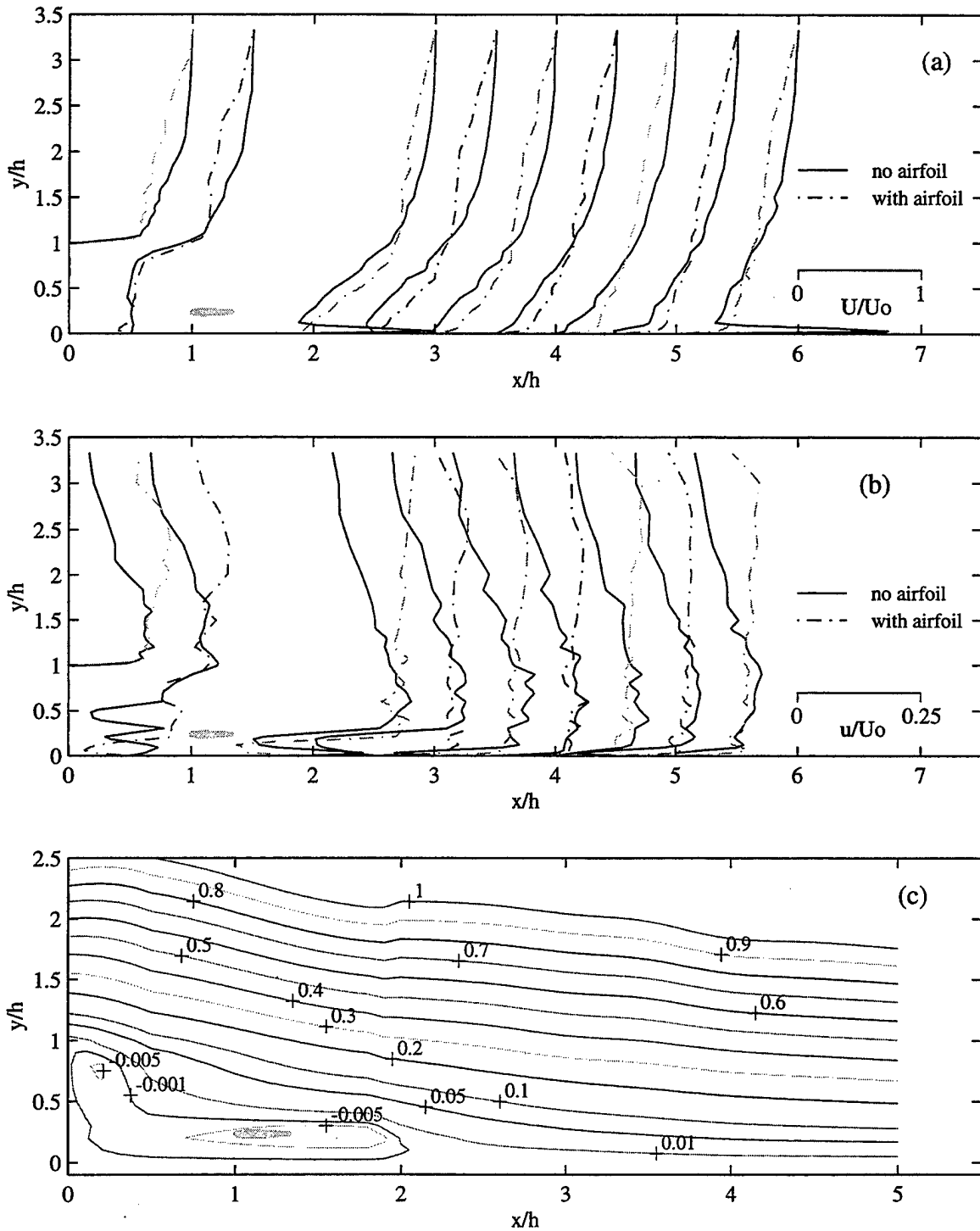


Figure 5.4.26 (a) velocity, (b) turbulence intensity, (c) streamlines of the backward-facing step. 10mm airfoil installed at $(1.83h, 0.2h)$, oscillation frequency $f=5$ Hz, amplitude $H'=0.25$. Short, blunt leading edge upstream plate.

VI. CONCLUSIONS

The flow entrainment and the propulsive wake structure induced by a flapping airfoil located in either a zero-velocity or low-velocity flow have been investigated using dye flow visualization and single component LDV measurements. The results confirm previous visualizations and measurements which identified an asymmetric wake behavior as soon as a critical plunge velocity was exceeded. They also clarify the flow behavior induced by the flapping airfoil for the case of vanishing free-stream velocity.

Also, the effects of a small airfoil oscillated in plunge in a backward-facing step flow have been explored using dye flow visualization and single component LDV measurements for a Reynolds number of 10,000 and a step aspect ratio of 12.33. Results of mean velocity and turbulence intensity for a backward-facing step flow with two-dimensional upstream flow condition are consistent with those reported in the literature. It has been shown that if the flow is three-dimensional near the edge of the step, the reattachment length is reduced from 5.2 to 3.0 step heights. The flow characteristics for various locations of a plunging airfoil, various frequencies of oscillation and amplitude and two different sizes of airfoil have been studied. Results indicate that the global flow behavior in terms of the size of the separation bubble is not significantly modified when the airfoil is not oscillating unless it is located within the separated shear layer close to the zero mean streamwise velocity contour. The most effective location for the airfoil is closest to the step and to the wall, followed by the one location within the separated shear layer. The effectiveness of a plunging airfoil increases with frequency and amplitude of oscillation as well as with the size of the airfoil. The reattachment length has been shown to be reduced by as much as over 70%. It has also been shown that a plunging airfoil can still perform effectively when the upstream flow condition is three-dimensional .

LIST OF REFERENCE

- Abott, D.E. and Kline, S.J., "Experimental Investigation of Subsonic Turbulent Flow Over Single and Double Backward-Facing Step," *J. Basic Eng.*, Vol. 84, pp. 317-325.
- Adams, E.W. and Johnston, J.P., "Effects of The Separating Shear Layer on the Reattachment Flow Structure Part 1," *Experiments in Fluids*, Vol. 6, pp. 493-499, 1988.
- Armaly, B.F., Durst, F., Pereira, J.C.F. and Schonung, B., "Experimental and Theoretical Investigation of Backward-Facing Step Flow," *J. Fluid Mech.*, Vol. 127, pp. 473-496, 1983.
- Battacharjee, S., Scheelke, B. and Troutt, T.R., "Modification of Vortex Interactions in a Reattaching Separated Flow," *J. AIAA*, Vol. 24, pp. 623, 1986.
- Barton, I.E. "Laminar Flow Past an Enclosed and Open Backward-Facing Step," *Phys. Fluids.*, Vol. 110, pp. 171-194.
- Betz, A. "Ein Beitrag zur Erklarung des Segelfluges," *Z.F. Flugtechnik und Motorluftschiffahrt*, 3, pp. 269-272, 1912
- Bradshaw, P., "The Effect of Initial Conditions on the Development of a Free Shear Layer," *J. Fluid Mech.*, Vol. 26, pp. 225-236, 1966.
- Bradshaw, P. And Wong, F.Y.F., "The Reattachment and Relaxation of a Turbulent Shear Layer," *J. Fluid Mech.*, Vol. 52, No. 1, pp. 113-135, 1972.
- Bratt, J.B. "Flow Patterns in The Wake of an Oscillating Airfoil," *Aeronautical Research Council, R&M* 2773, 1953.
- Brown, G.L. and Roshko, A., "On Density Effects and Large Structure in Turbulent Mixing Layers," *J. Fluid Mech.*, Vol. 64, pp. 775-816, 1974.
- de Brederode, V. and Bradshaw, P., "Turbulent Structure of a Reattaching Mixing Layer," *J. Fluid Mech.*, Vol. 110, pp. 171-194.
- Dohring, C.M., "Experimental Analysis of the Wake of an Oscillating Airfoil," *Thesis, Naval Postgraduate School*, 1996
- Dohring, C.M., Platzer, M.F., Jones, K.D. and Tuncer, I., "Computational and Experimental Investigation of the Wakes Shed From Flapping Airfoils and their Wake Interference/Impingement Characteristics," *78th Agard Fluid Dynamics Panel Symposium. Paper 33:1-9*, 1996
- Eaton, J.K. and Johnston, J.P., "A Review of Research on Subsonic Turbulent Flow Reattachment," *J. AIAA*, Vol. 19, No. 9, pp. 881-882, July 1981.
- Etheridge, D.W. and Kemp, P.H., "Measurements of Turbulent Flow Downstream of a Rearward-Facing Step," *J. Fluid Mech.*, Vol. 86, No. 3, pp. 545-566, 1978.
- Freymuth, P., "Propulsive Vortical Signature of Plunging and Pitching Airfoils," *J. AIAA*, Vol. 26, No. 27, pp. 881-882, July 1988.

- Halfman, R.L., "Experimental Aerodynamic Derivatives of a Sinusoidally Oscillating Airfoil in Two-Dimensional Flow," NACA Rept. 1108, 1952.
- Hasan, M.A.Z., "The Flow Over A Backward-Facing Step Under Control Perturbation: Laminar Separation," *J. Fluid Mech.*, Vol. 238, pp. 73-96, 1992.
- Isomoto, K. and Hyonami, S., "The Effect of Inlet Turbulence Intensity on the Reattachment Process Over A Backward-Facing Step," *J. Fluids Eng.*, Vol. 11, pp. 87-91, 1989.
- Jones, K.D., Dohring, C.M., Platzer, M.F., "Wake Structures Behind Plunging Airfoils: A Comparison of Numerical and Experimental Results," *AIAA* paper 96-0078, 1996.
- Kasagi, N. and Matsunaga, A., "Three-Dimensional Particle-Tracking Velocimetry Measurement of Turbulence Statistics and Energy Budget in A Backward-Facing Step Flow," *Int. J. Heat and Fluid Flow*, Vol. 16, pp. 477-485, 1995.
- Katz, J. and Weihs, D., "Behavior of Vortex Wakes from Oscillating Airfoils," *J. Aircraft*, Vol. 15, No. 12, Dec., pp. 861-863, 1978.
- Katzmayr, R., "Effect of Periodic Changes of Angle of Attack on Behavior of Airfoils," *NACA TM147*, 1922.
- Knoller, R., "Die Gesetze des Luftwiderstandes," *Flug-und Motortechnik(Wien)*, pp. 1-7, 1909.
- Koochesfahani, M.M., "Vortex Patterns in the Wake of an Oscillating Airfoil," *J. AIAA*, Vol. 27, No. 9, Sep., 1989.
- Otugen, M.V., "Expansion Ratio Effects on the Separated Shear Layer and Reattachment Downstream of a Backward-Facing Step," *Experiments in Fluids*, Vol. 10, pp. 273-280, 1991.
- Roos, F.W. and Kegelmann, J.T., "Control of Coherent Structures in Reattaching Laminar and Turbulent Shear Layer Airfoils," *J. AIAA*, Vol. 24, 1956.
- Schmidt, W., "Der Wellpropeller, ein neuer Antrieb fur Wasser-, Land- und Luftfahrzeuge," *Zeitschrift Flugwissenschaften*, Band 13, Heft 12, pp. 472-479, 1965
- Suzuki, H., Kida, S., Nakamae, T. and Suzuki, K., "Flow and Heat Transfer Over a Backward-Facing Step with a Cylinder Mounted near its Top Corner," *Int. J. Heat and Fluid Flow*, Vol. 12, No. 4, pp. 353-359, 1991.
- Thangam, S. and Knight, D.D., "Effect of Step Height on the Separated Flow Past a Backward-Facing Step," *Phys. Fluids A*, Vol. 1, No. 3, pp. 604-606, 1989.
- Zaman, K.B.M.W. and Hussain, A.K.M.F., "Vortex pairing on a Circular Jet Under Controlled Excitation, Part 1," *J. Fluid Mech.*, Vol. 101, pp. 449, 1981.

INITIAL DISTRIBUTION LIST

1. Defense Technical Information Center.....2
8725 John J. Kingman Rd., STE 0944
Ft. Belvoir, Virginia 22060-6218

2. Dudley Knox Library.....2
Naval Postgraduate School
411 Dyer Rd.
Monterey, California 93943-5101

3. Professor R. Panholzer, Code SS/PA.....1
Space Systems Academic Group
Naval Postgraduate School
Monterey, California 93943-5101

4. Professor D. J. Collins, Code AA/CO.....1
Department of Aeronautics and Astronautics
Naval Postgraduate School
Monterey, California 93943-5101

5. Professor M. F. Platzler, Code AA/PL.....10
Department of Aeronautics and Astronautics
Naval Postgraduate School
Monterey, California 93943-5101

6. Dr. K. D. Jones, Code AA/JO.....1
Department of Aeronautics and Astronautics
Naval Postgraduate School
Monterey, California 93943-5101

7. Dr. I. H. Tuncer, Code AA/TU.....1
Department of Aeronautics and Astronautics
Naval Postgraduate School
Monterey, California 93943-5101

8. Professor R. Howard, Code AA/Ho.....1
Department of Aeronautics and Astronautics
Naval Postgraduate School
Monterey, California 93943-5101

9. Professor J. C. S. Lai, Code AA/La.....1
Department of Aeronautics and Astronautics
Naval Postgraduate School
Monterey, California 93943-5101

10. Professor T. R. McNelley, Code ME/MC.....1
 Department of Mechanical Engineering
 Naval Postgraduate School
 Monterey, California 93943-5101

11. Professor M. D. Kelleher, Code ME/KK.....1
 Department of Mechanical Engineering
 Naval Postgraduate School
 Monterey, California 93943-5101

12. Professor P. J. Marto, Code ME/MX.....1
 Department of Mechanical Engineering
 Naval Postgraduate School
 Monterey, California 93943-5101

13. Professor T. Sarpkaya, Code ME/SL.....1
 Department of Mechanical Engineering
 Naval Postgraduate School
 Monterey, California 93943-5101

14. Professor D. Canright, Code MA/CA.....1
 Department of Mathematics
 Naval Postgraduate School
 Monterey, California 93943-5101

15. Naval/Mechanical Engineering, Code 341
 700 Dyer Rd, Rm 115
 Monterey, California 93943-5101

16. Dr. E. Rood.....1
 Office of Naval Research
 800 North Quincy Street
 Arlington, Virginia 22217-5660

17. Dr. S. Lekoudis.....1
 Office of Naval Research
 800 North Quincy Street
 Arlington, Virginia 22217-5660

18. Lt. Col. Jiannwoei Yue.....1
 201-3 Chang-Ann Rd. Second Section
 Taichung, 40727 Taiwan
 Republic of China